

FINAL REPORT

**Extension and Input Refinement to the ARB Wildland Fire Emissions
Estimation Model**

ARB Contract Number: 00-729

Prepared by:

Nicholas Clinton, Ruiliang Pu, Peng Gong, Yong Tian

Project Team:

Peng Gong – Principal Investigator

Nicholas Clinton – Staff Research Associate

Ruiliang Pu – Staff Research Associate

Yong Tian – Staff Research Associate

Center for the Assessment and Monitoring of Forest and Environmental Resources
College of Natural Resources
Gianinni Hall
University of California
Berkeley, CA 94720

Prepared for:

Air Resources Board
California Environmental Protection Agency

Submitted June 15, 2003

Copyright © 2003 by the Regents of the University of California. All rights reserved.

Disclaimer

The statements and conclusions in this report are those of the University of California and not necessarily those of the California Air Resources Board. The mention of commercial products, their source, or their use in connection with material reported herein is not to be construed as actual or implied endorsement of such products.

Acknowledgements

Completion of this project would not have been possible without the cooperation and assistance of various individuals in academia and government.

We are grateful for assistance, backing and partnership we have enjoyed from our project management including Patrick Gaffney, Klaus Scott, and Mike FitzGibbon at the California Air Resources Board. Their invaluable guidance and steering kept the project on track.

The North American Fire Mapping Project participants were very helpful in critique and review of the fire mapping portion of this project. They also made valuable contributions to the development of fire detection algorithms.

This report was submitted in fulfillment of ARB Contract Number 00-729, Extension and Input Refinement to the ARB Wildland Fire Emissions Estimation Model, by the University of California under the sponsorship of the California Air Resources Board. Work was completed as of June 15, 2003.

Table of Contents

Disclaimer	ii
Acknowledgements	iii
Table of Contents	4
Preface.....	5
Executive Summary	6
Section 1 – Fire Mapping Using Remote Sensing	10
Introduction.....	10
Fire Mapping Algorithms	11
Data sources	13
Methods.....	13
AVHRR data preparation.....	13
Hotspot detection algorithm.....	13
Burn scar mapping algorithm.....	16
Comparison to Fire Activity Data.....	20
Post-Processing.....	24
Results and Analysis	25
Burnt area mapping.....	26
Accuracy Assessment	32
Discussion.....	37
References.....	39
Section 2 – NFDR-TH Input Enhancement.....	43
Introduction.....	43
Methods and Results.....	45
Discussion.....	48
Conclusion	49
Section 3 – Daily Emissions Allocation	50
Introduction.....	50
Methods and Results.....	50
Discussion.....	55
Conclusion	56
References.....	56
Section 4 – Adding Additional Pollutants to Emissions Estimates.....	57
Introduction.....	57
Methods and Results.....	57
Discussion.....	59
Conclusion	61
References.....	61
Section 5 – Development of Web and Desktop Tools for Fire Emission Estimation	63
Introduction.....	63
Appendix.....	64
• Wildland Fire Emissions Estimation System, Version 4 (Visual Basic), <i>Programmer’s Guide and Usage Notes</i>	64
• Wildland Fire Emissions Thematic Mapper, <i>User and Configuration Guide</i>	64

Preface

This report is organized into four main sections, each roughly corresponding to the tasks in the original scope of work for this project. This structure is intended to clarify the reporting, since the sections describe very different kinds of work, each task being a semi-independent project. Each section has approximately the same format and includes: introduction, method, results, discussion, and conclusion. The sections are:

1. Remote sensing (RS) based fire mapping. This was the first task, and largest project component. Also includes comparison of RS data to California Department of Forestry (CDF) fire history data.
2. NFDR-TH spatial moisture input. Enhancement of emissions estimation inputs to include localized fuel moisture data.
3. Daily emissions allocation. Increasing the temporal resolution of emissions estimates to compute daily fire emissions.
4. Emissions expansion. Addition of pollutants estimated by the system to include NO_x, SO_x, N₂O, ammonia, methane, total non-methane hydrocarbons, (in addition to the PM10, PM25, and CO previously computed).

The sub-contractual tasks of migrating the Emissions Estimation System to Visual Basic (for compatibility with ArcGIS 8.x) and developing a prototype web GIS for dissemination of emissions information were performed by VESTRA Resources of Redding, California. Their documentation of these tasks can be found in the appendix. The reports describe how to set up, operate and maintain the applications, as well as the basic components of the applications. The applications, as well as the documentation, are included on the companion CD.

Detailed information referenced by any of main sections is also provided in the appendix. The appendix is a repository of data and minutiae that are not of interest to the casual reader and includes large tables and Avenue scripts. The data may be useful for more technical inquiries, or as a reference for future research. The report makes frequent reference to Avenue scripts found in the appendix. The scripts can be referenced for a precise record of the geo-processing steps we used to generate and/or transform data.

The report also has a companion CD. The CD contains digital versions of this report, the data tables, geographic data products, and the updated Emission Estimation System (EES) for ArcView 3.x users. The supplementary CD is provided for potential users of information developed under the contract, but is not intended as the primary deliverable product.

Executive Summary

Fire mapping using Remote Sensing

Fire history data is an essential input to the Berkeley Fire Emissions Estimation System (EES). The standard, or default, fire data input is the California Department of Forestry and Fire Protection (CDF) historical database of fire occurrence. This dataset is subject to constraints of data availability from responsible agencies (for example the fire information from land controlled by the Bureau of Land Management), funding availability, and the chain-of-custody that the necessary data transfer and transformation entails. As an alternative, CAMFER (in collaboration with the North American Fire Mapping Project participants) has developed algorithms for remotely sensed fire detection and mapping using the Advanced Very High Resolution Radiometer (AVHRR) on board the National Oceanic and Atmospheric Administration’s (NOAA) polar orbiting satellites.

CAMFER adapted the Canadian Centre for Remote Sensing (CCRS) hotspot detection and burn scar mapping algorithms to California. These algorithms make use of thermal and near infrared channels for hotspot detection. The hotspots then function as input to the burn scar mapping algorithm, summarized in table 1. The burn scar mapping technique relies on the Normalized Difference Vegetation Index (NDVI) for determination of burned area.

Table 1. This algorithm processing chain is a modified version of the CCRS HANDS algorithm.

Step 0	AVHRR data preparation: two NDVI composites of a selected interval, one corresponding hotspot composite (fire mask)
Step 1	Normalize NDVI _{post} to NDVI _{pre} : means of NDVIs calculated only with interested land covers $Ratio.C = \frac{mean\ of\ NDVI_{pre}}{mean\ of\ NDVI_{post}}$ normalized NDVI _{post} = Ratio.C * NDVI _{post} , not hotspot pixels used for calculation of NDVI mean.
Step 2	Calculate NDVI difference: normalized NDVI _{post} – NDVI _{pre} , burn scar expected to have A negative value in the NDVI difference image.
Step 3	Confirm hotspot pixels (CBP) using NDVI difference: a CBP is assumed to have a negative NDVI difference, otherwise the hotspot pixel is considered as a false fire.
Step 4	Calculate NDVI difference statistics (mean, standard deviation, SD) of NDVI decrease for all CBPs for each land cover type, different land covers expected to have a different mean and SD.
Step 5	Select potential burn scar pixels (BSPs): NDVI difference of a potential BSP < (mean + c*SD), the potential BSPs selected for different land cover types with the mean and SD from Step 4.
Step 6	Apply a sieve filter to the selected BSPs: filter out a burnt patch of < 2 pixels, a burn patch less than 2 pixels is considered to be caused by noise.
Step 7	Confirm a BSP with a neighbor CBP and later on up to four neighbor confirmed BSPs to create connected burn patches, 1st iteration with a neighbor CBP, 2nd iteration with a neighbor CBP or a conformed BSP (CBSP), 3rd to 5th iteration with 2 to 4 CBSPs, after 5th iteration using 4 CBSPs only.
Step 8	Filter out a BSP patch of < 2 pixels: the patch of < 2 CBSPs is considered to be a false burnt patch, caused by noise.
Step 9	Output a burnt area mask (in TIFF format).

CAMFER created burn scar maps for 6 months in 1999 and 4 months in 1996 using 6 different sets of parameters for each year. We compared the resultant maps to CDF data using a GIS to quantify the differences between the datasets. Figure 1 shows an overlay of a 1999 fire map, a 1996 fire map, and the corresponding CDF data.

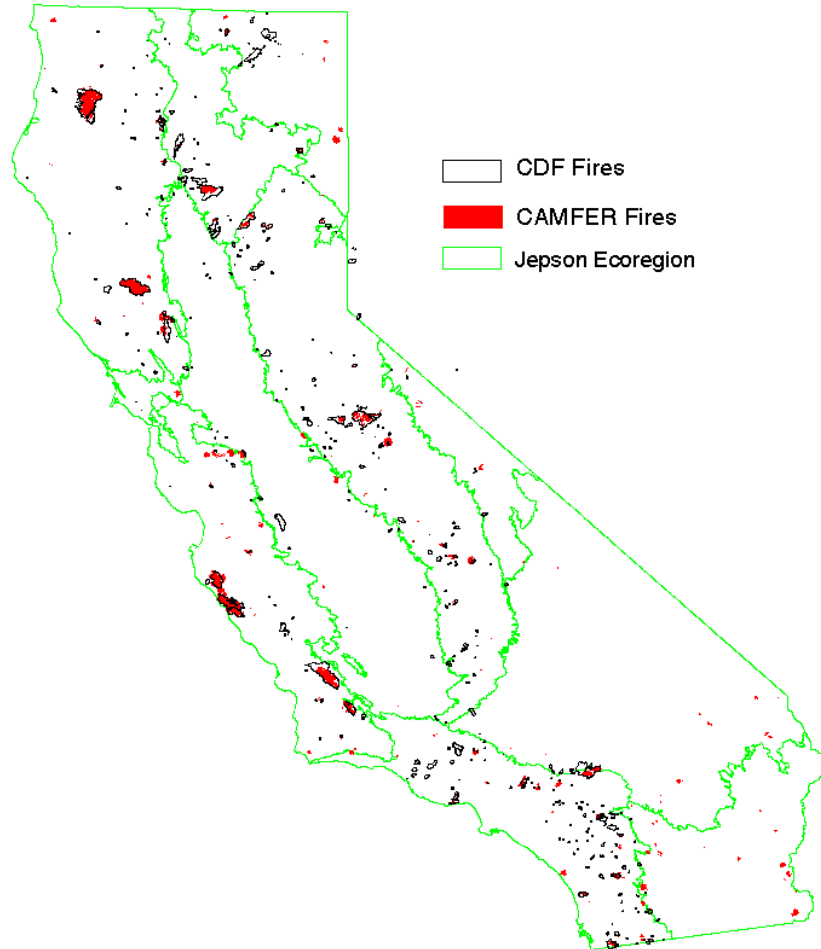


Figure 1. CAMFER and CDF fire overlay map.

Analysis of this data shows that the CDF versus remotely sensed mapped fires will differ based on annual or monthly NDVI differencing and the coefficient that is selected for the NDVI difference threshold. The degree of agreement between the CDF and remotely sensed data varies by vegetative cover type and Jepson eco region. We evaluated three different assessment techniques for comparing the CDF and CAMFER fire maps: polygon intersection, polygon overlay, and grid-polygon overlay. Depending on assessment type, the CAMFER satellite-based method captures between 45% and 67% of CDF mapped fires. There is better agreement between the datasets in forested land and for fires over 10,000 acres. The CAMFER maps have higher agreement with CDF reported fires and lower amounts of “false positives” in forestland than in grass or shrub dominated ecosystems.

The CAMFER method of fire mapping is limited by satellite overpass frequency that will not detect fast burning fires occurring between overpasses. Vegetation change not caused by fire but resulting in an NDVI decrease may result in “false detection” of burn area. Similarly, “re-greening” of burned area can result in an NDVI increase over burned areas depending on the NDVI difference interval. These effects are evident through overlay of hotspots, burn scar maps and the CDF data.

Future research is needed for validation of both the CDF and remotely sensed fire maps. Additional investigation into variations in mapping accuracy by cover type or region may enable optimization of thresholds and corresponding increases in satellite-based mapping accuracy. This type of research is somewhat constrained by uncertainty in the accuracy and completeness of the CDF dataset, therefore, additional ground truthing is required for true validation of remotely sensed fire map products.

NFDR-TH Fuel Moisture Spatial Inputs

Past CAMFER research indicated that the Emissions Estimation System (EES) is highly sensitive to the fuel moisture input implemented in the First Order Fire Effects Model (FOFEM). Fuel moisture is defined as the National Fire Danger Rating System Thousand Hour fuel moisture (NFDR-TH). In order to enhance EES performance, CAMFER sought a spatial, empirically based input of fuel moisture as an alternative to default user input. The United States Forest Service (FS) computes thousand hour fuel moisture at a national scope, on a daily basis, at 1 kilometer resolution. CAMFER began archiving these grids on a daily basis on November 20, 2002.

In order to provide an immediate NFDR-TH input for inclusion to current versions of the EES, CAMFER mined FS image archives to attain year 2000 NFDR-TH data. Only saved image data was available. To create electronic maps of these GIF images, we geo-referenced the images with a pre-prepared world file, remapped the categorical data to average values, and interpolated over areas that had map graphics in the original images. We then re-projected and clipped the resultant maps for compatibility with the EES, making them ready for input to the emissions calculations.

For input to the EES, we created monthly average moisture grids. The EES uses date information in the fire attributes to select the appropriate monthly grid and sample the NFDR-TH fuel moisture value at the location of each fire in the estimation. A run of year 2000 fire data from the CDF database shows a 60% increase in particulate emission estimates resulting from spatial input of NFDR-TH fuel moisture values.

Daily Emissions Allocation

For modeling purposes, ARB requires daily or even hourly temporal resolution of fire emissions estimates. CAMFER evaluated an estimation approach to generating this information based on the FARSITE model. This method proved far too data intensive to be practical for regular decomposition of fire area into daily polygons.

Instead, CAMFER obtained daily fire progression polygons (For the Plaskett II and Manter fires. ARB provided daily progression polygons for the McNally fire.) from

emergency response agencies involved in fire suppression. We used a sequence of Avenue scripts to build daily burn area polygons from fire progression polygons, perform estimates of daily emissions using the EES, then allocate the emissions to grids of various resolutions and the Central California Ozone Study (CCOS) modeling domain polygons.

The acquisition of geographic information at a daily resolution is possible from the Office of Emergency Services (OES) website, using remotely sensed fire detection data, and from FARSITE. Provided that daily burn area or fire progression polygons are available, the process of daily emissions estimation is straightforward and automatic. Allocation of the daily emissions to various other geographic zones is slightly more complex, but feasible with appropriate scripting. Daily data may be further decomposed into hourly emissions based on existing apportionment schemes.

Adding Additional Pollutants to Emissions Estimates

Only three pollutants are estimated by the currently released Forest Service First Order Fire Effects Model (FOFEM). In order to enhance the EES capability for estimating additional emissions, an expanded set of emission factors was needed. The modular structure of the EES facilitates this type of update through the replacement of the emission factor table. The emission factors for additional pollutants needed to conform to the format of this table, with different emission factors for three moisture regimes supported by FOFEM.

To add additional pollutants, CAMFER performed a literature search in order to obtain emissions information for CH₄, Total Non-Methane Hydro-Carbons (TNMHC), NH₃, N₂O, NO_x, and SO₂. We used FOFEM tables of combustion efficiencies (CE) by moisture regime and an equation for CO₂ production as a function of CE to derive a table of CO₂ emission factors in the same format as the “stock” FOFEM table that included CO. Using emission ratios to either CO or CO₂, depending on pollutant correlation to either smoldering or flaming combustion (respectively), we built an expanded table of emission factors. The new table is in the same format as the existing table, enabling control over emissions through the user defined moisture regime input. By maintaining a consistent format in the emission factors, we achieved integration of additional modeling capability without extensive modification of the EES.

Section 1 – Fire Mapping Using Remote Sensing

Introduction

Fire burn history data is an essential input to the Berkeley EES. The system can only estimate emissions (for inventory purposes rather than prediction purposes) where burn activity is known to have occurred. The standard, or default, input in this regard is the California Department of Forestry and Fire Protection (CDF) historical database of fire occurrence. This burn activity data is compiled through collaboration between CDF and the United States Forest Service (USFS). More information about this program is available at http://frap.cdf.ca.gov/data/fire_data/history/fire_historyfr.html. The website is very explicit about the limitations of this dataset. It is a compilation of data, from a variety of agencies, in various formats, that has been assembled into a layer of geographic information in polygon format. The data is not comprehensive. It is subject to constraints of data availability from responsible agencies (for example the fire information from land controlled by the Bureau of Land Management), funding availability, and the chain-of-custody that the necessary data transfer and transformation entails.

For these reasons, ARB is interested in a method of fire activity estimation alternative to the use of the CDF dataset. CAMFER (in collaboration with the North American Fire Mapping Project participants) has developed algorithms for remotely sensed fire detection and mapping using the Advanced Very High Resolution Radiometer (AVHRR) on board the National Oceanic and Atmospheric Administration's (NOAA) polar orbiting satellites. Remote sensing is the most efficient and economic means for monitoring fires over large areas on a routine basis, despite that it suffers from various limitations (Li et al. 2000a, b, Justice et al. 1993).

AVHRR data (onboard NOAA-14 and earlier satellites) are available at a nominal resolution of 1.1 km in five channels consisting of the visible, near-infrared (IR), mid-IR and two thermal-IR portions of the spectrum. The spectral resolution offers considerable benefits to fire monitoring (Harris 1996). Table 1 summarizes wavelength and physical characteristics of each AVHRR channel for fire detection. Channels 1 and 2 provide data capable of detecting, monitoring and measuring smoke emissions (Kaufman et al. 1990, Khazenie and Richardson 1993), but contain no thermal information. Channel 3 is extremely sensitive to sub-pixel burning. It is the most important channel for fire detection (Rauste et al. 1997, Franca et al. 1995, Pozo et al. 1997, Muirhead and Cracknell 1985, Setzer and Pereira 1991) although it has a relatively low temperature saturation point (~321K). Channels 4 and 5 are far less sensitive to sub-pixel burning, but they can frequently help detect fires when combined with other channels (Flasse and Ceccato 1996, Justice et al. 1996).

Table 1. Wavelength and physical characteristics of each AVHRR band used for fire detection

Channel	Wavelength (μm)	Characteristics
1	0.58 - 0.68	visible, reflection of solar light, removal of low clouds and bright surfaces, sensitivity to fire smoke
2	0.725 - 1.1	NIR, reflection of solar light, vegetation albedo drastically reducing after fire
3	3.55 - 3.95	MIR, reflection of solar light and MIR radiance, good for fire detection, saturation at 320K
4	10.3 - 11.3	Thermal Channel, thermal radiance
5	11.5 - 12.5	Thermal Channel, thermal radiance

Fire Mapping Algorithms

Wildfire mapping using NOAA/AVHRR data involves both active fire detection and burn scar mapping. Existing AVHRR-based fire detection algorithms can be grouped into two broad categories: (1) fixed threshold algorithms, (2) adaptive threshold contextual algorithms (Giglio et al. 1999). Fixed threshold algorithms apply empirically determined thresholds to discriminate fire pixels from their non-burning surroundings and clouds (Boles and Verbyla 2000). Threshold values are defined and fixed for given regions and seasons. Flannigan and Vonder Haar (1986) first used the fixed threshold method to identify fire pixels. If the temperature for both channel 3 and channel 4 exceeded the mean background temperature and if channel 3 was greater than channel 4 by a critical threshold, fire was assumed to exist. They detected 80% of unobstructed fires.

Kaufman et al. (1990) used a threshold-based fire detection method in an assessment of trace gases and particulates emission from fires in Brazil. They found lower threshold values resulted in an increased number of false fires caused by warm surface areas. Kennedy et al (1994) modified the threshold set by Kaufman et al (1990) using AVHRR data in West Africa and improved fire detection effectiveness.

Li et al. (1997, 2000a), Rauste et al. (1997), Pozo et al. (1997) and Arino and Melinotte (1998) employed fixed multiple thresholds applied to multiple channels to detect active fires in the Canadian boreal forests, Spain and Africa, respectively. They all achieved various degrees of success in fire detection. The advantages of fixed thresholds algorithms for active fire detection are that they are simple and require less computation. The limitations of these methods are that the fixed thresholds are only applicable to local to regional scales and a short fire season.

Instead of using fixed threshold values throughout an area, a category of contextual algorithms using adaptive thresholds was proposed. This method involves the computation of variable, pixel-specific thresholds based on pixels surrounding a potential fire pixel. Flexible threshold algorithms identify a fire pixel based on the level of contrast between the potential fire pixel and its "background" pixels, the definition of background varying with kernel size (Boles and Verbyla 2000).

Contextual algorithms are intended to be flexible and effective over different environmental conditions (Flasse and Ceccato 1996). Lee and Tag (1990) proposed one of the first contextual fire detection algorithms in their analysis of gas waste flares from AVHRR nocturnal data. A contextual algorithm adapted from Flasse and Ceccato (1996) is being used for the International Geosphere Biosphere Program, Data and Information Systems (IGBP-DIS) fire product (Malingreau and Justice 1997, Justice and Dowty 1994, Dwyer et al. 1998, Stroppiana et al. 2000).

Contextual methods have also been used for regional fire monitoring, for example, over central Africa (Eva and Flasse 1996). In principle, contextual methods are more versatile over a wide range of conditions than the fixed threshold approaches. It should be noted, however, if a set of thresholds were set too high for identifying potential fire pixels and background non-fire pixels, a large omission error would occur. Since the fire confirmation tests employed in the subsequent contextual algorithms work only on those potential fire pixels, the omission error problem is compounded (Li and Giglio 1999). Therefore, contextual algorithms are highly sensitive to the initial thresholds used to identify potential fire pixels.

Active fire detection as described using the methods above identifies only a portion of an entire burnt area over a certain region in a given season due to clouds and limitation in satellite over-passing frequency (Li et al. 2000b). Burnt scar mapping overcomes this problem to some extent. Extraction of burnt area information from AVHRR data can be done with any of the following three approaches: (1) application of multiple tests on spectral values or derived indices based on single date data; (2) temporal analysis; and (3) classical image segmentation techniques with single date or multi-temporal data (Arino et al. 1999). For the first approach, a post-fire image is needed. Based on the spectral difference between burnt and un-burnt areas in individual and/or a combination of channels (e.g., NDVI), burn scars can be detected (Razafimpanilo et al. 1995, Pereira 1999).

In the second approach, changes caused by fire activity are tracked for burnt scar mapping. For example, Kasischke and French (1995) used AVHRR data to map burn scars based on the decrease in NDVI, which took place after a large forest fire in Alaska. Martin and Chuvieco (1995) and Fernandez et al. (1997) also applied pre- and post-fire NDVI differences to map burn scars. It has been demonstrated that this method is more effective than those using only a single post-fire image, it minimizes the confusion with regard to some permanent land cover types that have spectral patterns similar to fire scars (Pereira et al. 1997). The third type of method involves image classification and post-classification comparison. Recently, a new burn scar mapping algorithm was developed that combined hotspot detection with NDVI differencing. Fraser et al. (2000) developed an algorithm named HANDS (Hotspot and NDVI Differencing Synergy) that combines the strengths of the two techniques while avoiding their limitations.

To obtain an estimation of burned area in California, for 1999 and 1996, we developed an integrated approach of mapping wildfires using the NOAA-14/AVHRR data. We

integrated the use of contextual information in a multi-channel fixed threshold algorithm (Li et al. 2000a) for hotspot detection, and adopted a synergistic approach, similar to HANDS, for burn scar mapping.

Data sources

Daily AVHRR-HRPT (High Resolution Picture Transmission format) images (1.1 km resolution at nadir) for 1996 and 1999 were acquired on board of NOAA-14 satellite during its daytime passes. The local passing time of NOAA-14 over California varied. Due to excessive cloudiness and data acquisition problems, 6 months in 1999 (May through October) and 4 months in 1996 (July through October) were used for analysis.

Methods

AVHRR data preparation

We used the Geocomp-n (PCI Geomatics company, Canada, 1999) to pre-process daily NOAA/AVHRR data. The Geocomp-n correction is accomplished in two stages: Geocoding and compositing. At the geocoding stage, the radiometric correction and calibration, and spatial geometric correction are applied to 5 channels of AVHRR data with a calibration auxiliary file, orbit parameter file and georeferenced chip images. The outputs from this stage are reflectance at the top of the atmosphere from channels 1 and 2 and brightness temperature (Kevin) from channels 3-5. The geometric location accuracy at this stage reaches subpixel levels of 1 kilometer or less. In the composite stage, the Geocomp-n composites the same-day images into one composite image file for later use (i.e., hotspot detection and burn scar mapping as below).

Hotspot detection algorithm

The active fire detection algorithm used in this study is based on the algorithm of Li et al. (2000a, hereafter called the CCRS algorithm) with modification for California. Compared to other algorithms, the CCRS algorithm is most effective for detection of large area fires over the boreal forest in Canada (Li et al. 2000c). Based on the fixed threshold tests in the CCRS algorithm, we added some new tests to deal with the heterogeneous landscape in California. The tests are divided into two major stages: identifying potential fire pixels and eliminating false fire pixels. For the latter stage, we added a function that considers background effects. As with the CCRS algorithm, thresholds of all tests are optimized for detection of “real” fires by eliminating as many as “false” fires as possible. Through a trial-and-error approach, we chose the threshold values using training data sets.

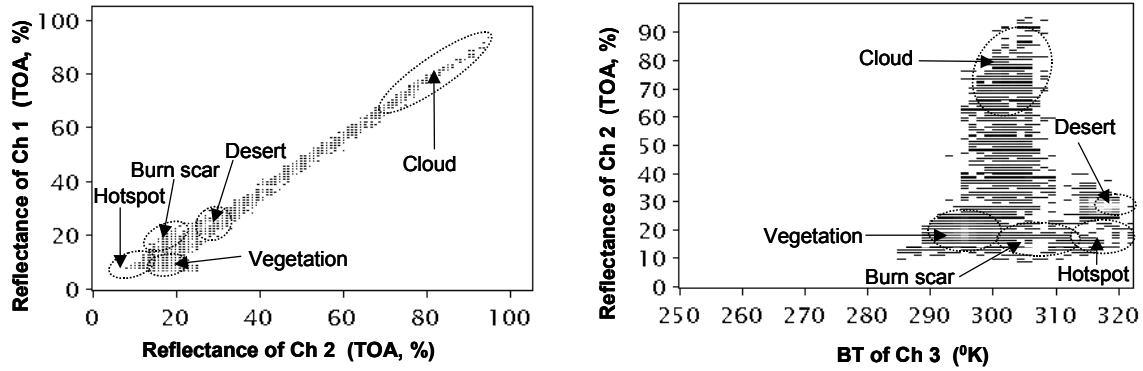


Figure 2(a), left, and 1(b), right. Spectral correspondence of hotspots, burn scars, and selected land cover types. These features intersect slightly in spectral space.

Figure 1 shows a schematic representation of the spectral correspondences of several known land cover types, especially hotspots and burn scars, helped us determine the thresholds. From Figure 1, it is evident that the hotspot and burn scar types have some intersection in the spectral space as well as overlap with other land cover types. Identification of fire pixels is difficult if only a few tests are done. Our multi-channel threshold algorithm is summarized with the CCRS algorithm in Table 2.

Table 2. Comparison of algorithms used for hotspot detection by CAMFER and CCRS

Test #	CAMFER (NOAA-14)	CCRS (NOAA-14)
1	T3 > 315K	T3 > 315K
2	T3-T4 >= 14K	T3-T4 > 14K
3	T4 >= 260K	T4 > 260K
4	R2 <= 22%	R2 < 22%
4, cont.	If 22% < R2 <= 30%, and R2 < (mean of 8 neighbor pixels - 1%), and T3 > (mean of 8 neighbor pixels + 5K), then fire.	N/A
5	Elimination of water bodies, urban, agricultural area, dune and desert.	Elimination of cropland, grassland and water bodies.
6	T4-T5 < 4K, and T3-T4 >= 19K	T4-T5 < 4.1K, and T3-T4 >= 19K
7	R1+R2 <= 75%	N/A
8	R1-R2 > 1%	N/A
9	Elimination of single pixel fires	Elimination of single pixel fires

Table 2 indicates that, as in most previous work (Li et al. 2000a, Li and Giglio 1999, Arino and Melinotte 1998, Franca et al. 1995, Justice et al. 1996, Kennedy et al. 1994), the brightness temperature (T3) of AVHRR channel 3 (centered around 3.7 μm) is used first to catch all potential fire pixels. We selected the threshold for channel 3 based on the assumption that fires at the sub-pixel level will generate a temperature that approaches the channel saturation point (~320K, in this study, it is 322K). Since the middle-infrared channel is very sensitive to thermal radiation and given the low saturation point, this assumption is reasonable (Justice et al. 1996). The wavelength of Channel 3 corresponds to the peak radiation from objects with a temperature around 800K, approximately the

temperature for burning biomass (Kennedy et al. 1994). Most wildfires have a large range of temperature (500K to 1000K) with a variable fraction of burning area within a pixel (Li et al. 2000a). For potential fire identification, Li et al. (2000a) used a threshold of 315K in boreal forests and Kaufman et al. (1990) used 316K in tropical forests. We chose 315 K for California.

At the second stage, all tests are for removing false fires after the initial potential fire detection. The thresholds chosen for tests 2, 3, 5, 6, and 9 are the same or similar to the corresponding tests in the CCRS algorithm (Li et al. 2000a). The threshold of test 2 (T3-T4, brightness-temperature difference between AVHRR channels 3 and 4) is set at 14K. This test eliminates false fires caused by a warm background, such as bare soils, because this type of warm background can saturate channel 3. It is known that in the case of biomass burning, channel 3 receives much more radiant energy than channel 4 does and thus the value of T3-T4 is high (Kennedy et al. 1994, Li et al. 2000a). Test 3 (set T4 \geq 260K) is for eliminating those pixels containing high reflective clouds. Although test 1 (T3 > 315K) can filter out cloudy pixels, many bright and highly reflective cloud pixels may still pass the test. The purpose of test 5 is to focus hotspot detection on wilderness areas. Test 6 is for eliminating false fire pixels caused by thin cirrus clouds and further removing the false fires caused by warm backgrounds. Test 9 is for limiting those confirmed fire pixels not surrounded by another fire pixel within a 3×3 window. We assumed that, in most cases, single fire pixels are caused by sub-pixel contamination and other noise, such as a forest pixel containing a water body with an insufficient amount of sun glint to be eliminated in test 8.

Although we tried to adjust thresholds for various tests in the CCRS algorithm based on the California training data set, there remained many false positives. In consideration of the difference between the relatively “cold background” of the Canadian boreal forests, the relatively “warm background” of northern California, the “hot background” of southern California brush land, and the sun glint problem caused by the coastline and many inner lakes in California, we added three more tests to remove false fires.

We added tests 4, 7, and 8 to the CCRS algorithm. In addition to the $R2 < 22\%$ threshold, effects of surrounding pixels on the central pixel in AVHRR channels 2 and 3 ($R2$ and $T3$) are taken into consideration. Test 4 for $R2$ involves the following assessment: if $R2 < 22\%$, then the subtest is passed, if $R2 > 30\%$ then the subtest is failed, else if $R2$ is between 22% and 30%, and $R2 < \text{the mean of its 8 surrounding pixels} - 1.0\%$, then the subtest is passed. When $R2$ is between 22- 30%, there are two scenarios for a vegetated pixel. The first is partial burning in a pixel at the canopy or ground level. In this scenario, it is unlikely that the near infrared reflectance, $R2$ of that pixel, will drop below 22%. Nevertheless, $R2$ does reduce dramatically when compared with surrounding pixels (e.g., most normal forest vegetation has greater than 30% reflectance for $R2$).

In the second scenario, non-fire pixels may also fall into the range of 22-30%, but their $R2$ s are equal or close to those of their surrounding pixels. Therefore, the subtest is designed to retain true fire pixels and remove false positives. Test 4 for $T3$ is as follows: if $T3$ is greater than the mean of its 8 surrounding pixels + 5K, then the subtest is passed.

If a pixel is composed of varied proportions of “warm” and “cold” components (e.g., bare soil and water body), it is possible that the pixel will pass Test 2 (Li et al. 2000c). However, if the T3 value of the pixel is similar to the values of its surrounding pixels, then the pixel may be considered a false fire and removed. In the above test, if any one of the 8 surrounding pixels is a potential fire pixel, it will first be replaced by the average pixel value of the same land cover type to which this particular pixel belongs before the fire.

Test 4 can effectively remove false fires caused by highly reflecting clouds, bright surfaces and warm backgrounds. The newly added Test 7 is for further elimination of highly reflecting clouds and bright surfaces. At particular sun-earth-satellite geometric configurations, sun glint on water causes the algorithm to falsely detect fire. This problem is critical along the coastline, but is also caused by inland water logged areas such as irrigated regions, marshes, and lakes of various sizes (Malingreau and Justice 1997). Since the values of R1 and R2 are very close to each other over a sun glint pixel, sun glint pixels can be removed in the newly added Test 8.

Table 2 provides a complete comparison of all tests for the two algorithms designed by CCRS and us. As an evolution from the CCRS algorithm, our algorithm adds more steps to address the effects of surrounding pixels, sun glint, and highly reflective clouds and surfaces. Our algorithm is more computationally intensive, but this processing is necessary over the heterogeneous California landscape.

Burn scar mapping algorithm

To assess burnt areas during a fire season in California, a multi-temporal NDVI differencing technique is needed. We adopted the idea of the HANDS procedure (Fraser et al. 2000) for mapping burnt areas in California, modified and implemented in PCI EASI script. The processing chain of the modified HANDS procedure is as follows:

Step 0. AVHRR data preparation. The data preparation procedure is as described above. The burn scar mapping algorithms require three critical inputs: “before” and “after” NDVI composites, and a daily hotspot composite (a fire mask) corresponding to the same interval as the NDVI composites. The fire mask is created using the hotspot detection algorithm described above. The NDVI composites can be created based on monthly, annual, or other intervals of interest that span a period for which fires are to be mapped.

Step 1. NDVI composite normalization. To compensate for any systematic NDVI variation unrelated to fire, post-fire NDVI (NDVI_{post}) composites are normalized to the pre-fire NDVI (NDVI_{pre}) composite. This is done by calculating a ratio, Ratio_C as follows:

$$(1) \quad \text{Ratio_C} = \text{Average of NDVI}_{\text{pre}} / \text{Average of NDVI}_{\text{post}}.$$

Hotspot pixels are excluded from this calculation. NDVI_{post} is then re-scaled by Ratio_C:

$$(2) \quad \text{NDVI}_{\text{norm-post}}(i,j) = \text{Ratio_C} * \text{NDVI}_{\text{post}}(i,j)$$

NDVI variation is associated with seasonal or inter-annual variation of vegetation phenology, depending on the time interval used between NDVI composites (Kasischke and French, 1997). Fraser et al. (2000) first calculated the difference between the two averages of NDVI composites, and added the difference to the post-fire NDVI to ensure that both NDVI composites have the same average. We multiplied the NDVI value for each post-fire pixel by a ratio to effect the normalization. This multiplicative factor ensures that the rescaled values are proportionally adjusted.

Step 2. Calculate NDVI difference. The pre-fire NDVI composite was subtracted from the normalized post-fire NDVI ($\text{NDVI}_{\text{norm-post}}$) composite to obtain the NDVI difference ($\text{NDVI}_{\text{diff}}$):

$$(3) \quad \text{NDVI}_{\text{diff}}(i,j) = \text{NDVI}_{\text{norm-post}}(i,j) - \text{NDVI}_{\text{pre}}(i,j)$$

In the resulting NDVI difference image, burnt pixels are expected to have a negative value.

Step 3. Confirm hotspots using NDVI difference. A hotspot pixel having an NDVI decrease is a "Confirmed Burn Pixel (CBP)." Otherwise the hotspot pixel is considered a false fire, which may be caused by either a small fire causing insignificant vegetation change at the 1 km² scale, or other noise. In this way, all hotspot pixels with an NDVI decrease become *confirmed* burn pixels.

Step 4. Calculate NDVI_{diff} statistics. The mean and standard deviation (SD) of NDVI decreases for all CBPs are calculated for each land cover type separately. Land cover types consist of scrub and chaparral, grassland, marsh, riparian forest, woodland, rangeland, forests, and barren land. We used the GAP vegetation data to delineate these land cover types. Unlike Fraser et al. (2000) who did not separately calculate the mean and SD for each land cover type, we believe the magnitude of NDVI change varies over different land covers. We adjusted the algorithm to account for variation in NDVI differencing by ecosystem type.

Step 5. Select potential Burn Scar Pixels (BSPs). We used different mean and SDs of NDVI decreases to select potential Burn Scar Pixels (BSPs). We tested whether a pixel satisfies the condition:

$$(4) \quad \text{NDVI}_{\text{diff}}(i,j,k) < (\text{mean}_k + c * \text{SD}_k),$$

If this test is satisfied, then the pixel is selected as a *potential* BSP, where mean_k and SD_k are the mean and SD of NDVI decrease corresponding to the kth land cover type. The coefficient of c is a constant determined by analyzing actual burnt areas. The mean and SD of NDVI decrease are specific to land cover types, but the constant is applied across all land covers. We experimented with various values for c in an effort to optimize burn

area mapping with this constant.

Step 6. *Filtering the potential BSPs.* Potential burnt patches less than 2 pixels in size are discarded. This step smoothes burnt area boundaries and separates patches from the surrounding background noise resulting from the NDVI differencing (Fraser et al., 2000).

The remaining three steps are different from those by Fraser et al. (2000) for the convenience of scripting in PCI.

Step 7. *Confirm a potential BSP.* Potential BSPs are confirmed iteratively. A BSP is confirmed in one of two ways: by having a neighboring CBP, or by having one to four *previously* confirmed neighbor BSPs. In the 1st iteration, BSPs are confirmed by having one or more adjacent (neighboring) CBPs. In the 2nd iteration, a BSP can be confirmed by either a neighboring CBP *or* a confirmed BSP. In the 3rd to 5th iterations, a BSP is confirmed by having 2 to 4 *previously* confirmed BSPs as neighbors. After the 5th iteration, a BSP is confirmed by having 4 *previously* confirmed BSPs as neighbors. In this way, burn areas are “grown” outwards from CBPs.

Step 8. *Filter out confirmed burnt patches that are less than 2 pixels.* A confirmed burn patch of less than 2 pixels in size is considered to be a “false detection” and is eliminated. Therefore a 2 square kilometer fire is the minimum fire size mapped by this algorithm.

Step 9. *Output a burnt area mask.* After passing all the 8 steps as described above, a burned area map spanning the time interval of interest is output in TIFF format.

The processing chain, presented above and summarized in Table 3, is fully automated using EASI scripts. EASI is the proprietary scripting language for PCI, the image processing software we used for this project. The results from critical steps are illustrated in Figure 4 and will be analyzed in the following section. With the goal to map cumulative burnt area during a complete fire season, we evaluated two approaches utilizing different NDVI differencing intervals. The first method employs monthly NDVI differences. In this method, the fire season is divided into monthly periods each corresponding to a monthly hotspot composite. Steps 1 through 9 are repeated for each month to create monthly burn area maps. Finally, results for each month are combined to derive a burn area map for the entire fire season. Alternatively, the monthly hotspot composites can be combined to create an annual fire mask and steps 1 through 9 are run once, for an annual NDVI difference.

Table 3. Summary of the burn scar algorithm processing chain. This algorithm is a modified version of the CCRS HANDS algorithm.

Step 0	AVHRR data preparation: two NDVI composites of a selected interval, one corresponding hotspot composite (fire mask)
Step 1	Normalize NDVI _{post} to NDVI _{pre} : means of NDVIs calculated only with interested land covers $Ratio.C = \frac{\text{mean of NDVI}_{pre}}{\text{mean of NDVI}_{post}}$ normalized NDVI _{post} = Ratio.C * NDVI _{post} , not hotspot pixels used for calculation of NDVI mean.
Step 2	Calculate NDVI difference: normalized NDVI _{post} – NDVI _{pre} , burn scar expected to have A negative value in the NDVI difference image.
Step 3	Confirm hotspot pixels (CBP) using NDVI difference: a CBP is assumed to have a negative NDVI difference, otherwise the hotspot pixel is considered as a false fire.
Step 4	Calculate NDVI difference statistics (mean, standard deviation, SD) of NDVI decrease for all CBPs for each land cover type, different land covers expected to have a different mean and SD.
Step 5	Select potential burn scar pixels (BSPs): NDVI difference of a potential BSP < (mean + c*SD), the potential BSPs selected for different land cover types with the mean and SD from Step 4.
Step 6	Apply a sieve filter to the selected BSPs: filter out a burnt patch of < 2 pixels, a burn patch less than 2 pixels is considered to be caused by noise.
Step 7	Confirm a BSP with a neighbor CBP and later on up to four neighbor confirmed BSPs to create connected burn patches, 1st iteration with a neighbor CBP, 2nd iteration with a neighbor CBP or a conformed BSP (CBSP), 3rd to 5th iteration with 2 to 4 CBSPs, after 5th iteration using 4 CBSPs only.
Step 8	Filter out a BSP patch of < 2 pixels: the patche of < 2 CBSPs is considered to be a false burnt patch, caused by noise.
Step 9	Output a burnt area mask (in TIFF format).

For 1996 and 1999, we performed burn scar mapping using three different values of *c* (step 5 of burn scar mapping algorithm) for each of the two NDVI differencing methods. This resulted in 6 separate burn scar maps for each of the two years. We exported these maps from PCI image files to TIFF files for analysis and evaluation using GIS software. Table 4 shows the channel of the PCI file from which the data originated, the value of *c* used, the NDVI differencing technique and the resultant filename and acreage. ‘Channel,’ in this context, refers to the PCI image file channel used for map production, rather than the AVHRR channel.

Table 4. Summary of parameters used in the production of burn scar maps.

Year	Channel	Filename	NDVI	c	Total Acreage
1999	1	99ch1*.*	annual	0.4	659,485
1999	2	99ch2*.*	annual	0.55	858,269
1999	3	99ch3*.*	annual	0.45	760,261
1999	4	99ch4*.*	monthly	0.05	685,745
1999	5	99ch5*.*	monthly	0.15	731,921
1999	6	99ch6*.*	monthly	0.25	900,074
1996	1	99ch1*.*	annual	0.25	524,930
1996	2	99ch2*.*	annual	0.255	750,614
1996	3	99ch3*.*	annual	0.23	526,244
1996	4	99ch4*.*	monthly	0.25	825,622
1996	5	99ch5*.*	monthly	0.1	563,005
1996	6	99ch6*.*	monthly	0.05	424,659

Comparison to Fire Activity Data

Only a small number of fire detection algorithms have been rigorously validated. In most cases, due to the lack of ground truth data in most regions, only cursory validations were conducted by comparing against fire smoke plumes (Li and Giglio 1999). For hotspots, we conducted extensive human inspection of satellite composite images. Due to the sensitivity of fire smoke plume reflection in channels 1 and 2, it is possible to use the composite image to visually confirm fires by the presence of smoke. Comparing hotspots detected by our method with corresponding satellite imagery, we found that most hotspots had accompanying smoke plumes. More quantitative approaches have also been employed. Some research simply reports percent of burn scars detected in the study area (Bourgeau-Chavez et al. 1997). Fraser et al. (2000) report percent of burn scars detected as well as area correlations between ground truth data and the results of the HANDS algorithm. Other authors have devised elaborate schemes of accuracy quantification (Rommel and Perera, 2001) by describing “accuracy response variables.” Both Fraser et al. (2000) and Rommel and Perera (2001) rasterized ground truth data before comparison to the remotely sensed burn scars.

CAMFER has employed a variety of validation approaches in order to describe the difference between CDF reported fires and AVHRR burn scar mapping. However, a completely comprehensive layer of burn areas in California does not exist. This paucity of reliable and spatially referenced data about fires complicates the validation of the CAMFER burn scar maps. The CDF layer is beset by problems already described. However, the CDF data is the only statewide polygon coverage available and is useful for purposes of spatial comparison to the CAMFER burn scar maps. As such, the analysis is more of a “confirmation” than a true “validation.”

The first stage of comparison between datasets involves transformation of the data to equivalent projections and/or formats. The AVHRR data is imported (by the PCI Geocomp software package) to the Lambert Conformal Conic (LCC) projection, and the CDF data is in the Teale Albers projection. Since the LCC projection does not preserve area (Snyder 1987), there is some distortion that occurs in the re-projection of the AVHRR fire map to Albers. We noted a decrease in the area of fire polygons (approximately 11%) when converting from LCC to Albers. The LCC projection parameters built into the PCI software use standard parallels of 49 and 77 degrees north latitude. These parameters are appropriate for Canadian mapping purposes, but may contribute to distortion of the data when used for creating maps in California and the continental United States.

In transforming the data for validation purposes, we attempted to minimize distortion of the data that results from changing format and projection. In order to facilitate geographic analysis, we converted the TIFF images exported by PCI to grids using Arc/INFO. In this step, pixels were converted directly to grid cells with no re-sampling or re-distribution of the raster data. We used a region grouping command to group the cells into “fires” by assigning continuous groups of cells the same id number. We then

converted the grids to polygons, with each grouping of cells becoming a polygon. Diagonal neighbors were not grouped and received unique polygon identification numbers. The final step was the re-projection and “building” of the polygons, using Arc/INFO. We scripted all these steps in Avenue. The script Startr.ave links scripts assignr.ave and convertr.ave to create a fully-automated process.

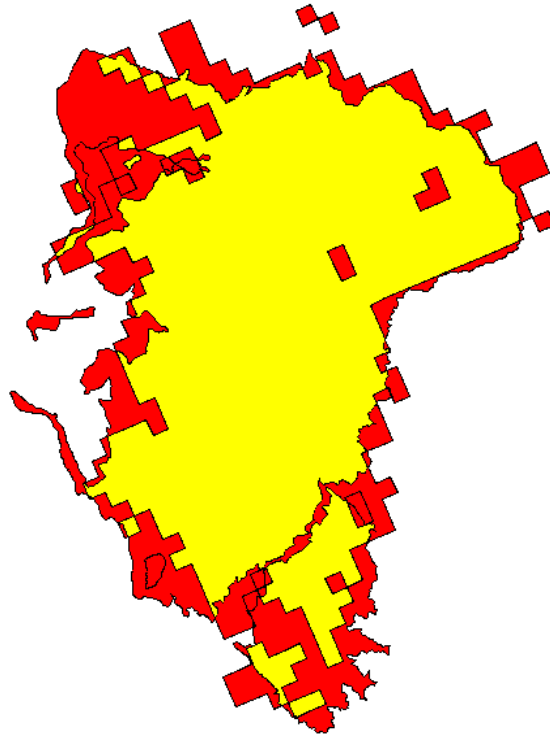


Figure 3. Geometric intersection of CDF and CAMFER polygons. An exact determination of overlapping area is possible with this method. Yellow represents the area of intersection between the datasets. Artifacts of the raster data structure are evident.

There are a variety of ways to compare the AVHRR mapped fires with the CDF fire database. Each method represents a different level of stringency in the evaluation of whether a fire is “matching” or not. The most stringent method is a geographic union of shapes. This approach is illustrated by Figure 3, which shows the intersecting area of the RS and CDF delineations of a large fire. The residual raster data structure is evident in the RS polygons, but these polygons are “split” by the boundary of the CDF fire perimeter. The resultant shapes represent exact overlap between the CDF designated burn area and the AVHRR fire detection.

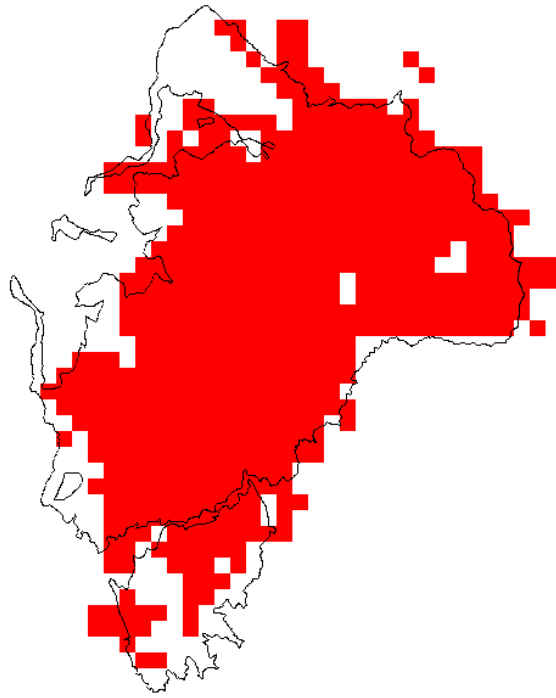


Figure 4. Polygon on grid overlay. The area of all cells more than half inside the polygon is counted, but cells outside the polygon are not. The different orientation is due to the LCC projection.

A slightly less stringent method, but possibly more relevant from a fire mapping perspective, is the polygon on grid overlay. This approach is illustrated by Figure 4. With this method, cells are not “split” by CDF polygon boundaries. Instead, cells in the grid with over half their area inside a CDF polygon are considered part of the set of overlay cells. For this reason, the exact overlay area is not computed, but the area of all cells “overlaid” by CDF mapped fires is added together as the area detected using the RS approach. This analysis was complicated by the fact that one or the other of the data sets had to be re-projected in order to perform this analysis. In order to avoid a re-sampling of the fire detection grid, we re-projected the CDF data to LCC and performed the analysis in the LCC projection. This results in a slight distortion of true area.

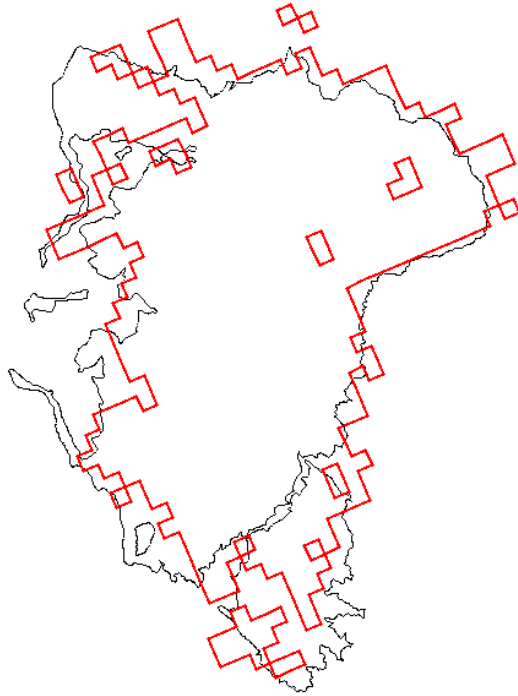


Figure 5. Polygon overlay. The vector based approach, performed in Albers, counts the entire area of intersection polygons, regardless of whether it is outside or inside the CDF polygon. The least restrictive of the comparison techniques.

The third method is a simple polygon overlay. This approach, the least restrictive in terms of horizontal overlap, is displayed in Figure 5. For this reason, positional errors in both datasets are minimized in terms of their contribution to validation results. The area of all CAMFER fire polygons that intersect CDF polygons is added as the “matched” area. Similarly, all CDF polygons that intersect CAMFER polygons are considered as “detected” fires. In this way, there is no minimum amount that polygons must intersect to be considered as matching. Figure 5 illustrates how two CDF fires may be intersected by one CAMFER fire and one CDF fire may be intersected by more than one CAMFER fire. These types of many to many or many to one correspondences complicate the construction of area correlations such as reported by Fraser et al. (2000).

An Avenue script (statmakr.ave) executes the polygon-grid overlay technique. The analysis performed in the LCC projection. The script tabulates the number of cells designated as “burned” in each CDF fire polygon and writes the information to a table. The process is repeated for each grid analyzed. We performed the geometric intersection method by manually entering commands to Arc/INFO for workstations. Using the “union” command, we created a polygon coverage in which intersecting areas and non-intersecting areas from both coverages are represented by polygons. Unique combinations of attributes identify the polygons as belonging to the CDF layer, the CAMFER layer, or both. We used the centroidmod.ave script to assign information about ecoregion and cover type to the polygons. The results from the intersection and the polygon-grid overlay are only reported on a limited basis. They are used in the

comparison of burn area confirmation techniques and in the more detailed analysis of selected burn scar maps.

We used a sequence of Avenue scripts to perform polygon overlay analysis on all the burn scar maps and aggregate the information to a single table. A single script (rslinr.ave) calls sub-procedures (centroidmod.ave, analyzer2.ave, combinertables2.ave) to allocate the polygons by ecoregion and land cover type, determine which polygons are in contact with each other, total the areas and build a table of the results. These tables are the primary source of the data used in the comparison between CAMFER and CDF fire maps. We also used the information in these tables to identify which burn scar maps were most accurate, to assess algorithm and threshold performance over different geographic and ecological areas, and to select burn scar maps for more detailed analysis. The information computed by the tables includes the area of CDF polygons that are overlaid by CAMFER polygons, and the area of CAMFER polygons that do *not* overlay any CDF fire polygons (presumed false detections). We used the ratio of these two data to determine the burn scar map on which to focus additional investigation. Since the 1999 channel 1 map had the highest ratio of CDF fires detected to CAMFER fires unmatched, we selected this map for further analysis. For comparison to a monthly NDVI differencing, we also discuss channel 4. The results are reported below.

Post-Processing

In order to temporally allocate the mapped burn area, we used the detected hotspots as a temporal reference. Hotspots used as input to the burn scar mapping algorithms were in the format of monthly images with the day of the month as cell value. We exported these to TIFFs, then used Avenue scripts (gridmakr**.ave, combinr.ave) to create grids with the cell value of the hotspots as the date. We used these grids to produce Euclidean Allocation grids of daily hotspot value. Euclidean Allocation is the raster based equivalent of the creation of Thiessen polygons around point features. This can be used as an interpolation technique, where areas of unknown value (in this case date of burn) are assigned the value from the closest area of *known* value. The assignr.ave script, also used to group regions of cells into polygons, uses the allocation grids to decompose the polygons temporally. The Euclidean Allocation grid is used to divide the polygon (fire) such that each area of the polygon receives a daily value based on the closest hotspot (a nearest neighborhood operation). The daily burn areas are closer to the hotspot of that daily value than any other hotspot. Through a spatial join, the daily polygons retain their unique identifier so that each polygon has a unique fire ID as well as a date field. The purpose of this exercise was to demonstrate that remotely sensed data could be used to produce polygon files with the required input information for the EES. No further analysis was performed on these shapefiles, but we used the date attributes to verify that CDF fires only partly overlapped by CAMFER fires had approximately the same date.

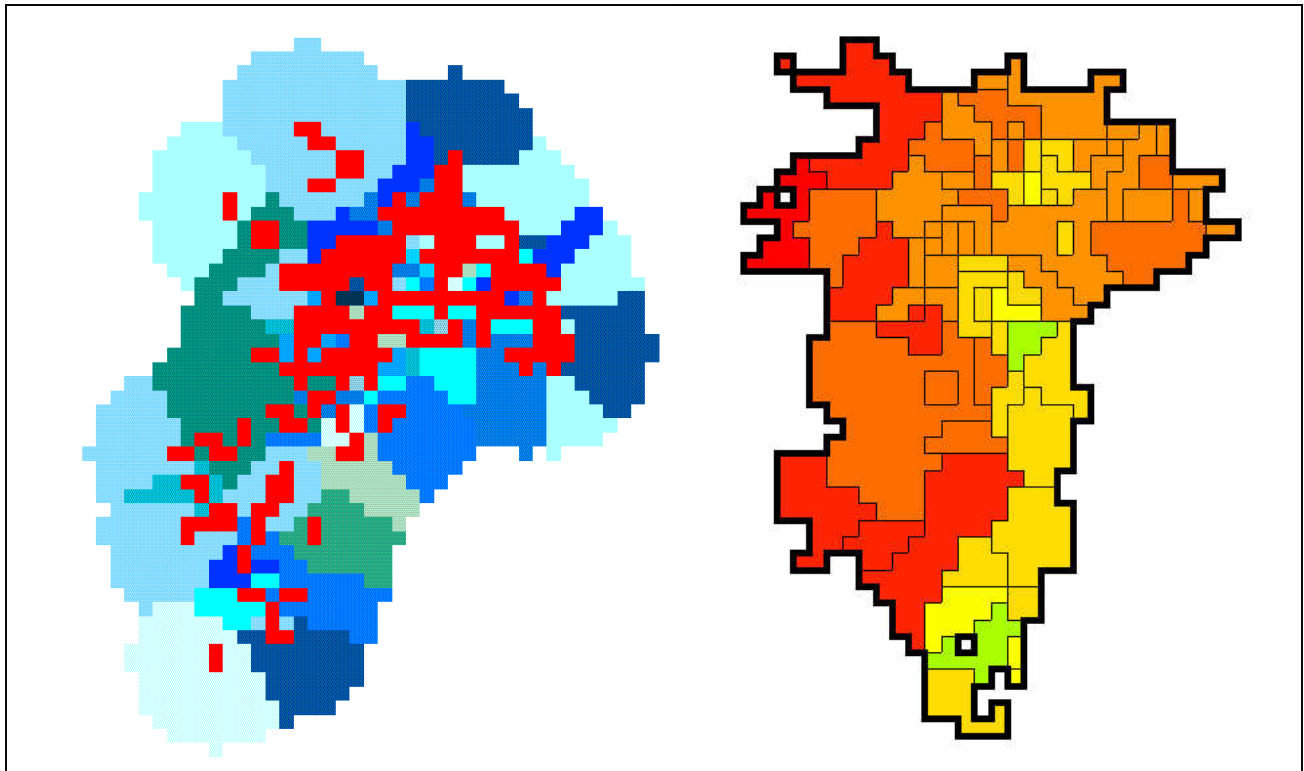


Figure 6(a), left, shows hotspots overlaid on a background Euclidean allocation grid created from the hotspots. Figure 6(b), right, shows the resultant temporal decomposition of burn area based on the date the hotspots

Results and Analysis

Hotspot detection

We applied the hotspot detection algorithm to AVHRR data for 6 months in 1999 and 4 months in 1996. This produced hotspot maps for the entire State of California at monthly intervals. Northern California hotspots are displayed in Figure 7. Following the monthly aggregation process and the assignment of the date as the cell value, we were able to “grow” the hotspots using a Euclidean allocation. This creates the grid of date values that we used in the temporal apportionment of burn area. Figure 6(a) shows an area of hotspots (corresponding to a large fire in Northern California) overlaid on the resultant Euclidean allocation grid. A simple grid multiplication of this grid and the burn scar maps enabled the estimation of when each part of the mapped burn area actually burned. A map of the temporally decomposed burn scar corresponding to the above hotspot images is shown in Figure 6(b).

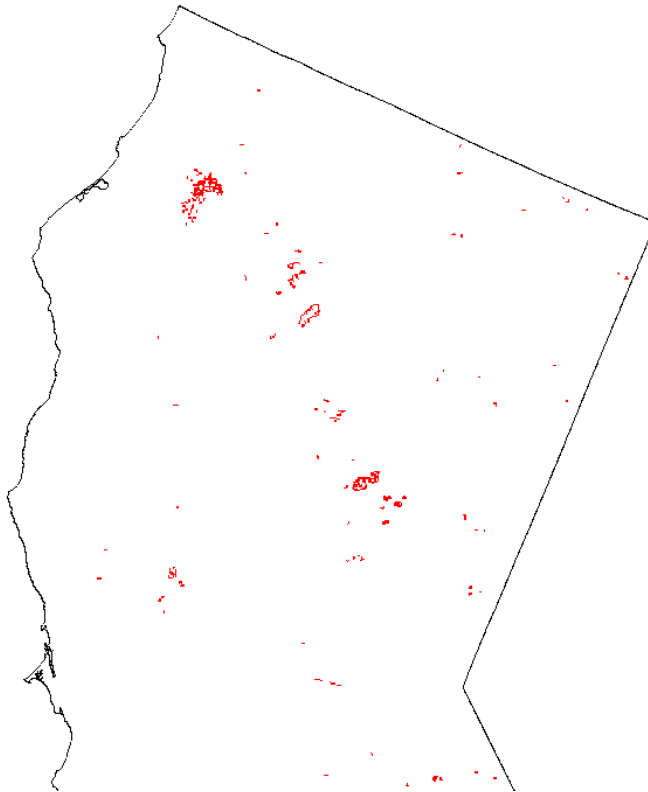


Figure 7. 1999 hotspots for Northern California. The large cluster on the upper left corresponds to the images in Figure 6.

Burnt area mapping

Figure 8(a-f) shows a progression of images illustrating the steps of burn scar mapping for September, 1999. Figure 8(a) shows part of the image of NDVI difference between the normalized post-fire and the pre-fire NDVI composites. On this image, burn scars are assumed to have an NDVI decrease. At the upper left of the image, a light patch caused by a plume of burning smoke appears almost every day during September 1-10. A dark gray area at the central bottom of the image is agricultural land, caused by low NDVI composite values, which is excluded from the wildfire map. Figure 8(b) is a confirmed burn pixel (CBP) map on which the CBPs were determined with the assumption that a real burning pixel has to be accompanied by an NDVI decrease. Most of the CBPs at the upper left of the image are located at the front part of smoke plumes shown in Figure 8(a) (upper left). There are a number of potential burn scar pixels (BSPs) in Figure 8(c). Among them only a small portion are due to fires. The solar-elevation change and phenological change in vegetation between early September and early October may be responsible to the large number of false positives. Figure 8(d) shows the effectiveness of filtering to remove burn patches smaller than three pixels. Figure 8(e) illustrates the usefulness of the confirmation approach utilizing confirmed neighbor BSPs and/or a neighbor CBP. After this confirmation, the number of burned scars is considerably reduced. Figure 8(f) also illustrates the effects of filtering.

Figure 8(a)

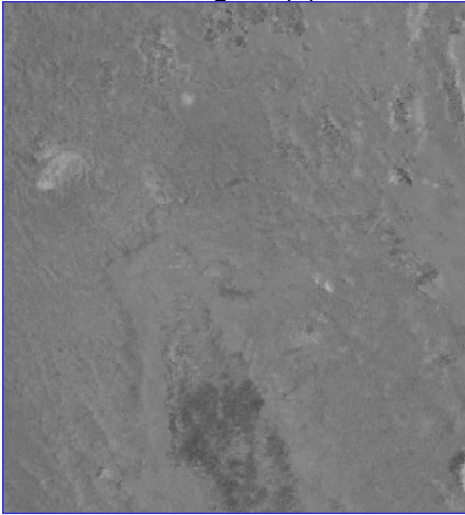


Figure 8(b)

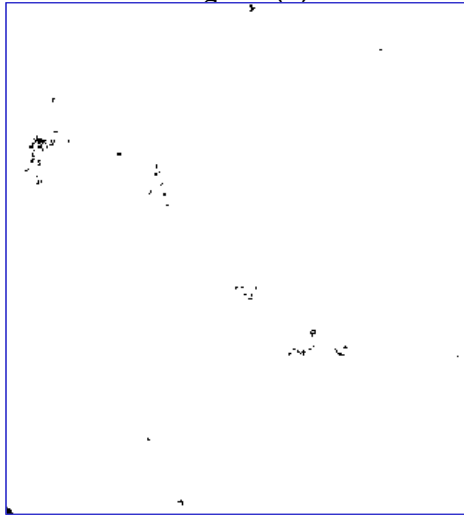


Figure 8(c)



Figure 8(d)

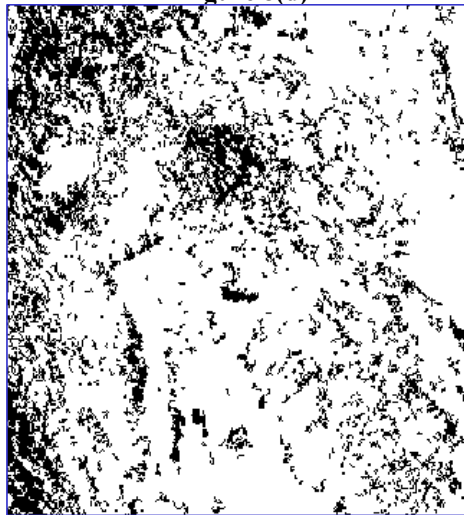


Figure 8(d)

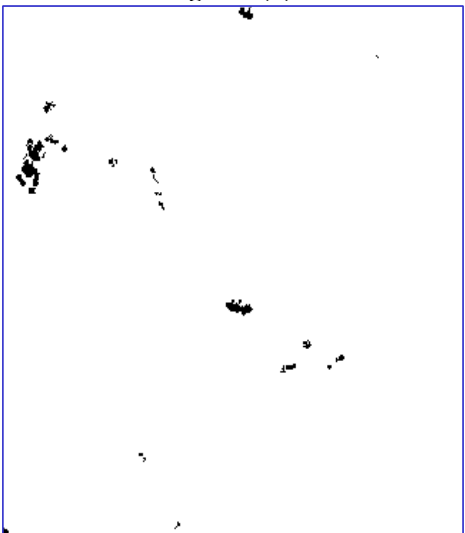


Figure 8(e)

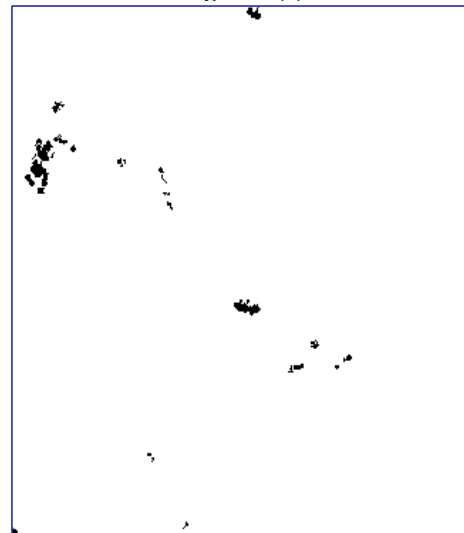


Figure 8(a)-8(e). Selected images from the steps of burn scar mapping.

The final product is displayed in grid format, LCC projection, for Northern California in Figure 9. This image displays a 1999 burn scar, produced using the hotspots shown in Figure 7 as input, and the parameters shown in Table 4 for channel 12 of the image file (Hereafter channel 1 map. We will name maps according to the PCI image channel from which they were created. See Table 4 for details.) As indicated in Table 4, we produced a range of burn scar maps using different parameters. Figure 10(a) displays 1999 channel 1 and figure 10(b) shows the channel 4 map of the same area. This figure illustrates the differences that result from using monthly (channel 4) versus annual (channel 1) differencing. Clearly, the two techniques have different outcomes in terms of the burn scar map.

These differences are quantified in Tables 5 and 6. These tables display mapping data by cover type, ecoregion and correspondence to fire polygons in the CDF data (using the polygon overlay analysis). For example, the channel 4 map has approximately 70,000 acres more mapped burn scars in the scrub type than channel 1. Channel 1 has approximately 66,000 acres more in the woodland type than channel 4. These discrepancies may be due to the different NDVI differencing techniques.

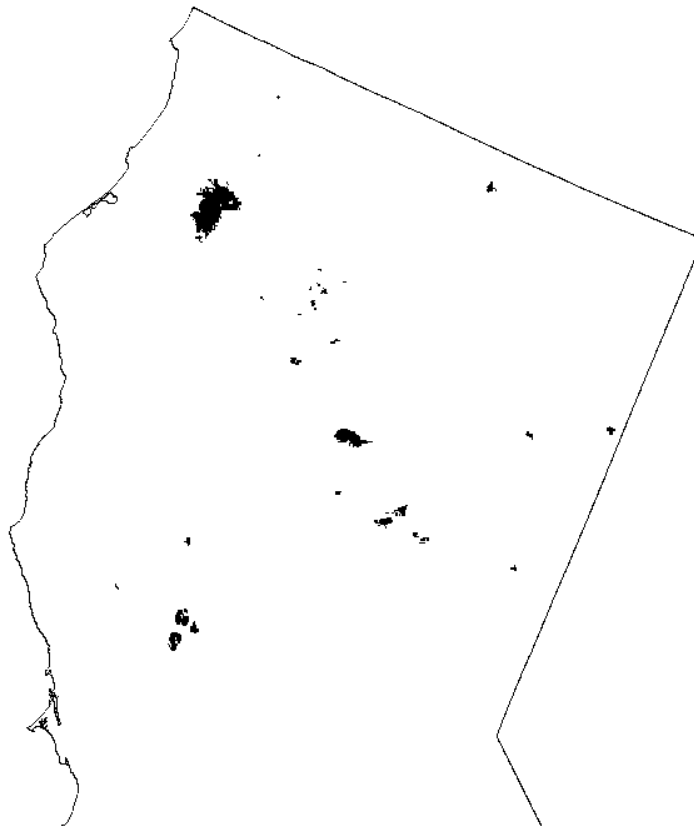


Figure 9. Burn scar map for northern California using 1999 channel 1 data. This map was produced using the hotspots in figure 6 as input.

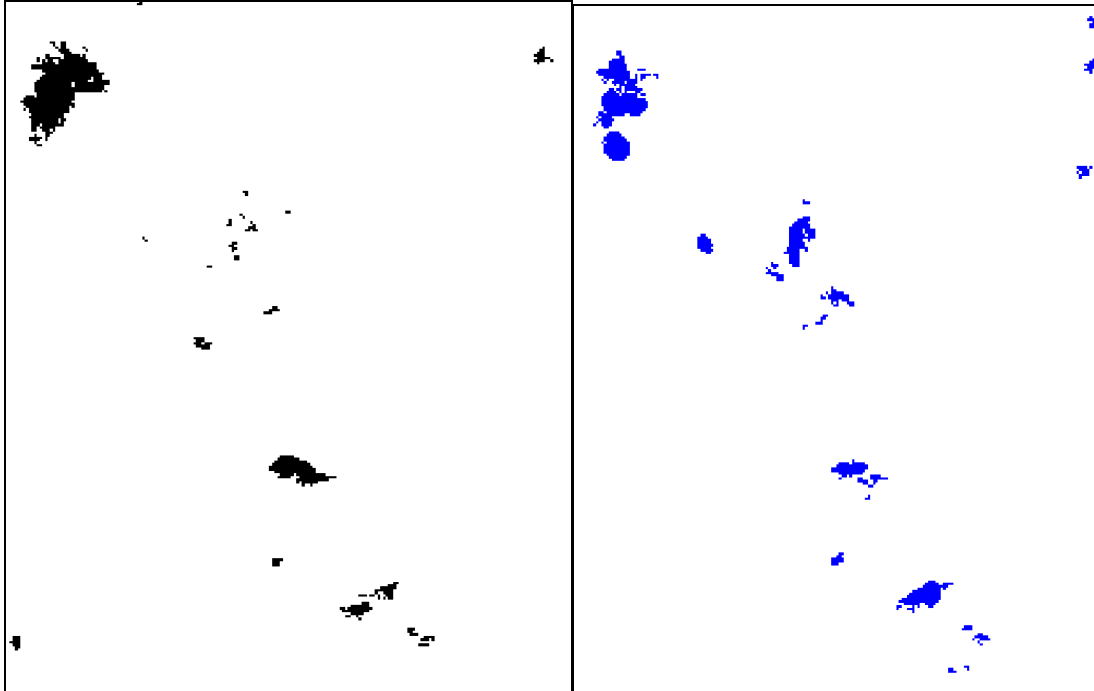


Figure 10(a), left, and 10(b), right. The same area is shown using annual NDVI differencing (a) and monthly NDVI differencing(b). The same fires are mapped differently depending on the NDVI differencing technique.

Table 5. Summary of CAMFER 1999 burn scar maps by cover type. Generated with polygon overlays.

Channel	NDVI	c	Open Dunes Land	Scrub	Grassland	Wetland	Riparian	Woodland	Forest	Total - All Categories
CAMFER Total Acreage of Mapped Fires										
6	monthly	0.25	218	0 482,872	34,058	3,702	619	125,996	252,609	900,074
5	monthly	0.15	218	0 336,461	33,372	3,471	0	121,227	237,172	731,921
4	monthly	0.05	218	0 340,410	31,818	3,471	0	85,603	224,225	685,745
2	annual	0.55	3,198	0 415,896	52,688	0	3,321	188,227	194,939	858,269
3	annual	0.45	3,238	0 326,901	51,228	0	3,113	193,592	182,189	760,261
1	annual	0.4	2,814	0 271,452	52,261	0	3,113	149,678	180,167	659,485
CAMFER Acreage of Fires that Overlap CDF Fires										
6	monthly	0.25	0	0 181,884	5,529	0	0	95,195	245,740	528,348
5	monthly	0.15	0	0 165,370	4,846	0	0	92,246	230,508	492,970
4	monthly	0.05	0	0 170,408	3,073	0	0	59,922	217,290	450,693
2	annual	0.55	0	0 280,501	25,275	0	0	123,482	189,012	618,270
3	annual	0.45	662	0 240,801	25,275	0	0	136,800	172,307	575,845
1	annual	0.4	662	0 212,436	22,403	0	0	114,543	172,221	522,265
CAMFER Acreage of Fires that Do NOT Overlap CDF Fires										
6	monthly	0.25	218	0 300,988	28,529	3,702	619	30,801	6,869	371,726
5	monthly	0.15	218	0 171,091	28,526	3,471	0	28,981	6,664	238,951
4	monthly	0.05	218	0 170,002	28,745	3,471	0	25,681	6,935	235,052
2	annual	0.55	3,198	0 135,395	27,413	0	3,321	64,745	5,927	239,999
3	annual	0.45	2,576	0 86,100	25,953	0	3,113	56,792	9,882	184,416
1	annual	0.4	2,152	0 59,016	29,858	0	3,113	35,135	7,946	137,220

Table 6. Summary of CAMFER 1999 burn scar maps by ecoregion. Generated with polygon overlays.

Channel	NDVI	c	Modoc Plateau	Northwest Coast	Cascade Range	Sierra Nevadas	East of Sierras	Central Valley	Central Coast	Mojave Desert	Southwest Coast	Sonoran Desert
CAMFER Total Acreage of Mapped Fires												
6	monthly	0.25	15,417	192,182	56,193	104,510	44,919	29,202	135,744	145,590	125,582	50,735
5	monthly	0.15	12,660	180,985	52,332	98,241	35,182	29,202	127,144	42,240	114,450	39,485
4	monthly	0.05	11,738	163,878	43,920	88,164	35,182	27,884	120,461	42,240	112,793	39,485
2	annual	0.55	12,874	202,627	44,043	52,847	9,524	16,408	291,516	89,434	117,232	21,764
3	annual	0.45	10,804	193,949	43,588	45,070	7,090	15,544	273,259	55,769	109,593	5,595
1	annual	0.4	9,649	183,835	40,406	36,950	3,547	14,887	240,339	30,606	94,083	5,183
CAMFER Acreage of Fires that Overlap CDF Fires												
6	monthly	0.25	5,544	189,905	55,278	90,151	5,306	3,735	110,566	0	67,863	0
5	monthly	0.15	4,620	179,167	51,417	84,976	5,085	3,735	103,037	0	60,933	0
4	monthly	0.05	3,927	162,509	42,777	75,978	5,085	2,417	98,310	0	59,690	0
2	annual	0.45	5,775	192,276	44,043	43,700	0	0	232,475	13,888	86,113	0
3	annual	0.55	4,851	185,403	43,588	36,127	0	0	216,375	13,046	76,455	0
1	annual	0.4	4,620	177,078	40,406	33,670	0	0	187,688	12,835	65,968	0
CAMFER Acreage of Fires that Do NOT Overlap CDF Fires												
6	monthly	0.25	9,873	2,277	915	14,359	39,613	25,467	25,178	145,590	57,719	50,735
5	monthly	0.15	8,040	1,818	915	13,265	30,097	25,467	24,107	42,240	53,517	39,485
4	monthly	0.05	7,811	1,369	1,143	12,186	30,097	25,467	22,151	42,240	53,103	39,485
2	annual	0.45	7,099	10,351	0	9,147	9,524	16,408	59,041	75,546	31,119	21,764
3	annual	0.55	5,953	8,546	0	8,943	7,090	15,544	56,884	42,723	33,138	5,595
1	annual	0.4	5,029	6,757	0	3,280	3,547	14,887	52,651	17,771	28,115	5,183

Tables 5 and 6 also show the effects of altering the coefficients of the NDVI thresholds on the resultant burn acreage mapped. Table 5 shows that mapping of shrub fires with the annual technique is very sensitive to the coefficient. The difference between coefficients is more manifest in the unmatched acreage than in the matched acreage. The effect of changing the coefficient is not nearly as evident in the grassland type. With a monthly differencing, the burn scar mapping is sensitive to the threshold in the forest type, slightly more so than the annual technique.

Figure 11. Burnscars generated with monthly (blue) and annual (green) NDVI differencing, overlaid on hotspots (red), and the corresponding CDF fire polygon (black).

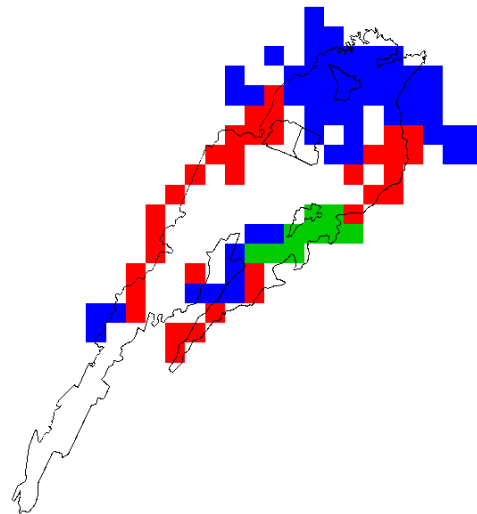


Figure 11 displays the channel 1 map, channel 4 map, hotspots, and the CDF data for a fire in Northern California. The data is arranged so that channel 1 is on top of channel 4, which is over the hotspots, the upper layers hiding the lower layers. This figure illustrates that monthly NDVI differencing captures some burn area not detected by the annual differencing. Similarly, the hotspots very neatly capture

the burn boundary but have not become part of either burn scar map. This image reveals the temporal sensitivity of the technique to “re-greening” or the re-vegetation of the burn area. The hotspots have not become part of the burn scar maps due to the fact that NDVI *increased* over those hotspot pixels. Whether this is due to natural or anthropogenic re-vegetation is unknown, but poses a limitation to the method in general. If the NDVI interval is not short enough to capture the burn scar before it re-vegetates, it will not be mapped (burn scar step #3).

Table 7. Mapping success of channels 1 and 4 by cover type. This data was generated using the polygon overlay analysis. Page 20 describes the various data categories and the method used to determine “matching” and “detection.” Only channels 1 and 4 for 1999 are reported here.

Channel 1 DATA	Land Cover Type								Total
	Open Land	Dunes	Scrub	Grassland	Wetland	Riparian	Woodland	Forest	
CDF # of fires	20	0	80	37	0	1	68	114	320
CDF acres of fires	5,795	0	235,361	24,585	0	55	213,079	301,831	780,706
CAMFER # of fires	6	0	51	21	0	5	42	41	166
CAMFER acres of fires	2,814	0	271,452	52,261	0	3,113	149,678	180,167	659,485
CAMFER # matched fires	1	0	10	5	0	0	19	32	67
CAMFER acres matched	662	0	212,436	22,403	0	0	114,543	172,221	522,265
CAMFER # unmatched fires	5	0	41	16	0	5	23	9	99
CAMFER acres unmatched	2,152	0	59,016	29,858	0	3,113	35,135	7,946	137,220
CDF # detected fires	0	0	14	4	0	0	15	23	56
CDF acres detected	0	0	159,622	5,028	0	0	158,722	255,078	578,450
CDF # undetected fires	20	0	66	33	0	1	53	91	264
CDF acres undetected	5,795	0	75,739	19,557	0	55	54,357	46,753	202,256
Channel 4 DATA									
CDF # of fires	20	0	80	37	0	1	68	114	320
CDF acres of fires	5,795	0	235,361	24,585	0	55	213,079	301,831	780,706
CAMFER # of fires	1	0	96	16	1	0	29	47	190
CAMFER acres of fires	218	0	340,410	31,818	3,471	0	85,603	224,225	685,745
CAMFER # matched fires	0	0	17	3	0	0	13	39	72
CAMFER acres matched	0	0	170,408	3,073	0	0	59,922	217,290	450,693
CAMFER # unmatched fires	1	0	79	13	1	0	16	8	118
CAMFER acres unmatched	218	0	170,002	28,745	3,471	0	25,681	6,935	235,052
CDF # detected fires	0	0	13	4	0	0	15	30	62
CDF acres detected	0	0	92,766	2,488	0	0	158,420	271,685	525,359
CDF # undetected fires	20	0	67	33	0	1	53	84	258
CDF acres undetected	5,795	0	142,595	22,097	0	55	54,659	30,146	255,347

The converse is also true. Due to the single NOAA overpass per day, quickly burning fires such as grass and shrub fires may not be detected as hotspots if the fire burns between overpasses. While the burn scar algorithms may detect an NDVI decrease, if there is no hotspot within or adjacent to the burn area, it will be discarded as a false positive (burn scar step #7). Table 7 illustrates this limitation. This table shows the results of the polygon overlay analysis for channel 1 and channel 4. The data indicate a large number of undetected CDF fires for both methods. Using the grid-polygon overlay technique, we evaluated the frequency of hotspots in fires. The data show that of 320 CDF mapped fires in 1999, 251 fires do not have any hotspots mapped within them. However, the burn scar algorithm provides for adjacency of hotspots as well by mapping burn scar pixels that have CBPs or BSPs next to them. Of the 251 CDF fires with no hotspots mapped inside them, only 7 of these fires had burn scars mapped within them by

the channel 1 map. These data indicate that the hotspot detection algorithm is a limiting factor for this method.

Table 8. Comparison of the three accuracy assessment methods. Figures 2-4 illustrate the techniques. Data is the acreage of CAMFER fires that correspond to fires in the CDF database.

Land Cover Type	Intersection	Grid Overlay - LCC	Polygon Overlay
Forest	177,349	199,981	172,221
Grassland	3,189	3,524	22,403
Open land	7	0	662
Riparian	0	0	0
Scrub	89,375	134,047	212,436
Wetland	0	0	0
Woodland	82,739	63,974	114,543
California Total	352,659	401,525	522,265
Jepson Ecoregion			
Cascade Ranges	38,236	41,706	40,406
Central Coast	103,157	118,578	187,688
East of Sierra Nevadas	0	0	0
Central Valley	1,242	1,401	0
Modoc Plateau	3,543	3,791	4,620
Mojave Desert	10,217	0	12,835
Northwest Coast	135,365	146,493	177,078
Sierra Nevadas	27,880	30,658	33,670
Sonoran Desert	0	0	0
Southwest Coast	33,019	58,899	65,968
California Total	352,659	401,525	522,265

Accuracy Assessment

Table 8 compares the three validation methods for a 1999 burn scar map using annual NDVI differencing and 0.4 as the c value (1999 channel 1). Different techniques allocate fires to different land cover types and ecoregions based on the rules of allocation. For the intersection method, “fires” are split into many polygons, each polygon being allocated based on its centroid. The grid overlay method relies on the CDF polygon centroid for allocation and the polygon overlay method relies on the CAMFER polygon centroid for allocation of CAMFER matched fires (CDF polygons are used for CDF detected fires). These allocation rules result in the slight discrepancies between cover types apparent in Table 8. However, the grand totals display general trends that result from the use of different techniques. CDF total acreage is 780,700. Therefore, “perfect” agreement (with CDF data) would be represented in Table 8 as 780,700 acres in the California total. As shown in Table 8, CAMFER agreement with CDF data varies by assessment technique between 45% and 67%.

Figure 12 illustrates how centroid based land cover and ecoregion assignments are sensitive to small variations in georeferencing. Fires on the boundary between zones may be mapped differently depending on the processing that has been performed for the accuracy assessment. For example, the reprojection of maps to Albers causes slight changes in positioning that can result in fires being allocated to a different category than in the LCC projection. The mapping of fires in the ‘open land’ category is evidence of

this effect. Any burn scar pixels in ‘open land,’ ‘riparian,’ or ‘wetland’ categories are systematically removed by the burn scar mapping algorithms. Table 8 shows how changing projection (compare the grid overlay data generated in the LCC projection to the polygon overlay data generated in the Albers projection) can effect a slight change in the position of fires relative to other geographic boundaries. The intersection method, by virtue of ‘splitting’ fire polygons (into intersected and non-intersected area), may map different parts of boundary fires, shown by Figure 12, into different categories.

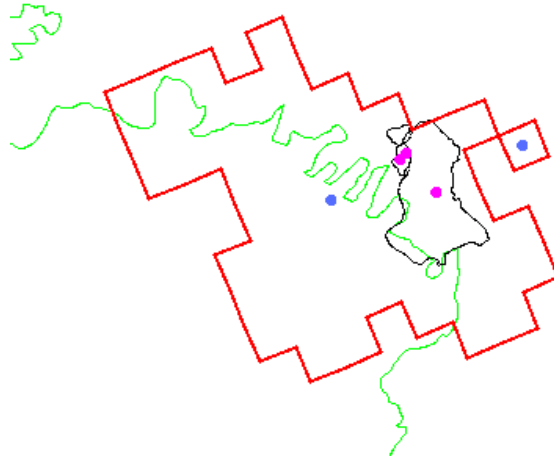


Figure 12. Centroid based allocation of fires. An ecoregion boundary is shown in green, CAMFER fire in red, CDF fire in black. Centroids appear as dots. Small changes in positioning can result in variations in cover or region assignments.

Table 9 displays intersection data for 3 categories based on the 1999 channel 1 map: areas where CAMFER polygons and CDF polygon intersect, areas of CAMFER polygons that do not overlap CDF data, and areas of CDF polygons that do not overlap CAMFER data. An ideal burn scar map (assuming, of course, that the CDF data is “true” and complete in terms of representing California burned acreage) would show 780,700 acres in the intersecting area column, and “0” acres of non-intersecting area. The data show that 45% of the area of CDF fires was intersected by CAMFER mapped burn scars. This statistic can be deceptive, however, since the full extent of mapped burn scars is not taken into account, only the intersection with CDF data. Positional error in one or both of the fire maps can skew estimates of accuracy through offset of the true location of the fire. The magnitude of the geometric intersection of fires is thus dependent on the position of the mapped perimeter. The differences in evaluation technique are displayed in table 8 (above). Tables 8 and 9 also indicate differences in success rates between both land cover types and ecoregions.

Table 9. Results of the geometric intersection. This method is illustrated by figure 2.

Land Cover Type	CDF and CAMFER intersecting area	CAMFER Only non-intersecting area	CDF Only non-intersecting area
Forest	177,349	43,006	123,753
Grassland	3,189	46,435	22,139
Open land	7	3,313	5,810
Riparian	0	3,114	55
Scrub	89,375	148,034	83,868
Wetland	0	1,175	0
Woodland	82,739	64,228	192,497
California Total	352,659	309,304	428,123
Jepson Ecoregion			
Cascade Ranges	38,236	2,250	120,784
Central Coast	103,157	135,905	20,463
East of Sierra Nevadas	0	3,547	4,055
Central Valley	1,242	15,354	12,170
Modoc Plateau	3,543	6,111	32,785
Mojave Desert	10,217	20,091	34,632
Northwest Coast	135,365	50,318	75,101
Sierra Nevadas	27,880	9,085	79,095
Sonoran Desert	0	5,184	5,150
Southwest Coast	33,019	61,461	43,888
California Total	352,659	309,304	428,123

These ecosystematic and regional trends are also evident in the polygon overlay analysis. The data for 1999 channels 1 and 4 by land cover is displayed in table 7. In terms of these data, the monthly and annual NDVI differencing methods are difficult to differentiate. There are similarities between mapped acreages despite very different thresholds (*c* values). However, certain discrepancies are notable. For example, for mapping of fires in the shrub type, channel 4 shows a large overestimate of burn area since the CAMFER matched acreage is 170,408 and the CDF detected acreage is only 92,766. While channel 1 also overestimates, the magnitude is much less, with 212,436 acres of CAMFER matched fires and 159,622 acres of CDF detected fires. The opposite is true for grassland, with channel 1 having a much larger overestimation. For forest and woodland types, both methods result in an underestimation of burned acreage. The data indicate a variation in mapping success between covertypes.

There are also differences by Jepson ecoregion of California. These data for the same two channels are displayed in table 10. This table shows distinct differences in mapping success by region of California. For example, both channels show unmatched fires in the Sonoran desert area, though channel 4 has a far larger amount. Channel 1 shows better success in Southern California (a large amount of chaparral dominated ecosystems) with a slight underestimate of burn area (CAMFER acres matched compared to CDF acres detected). Channel 4 shows a large overestimate in the same area. Data for the Sierra Nevadas shows channel 4 having a very accurate estimate of burn acres in this region. Channel 1, by contrast shows an approximate 50% underestimate.

Table 10. Mapping success of channels 1 and 4 by Jepson ecoregion. This data was generated using the polygon overlay analysis. Page 20 describes the various data categories and the method used to determine “matching” and “detection.” Only channels 1 and 4 for 1999 are reported here.

Channel 1 DATA	Jepson EcoRegion										Total
	Modoc Plateau	NW Coast	Cascade Range	Sierra Nevadas	East of Sierras	Central Valley	Central Coast	Mojave Desert	SWt Coast	Sonoran Desert	
CDF # of fires	15	46	24	92	9	25	27	2	77	3	320
CDF acres of fires	36,322	210,452	159,094	106,928	4,051	13,382	123,630	5,860	115,837	5,150	780,706
CAMFER # of fires	3	32	5	28	4	7	34	11	32	10	166
CAMFER acres of fires	9,649	183,835	40,406	36,950	3,547	14,887	240,339	30,606	94,083	5,183	659,485
CAMFER # matched fires	1	25	5	18	0	0	7	1	10	0	67
CAMFER acres matched	4,620	177,078	40,406	33,670	0	0	187,688	12,835	65,968	0	522,265
CAMFER # unmatched fires	2	7	0	10	4	7	27	10	22	10	99
CAMFER acres unmatched	5,029	6,757	0	3,280	3,547	14,887	52,651	17,771	28,115	5,183	137,220
CDF # detected fires	2	20	6	8	0	2	7	0	11	0	56
CDF acres detected	5,063	201,206	113,586	59,069	0	1,249	112,303	0	85,974	0	578,450
CDF # undetected fires	13	26	18	84	9	23	20	2	66	3	264
CDF acres undetected	31,259	9,246	45,508	47,859	4,051	12,133	11,327	5,860	29,863	5,150	202,256
<i>Channel 4 DATA</i>											
CDF # of fires	15	46	24	92	9	25	27	2	77	3	320
CDF acres of fires	36,322	210,452	159,094	106,928	4,051	13,382	123,630	5,860	115,837	5,150	780,706
CAMFER # of fires	5	23	16	37	18	8	23	37	19	4	190
CAMFER acres of fires	11,738	163,878	43,920	88,164	35,182	27,884	120,461	42,240	112,793	39,485	685,745
CAMFER # matched fires	1	21	13	19	1	1	9	0	7	0	72
CAMFER acres matched	3,927	162,509	42,777	75,978	5,085	2,417	98,310	0	59,690	0	450,693
CAMFER # unmatched fires	4	2	3	18	17	7	14	37	12	4	118
CAMFER acres unmatched	7,811	1,369	1,143	12,186	30,097	25,467	22,151	42,240	53,103	39,485	235,052
CDF # detected fires	2	23	6	13	1	2	6	0	9	0	62
CDF acres detected	5,063	201,429	111,942	74,573	11	1,249	111,985	0	19,107	0	525,359
CDF # undetected fires	13	23	18	79	8	23	21	2	68	3	258
CDF acres undetected	31,259	9,023	47,152	32,355	4,040	12,133	11,645	5,860	96,730	5,150	255,347

The data from tables 7 and 10 can also be used as an assessment of accuracy in general. The “Total” category at the right of the tables indicates overall mapping success. Some trends emerge from examination of these totals. The channel 1 burn scar map “detected” 578,450 acres of the mapped CDF fires. These fires correspond to 522,265 acres of CAMFER burn scars, making the remotely sensed detections a slight underestimate. However, there are 137,220 acres of unmatched fires in the CAMFER channel 1 map. It is unclear whether these unmatched fires are false detections, or actual detections of fires that are not represented in the CDF data. The average size of CDF fires detected is 10,329 acres. The average size of undetected fire is 766 acres. CAMFER’s AVHRR mapping algorithms are far more effective for large fires than for small fires. The average size of a matched CAMFER fire is 7795 acres. This observation could result from the underestimation of burned acres by the CAMFER algorithm, or it could indicate that, on average, single large fires in the CDF database were mapped as two or more smaller fires.

Table 11. Success of CDF fire detection as a percent for all 1999 channels. Computed using the polygon overlay technique.

CHANNEL	Land Cover Type								Total - All Categories
	Open Land	Dunes	Scrub	Grassland	Wetland	Riparian	Woodland	Forest	
6	0.0%	N/A	39.4%	20.6%	N/A	0.0%	74.3%	91.9%	68.4%
5	0.0%	N/A	39.4%	20.6%	N/A	0.0%	74.3%	91.6%	68.2%
4	0.0%	N/A	39.4%	10.1%	N/A	0.0%	74.3%	90.0%	67.3%
3	0.0%	N/A	67.8%	20.5%	N/A	0.0%	74.8%	84.5%	74.2%
2	0.0%	N/A	81.0%	20.5%	N/A	0.0%	74.8%	86.7%	79.0%
1	0.0%	N/A	67.8%	20.5%	N/A	0.0%	74.5%	84.5%	74.1%

Table 11 shows CDF detection percentages (calculated as acreage of CDF fires detected divided by total CDF fire acreage in each cover type) without regard for false detections. This table indicates striking differences between the cover types. The forest type stands out as having the most accuracy of mapped fires. Table 12 shows CAMFER unmatched acres as a percent of CAMFER acre totals for each cover type. Table 11 and 12 must be considered in conjunction in order to accurately assess mapping success. While some combination of differencing method and threshold may contribute to accurate mapping of burn areas, there is a trade-off with “false” positives. In some cases, however, it is possible to reduce the amount of “false” positives without a corresponding compromise in detection success. Whether these unmatched CAMFER fires are actually false positives (commission errors) is difficult to determine given the incompleteness of the CDF dataset.

Table 12. CAMFER unmatched fires as a percent for all 1999 channels. Computed using the polygon overlay technique.

CHANNEL	Land Cover Type								Total - All Categories
	Open Land	Dunes	Scrub	Grassland	Wetland	Riparian	Woodland	Forest	
6	100.0%	N/A	62.3%	83.8%	100.0%	100.0%	24.4%	2.7%	41.3%
5	100.0%	N/A	50.9%	85.5%	100.0%	N/A	23.9%	2.8%	32.6%
4	100.0%	N/A	49.9%	90.3%	100.0%	N/A	30.0%	3.1%	34.3%
3	79.6%	N/A	26.3%	50.7%	N/A	100.0%	29.3%	5.4%	24.3%
2	100.0%	N/A	32.6%	52.0%	N/A	100.0%	34.4%	3.0%	28.0%
1	76.5%	N/A	21.7%	57.1%	N/A	100.0%	23.5%	4.4%	20.8%

Discussion

The validation of the burn area mapping performed using the above methods described here is complicated by uncertainty in the CDF database. For example, not all fires occurring in California during 1999 and 1996 are mapped in the CDF data. Figure 13 duplicates the CDF status map appearing on the CDF website. Southeastern California and the Central Valley stand out as part of the huge area of California designated “perimeters not contributed.” Perhaps not coincidentally, the Central Valley and Sonoran Desert ecoregions have large amounts of unmatched CAMFER fires (see table 10). Given this lack of ground “truth” information from any responsible agency, it is impossible to classify the fires that CAMFER mapped in these areas as “false detections.” Similarly, areas of California in the central and South coasts have not been updated since 1997.

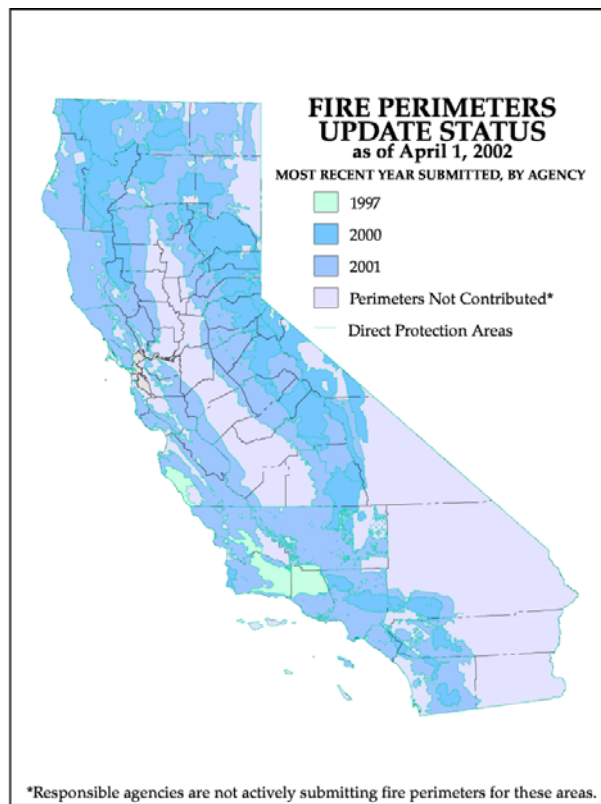


Figure 13. CDF status map (reproduced from FRAP website) for the fire history database. Note the large area designated as "perimeters not contributed."

There is an unknown amount of horizontal error in the CDF data. This uncertainty with regard to positional accuracy is compounded by the uncertainty of horizontal position in the AVHRR data. This lack of information on positional accuracy makes validation more difficult. The differences between the intersection, grid-polygon, and polygon-polygon accuracy assessments highlight the fact that errors in position can skew estimates of map accuracy. While this is obviously of concern for the purposes of validation, it is also of concern in terms of product quality. Positional errors in the maps can affect secondary

functions of the maps, for example as input to an Emissions Estimation System. A change in position of a fire will affect the amount of estimated emissions from that fire as well as the location at which the emissions enter the atmospheric environment. A true validation of burn scars remains an outstanding issue.

Our geographically based analysis elucidates different degrees of mapping success in different ecosystems and ecoregions. These results are crucial in the adjustment and modification of the algorithms to achieve better mapping success over heterogeneous landscapes. The data suggest that “fine tuning” of the parameters may be possible between vegetation cover types in order to minimize false positives while maximizing detection rate. As evidenced by the data in tables 11 and 12, there is not necessarily a direct tradeoff. But the maximization of detection and simultaneous minimization of false positives may require more complex processing. That type of optimization would need to occur differently over different cover types. Additional research is needed to address these questions.

The issue of “false detections” will also require additional research. At this time, it is difficult to assess the degree of map accuracy when parts of the ground “truth” dataset are incomplete. In some ways, lack of data over some geographic areas, in combination with commission errors and other anomalies in the CDF data, casts doubt on the accuracy of the dataset as a whole. This is unfortunate since this is the best data available for a detailed analysis of fire mapping, but without definitive knowledge of the data, it is very difficult to “validate” independent fire mapping products. More research is needed to assess the accuracy of the CDF data, provide independent verification of remotely sensed burn scars, and develop more in depth comparisons and validation of the datasets.

Conclusion

Through a modification of CCRS algorithms, we were able to successfully map wildfires in California using satellite based remote sensing technology. The mapping is, in general, more successful for large fires, over 10,000 acres and fires in forested ecosystems. Depending on the type of comparison selected, the CAMFER technique is able to map between 45% and 67% of CDF mapped burn area. A geometric intersection based comparison indicates that only 45% of fire area in the CDF database was mapped by the CAMFER method. If the rules for matching are relaxed, and one assumes that fires are “matched” even if the boundaries do not coincide exactly, then 67% of the CDF fire area was mapped using the CAMFER method. The true accuracy of the CAMFER method is unclear due to the fact that fire detections made using the remotely sensed data may not in fact be errors of commission in the CAMFER data, rather errors of omission in the CDF data.

The method is currently limited by the frequency of satellite overpasses available for hotspot detection. Because the method relies on hotspots as input to burn scar mapping, limitations to either hotspot detection or NDVI differencing will result in a corresponding decrease in quality of the final product. The NDVI differencing is also limited by data

availability, and complicated by phenological changes in vegetation that produce similar effects to burning in terms of decreasing NDVI.

These limitations may be mitigated through the use of different differencing techniques and thresholds in different land cover types. This should be a topic for future research. Additional work is also needed in the collection and verification of ground truth data needed for validation. Currently, efforts to validate remotely sensed burn scar maps are restricted by a lack of and/or uncertainty in fire history databases maintained by the state of California. The quality of data available for validation limits its efficacy to provide a reference against which remotely sensed burn scar maps can be fully judged.

References

Arino O, Piccolini I, Siegert F, Eva H, Chuvieco E, Martin P, Li Z, Fraser RH, Kasischke E, Roy D, Pereira J, Stroppiana D (1999) Burn scars mapping methods. *Forest Fire Monitoring and Mapping: A Component of Global Observation of Forest Cover, Report of a Workshop*, Edited by F. Ahern, J-M Gregoire and C. Justice, November 3-5, 1999, Joint Research Centre, Ispra, Italy, pp. 198-223.

Arino O, and Mellinotte JM (1998) The 1993 Africa fire map. *Int. J. Rem. Sens.* **19**, 2019-2023.

Boles SH, and Verbyla DL (2000) Comparison of three AVHRR-based fire detection algorithms for interior Alaska. *Remote Sens. Environ.* **72**, 1-16.

Bourgeau-Chavez, L.L., Harrell, P.A., Kasischke, E.S., French, N.H.F. 1997. The detection and mapping of Alaskan wildfires using a spaceborne imaging radar system. *International Journal of Remote Sensing*. Vol.18. No.2. PP.355-373

Di, L and Rundquist DC (1994) A one-step algorithm for correction and calibration of AVHRR level 1b data. *P. E. & R. S.* **60**, 165-171.

Dwyer, E, Gregoire JM, and Malingreau JP (1998) A global analysis of vegetation fires using satellite images: Spatial and temporal dynamics. *Ambio* **27**, 175-181.

Eva H., and Flasse S (1996) Contextual and multiple-threshold algorithms for regional active fire detection with AVHRR data. *Rem. Sens. Rev.* **14**, 333-351.

Eva H. and Lambin EF (1998) Burnt area mapping in central Africa using ATSR data. *Int. J. Remote Sensing* **19**, 3473-3497.

Fernandez A., Illera P, and Casanoca JL (1997) Automatic mapping of surfaces affected by forest fires in Spain using AVHRR NDVI composite image data. *Remote Sens. Environ.* **60**, 153-162.

Flannigan MD, and Vonder Haar TH (1986) Forest fire monitoring using NOAA satellite

AVHRR. *Can. J. Forest Res* **16**, 975-982.

Flasse SP, and Ceccato P (1996) A contextual algorithm for AVHRR fire detection. *International Journal of Remote Sensing* **17**, 419-424.

Franca JR, J.M. Brustet JM, Fontan J (1995) Multispectral remote sensing of biomass burning in West Africa. *J. Atmos. Chem.* **22**, 81-110.

Fraser RH, Li Z, and Cihlar J (2000) Hotspot and NDVI Differencing Synergy (HANDS): A New Technique for Burned Area Mapping. *Remote Sensing of Environment* **74**, 362-376.

Giglio L, Kendall JD, and Justice CO (1999) Evaluation of global fire detection using simulated AVHRR infrared data. *Int. J. Rem. Sens.* **20**, 1947-1985.

Harris, AJL (1996) Towards automated fire monitoring from space: semi-automated mapping of the January 1994 New South Wales wildfires. *Int. J. Wildland Fire.* **6**, 107-116.

Justice C, Malingreau JP, and Setzer AW (1993) Remote sensing of fires: Potential and limitations. *Fire in the Environment* (P.J. Crutzen and J.G. Goldammer, Eds.), pp. 77-88

Justice CO, and Dowty P (editors) (1994) IGBP-DIS satellite fire detection algorithm workshop technical report. *IGBP-DIS Working Paper9, NASA/GSFC, Greenbelt, Maryland, USA, February, 1993.*

Justice CO, Kendall JD, Dowty PR, Scholes RJ (1996) Satellite remote sensing of fires during the SAFARI campaign using NOAA advanced very high resolution radiometer data. *J. Geophys. Res.* **101**, 23851-23863.

Kaufman YJ, Setzer A, Justice C, Tucker CJ, Pereira MC, and Fung I (1990) Remote sensing of biomass burning in the tropics. *Fires in the Tropical Biota, Ecosystem Processes and Global Changes* (Goldammer JG, Ed.), 371-399.

Kasischke ES and Nancy HFF (1995) Locating and Estimating the Areal Extent of Wildfires in Alaskan Boreal Forests Using Multiple-Season AVHRR NDVI composite data. *Remote Sens. Environ.* **51**, 261-275.

Kasischke ES and French NNH (1997) Constraints on using AVHRR composite index imagery to study patterns of vegetation cover in boreal forests. *Int. J. Remote Sens.* **18**, 2403-2426.

Kennedy PJ, Belward AS, Gregoire JM (1994) An improved approach to fire monitoring in West Africa using AVHRR data. *Int. J. Remote Sens* **15**, 2235-2255.

Khazenie N and Richardson KA (1993) Detection of oil fire smoke over water in the

Persian Gulf region. *P. E. R. S.* **59**, 1271-1276.

Lee TM, and Tag PM (1990) Improved detection of hotspots using the AVHRR 3.7 um channel. *Bull. Amer. Meteor. Soc.* **71**, 1722-1730.

Li Z, Cihlar J, Moreau L, Huang F and Lee B (1997) Monitoring fire activities in the boreal ecosystem. *J. Geophys. Res.* **102**, D24, 29611-29624.

Li Z and Giglio L (1999) A review of AVHRR-based fire detection algorithms. *Forest Fire Monitoring and Mapping: A Component of Global Observation of Forest Cover, Report of a Workshop*, Edited by F. Ahern, J-M Gregoire and C. Justice, November 3-5, 1999, Joint Research Centre, Ispra, Italy, pp. 175-197.

Li Z, Nadon S, Cihlar J (2000a) Satellite-based detection of Canadian boreal forest fires: Development and application of the algorithm. *Int. J. Rem. Sens.*, **21**, 3057-3069.

Li Z, Nadon S, Cihlar J, Stocks B (2000b) Satellite-based mapping of Canadian boreal forest fires: Evaluation and comparison of algorithms. *Int. J. Rem. Sens.* **21**, 3071-3082.

Li Z, Kaufman YJ, Ichoku C, Fraser R, Trishchenko A, Giglio L, Jin J (2000c) A review of satellite fire detection algorithms: principles, limitations, and recommendations, *Submitted to Remote Sensing of Environment*

Malingreau JP and Justice CO(editor) (1997) *Definition and Implementation of A Global Fire Product Derived from AVHRR Data*, 3rd IGBP-DIS Fire Working Group Meeting Report, IGBP-DIS Working Paper 17, Toulouse, France, 13-15 November 1996.

Martin MP, and Chuvieco E (1995) Mapping and evaluation of burned land from multitemporal analysis of AVHRR NDVI images. *EARSEL Adv. Rem. Sen.* **4**, 7-13.

Muirhead K and Cracknell A (1985) Straw burning over Great Britain detected by AVHRR. *Int. J. Rem. Sens.* **6**, 827-833.

Pereira JMC (1999) A comparative evaluation of NOAA/AVHRR vegetation indexes for burned surface detection and mapping. *IEEE Trans. Geosci. Remote Sens.* **37**, 217-226.

Pereira JMC, Chuvieco E, Beudoin A, and Desbois N (1997) Remote sensing of burned areas: a review - In: *A Review of Remote Sensing Methods for the Study of Large Wildland Fires* (E. Chuvieco, ED.) Departamento de Geografia, Universidad de Alcala, Alcala de Henares, pp. 127-184.

Pozo D, Olmo EJ, and Alados-Arboledas L (1997) Fire detection and growth monitoring using a multitemporal technique on AVHRR mid-infrared and thermal channels. *Remote Sens. Environ.* **60**, 111-120.

Rauste Y, Herland E, Frelander H, Soini K, Kuoremaki T, and Ruokari A (1997)

Satellite-based forest fire detection for fire control in boreal forests. *Int. J. Rem. Sens.* **18**, 2641-2656.

Razafimpanilo H, Frouin R, Iacobellis SF, and Somerville RCJ (1995) Methodology for estimating burned area from AVHRR reflectance data. *Rem. Sen. Environ*, **54**, 273-289.

Rommel, Tarmo K., Ajith H. Perera. 2001. Fire mapping in a northern boreal forest: assessing AVHRR/NDVI methods of change detection. *Forest Ecology and Management*. No.152. pp. 119-129

Sandberg D, Hardy CC, Ottmar RD, Snell JAK, Acheson AL, Peterson JL, Seamon P, Lahm P, and Wade D (1999) *National Strategic Plan: Modeling and Data Systems for Wildfire and Air Quality*, General Technical Report PNW-GTR-450, Pacific Northwest Research Station, USDA Forest Service.

Setzer AW and Malingreau JP (1996) AVHRR monitoring of vegetation fires in the tropics: Toward the development of a global product. *Biomass Burning and Global Change*, (ed. J.S. Levine), p. 25-39, The MIT Press, Cambridge, Massachusetts, London, England.

Setzer AW and Pereira MC (1991) Amazonian biomass burnings in 1987 and an estimate of their tropospheric emission. *Ambio* **20**, 19-22.

Snyder, John P. 1987. "Map Projections – A Working Manual" USGS Professional Paper 1395. US Govt. Printing Office. Washington DC.

Stroppiana D, Pinnock S, and Gregoire JM (2000) The global fire preoduct: daily fire occurrence from April 1992 to December 1993 derived from NOAA AVHRR data. *Int. J. Remote Sensing* **21**, 1279-1288.

Section 2 – NFDR-TH Input Enhancement

Introduction

In order to provide fire or region specific inputs to the emissions estimation process, the CAMFER EES (Emission Estimation System) accepts a variety of user data corresponding, in general, to the required inputs for the FOFEM model (Reinhardt et al. 1997). As an initial investigation into model performance, CAMFER performed a preliminary sensitivity analysis of these inputs (Scarborough et al. 2001). We identified thousand hour fuel moisture as a critical input, the EES emission estimates being very sensitive to the value of this fuel moisture parameter. In order to improve the reliability of emissions estimates and facilitate emissions estimation at a large geographic scale, ARB is interested in using an empirically based, spatial input of thousand hour fuel moisture to the EES. The USDA Forest Service creates a grid of Thousand Hour fuel moisture through the National Fire Danger Rating System (NFDR-TH). This grid has a 10-kilometer spatial resolution, daily temporal resolution, and national scope. This section describes the integration of NFDR-TH grid input capability to the CAMFER EES.

The FOFEM based emission estimation engine of the CAMFER EES accepts two moisture inputs: NFDR-TH and “moisture conditions.” These parameters affect the consumption and emissions for dead and downed woody debris over 3 inches in diameter (thousand hour fuels) and duff. The NFDR-TH input affects consumption, and the “moisture conditions” input affects the apportionment of flaming and smoldering phases of combustion. While these inputs are linked, CAMFER retained two separate inputs in order to distinguish between the categorical “moisture conditions” variable and the continuous NFDR-TH variable. This distinction allows more control over processing and a separate adjustment of fuel consumption and emissions generation.

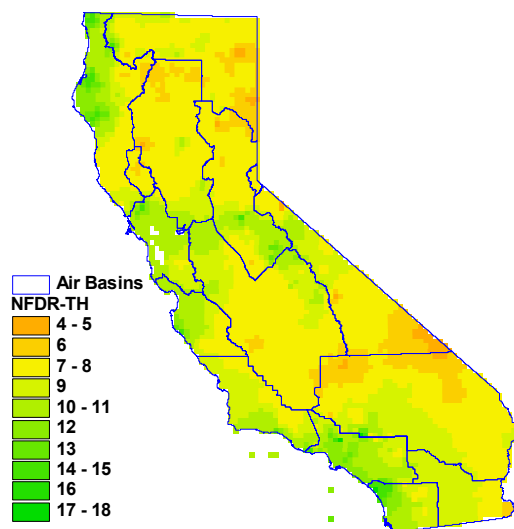


Figure 14. Late fall map of NFDR-TH. There is significant spatial variability in the magnitude of this value, especially along an East-West transect.

The NFDR-TH fuel moisture input, as an empirical value rather than “expert judgment,” is both temporally and spatially variable. Figure 14 displays an NFDR-TH grid for a late fall day in California. For a transect in Northern California, the value can be seen to increase by almost 10 percentage points from the coast to the Eastern California border. This magnitude of change has significant effects on resultant emissions estimates (Scarborough et al. 2001). In order to improve the accuracy of the emissions estimation, a geographic and temporal distinction of the NFDR-TH value must be made between fires, rather than using the default value (currently 20%) for all fires in the dataset.

This distinction is possible by adapting the EES to accept an NFDR-TH grid as input. The Forest Service creates this product as part of the Wildland Fire Assessment System (WFAS, www.fs.fed.us/land/wfas/welcome.html). Measurements from weather stations scattered throughout the U.S. are interpolated to produce a continuous, 10 kilometer resolution grid (Burgan et al. 1997). This information is distributed on a daily basis as stylized images on the WFAS website. Figure 15 shows an example of these images. These images are archived for the past several years. The information is also available, on the day of release only, as a grid dataset. To our knowledge, the underlying data are not archived. This limits temporal availability of the grid to the current day. Clearly, the currency of the data constrains its utility as an input for all but the most recent of fires.

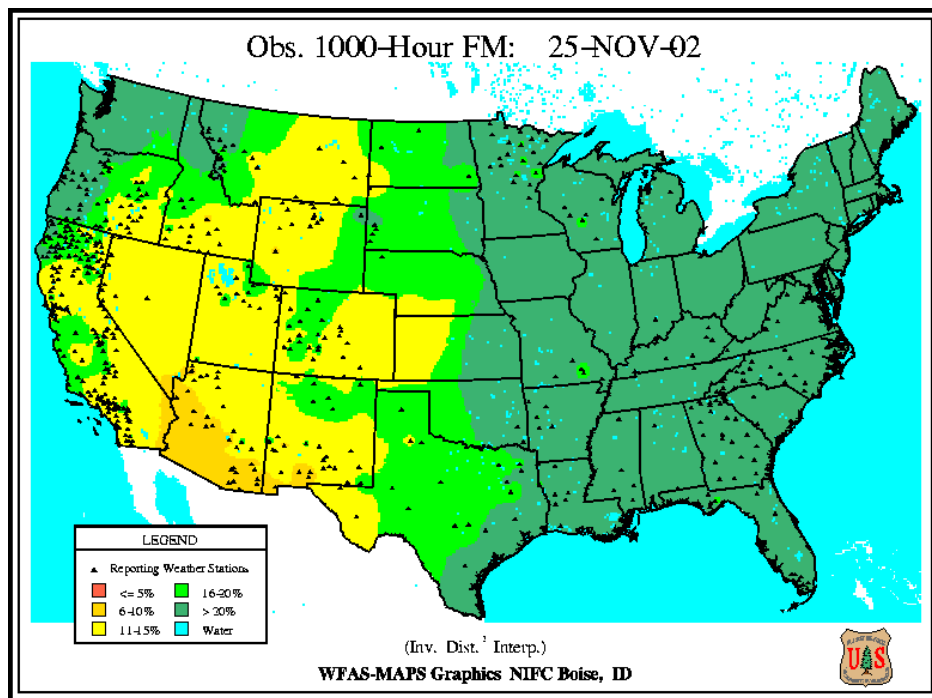


Figure 15. Example of archived images of Forest Service NFDR-TH maps. This image corresponds to a November 25 map. Weather stations are displayed as black triangles.

Methods and Results

In order to accumulate enough data to provide temporal resolution of the NFDR-TH input, CAMFER, through an agreement with the Forest Service, is now archiving the NFDR-TH grids on a daily basis. The grids are posted to a Forest Service FTP site in Gzipped Arc/INFO export file format. A combination of scripts logs on to the Forest Service site and “gets” the export files every day. This archiving began on November 25, 2002. Until a “season” (roughly defined as May through November) of these grids have been archived, there is relatively little value in using the data already obtained for emissions estimation. This is due to the limited temporal scope of moisture conditions that the grids represent.

In order to provide ARB with a more immediate method of enhancing the EES with a spatial NFDR-TH input, CAMFER "mined" the Forest Service image archive to obtain NFDR-TH graphics for the year 2000. These graphics are GIF images of categorical NFDR-TH values (see legend of FS image, above) for the continental US. Unlike the grids we obtain directly from the Forest service, the images have 6165 meter resolution.

The images available through this online archive are not geo-referenced or distributed in a format readily input to the GIS. Processing is required in order to convert the images to information that can function as input to the EES. The data must be geographically located and the images must be "cleaned" in order to remove graphical representations of weather stations, state boundaries, lakes, etc. Utilizing MS Internet Explorer, we duplicated the directory structure used by the Forest Service image archive, then manually downloaded each GIF image, using Explorer to convert the files to a bitmap format. These bitmaps are geographically located with a pre-made bitmap world file. The script (fdimport.ave) gets the images from the local directories, geo-references the images using the pre-made world file, then converts them to a grid format using a custom color reclassification scheme. This reclassification assigns NFDR-TH moisture content to each cell based on the Forest Service legends. So for a given set of rendering schemes, we produced moisture data that is based on the average of the moisture ranges reported. These ranges are shown in Table 13. The same script also converts the images to grid format.

Table 13. Reclassification scheme of categorical data displayed in the Forest Service image archives.

Forest Service Category	Mapped NFDR-TH Value
<=5%	3
6%-10%	8
11%-15%	13
16%-20%	18
>20%	24

The grids made directly from the images have large gaps in the data as a result of the graphics placed on the images to represent weather stations. We created another script (nibbler.ave) to interpolate moisture value over gaps in the data. This script uses a "majority filter" with a 9x9 kernel size to interpolate NFDRTH values in areas where the

image showed lake or weather station graphics. This process, while slightly modifying the moisture category boundaries, results in conterminous grids over California. In some cases, new gaps were formed as a result of the filtering steps, but of considerably less extent than the input grids. In order to a sequence of grids that could be readily incorporated as input to the EES, we created a script (avgmakr.ave) to go through the directories and create grids representing the average moisture conditions for each month. We used Arc/INFO to clip the grids to California and re-project them to Teale Albers.

Table 14. Image availability for year 2000 NFDR-TH moisture maps in the Forest Service archive. These images were used in the creation of monthly average grids.

<i>Month</i>	<i>Number of images</i>
January	31
February	28
March	31
April	29
May	16
June	30
July	25
August	29
September	29
October	24
November	27
December	27
Total	326

There are several reasons for creating monthly average fuel moisture maps. Not every day of the year was represented in the Forest Service image archive, so the use of averages allows a spatial moisture input for every fire, regardless of whether the particular burn day was represented in the archive. Table 14 shows the image availability for each month in year 2000. As indicated by the table, some months are better represented than others. Using monthly average grids also allows generalization of the data to other fire years. While moisture conditions will not be identical from year to year, trends of fuel moisture in California's Mediterranean climate will be similar between years. Monthly averages capture these trends and avoid the application of daily moisture conditions that will almost certainly not be applicable to the same date in other years. Finally, monthly grids are far easier to store and manipulate than 365 separate grids. The use of only 12 grids reduces data storage and file maintenance requirements. The July average grid is shown in Figure 16. This grid reflects a continuous range of moisture values, rather than a limited range of categorical values. This added complexity of the moisture range results from the monthly averaging process.

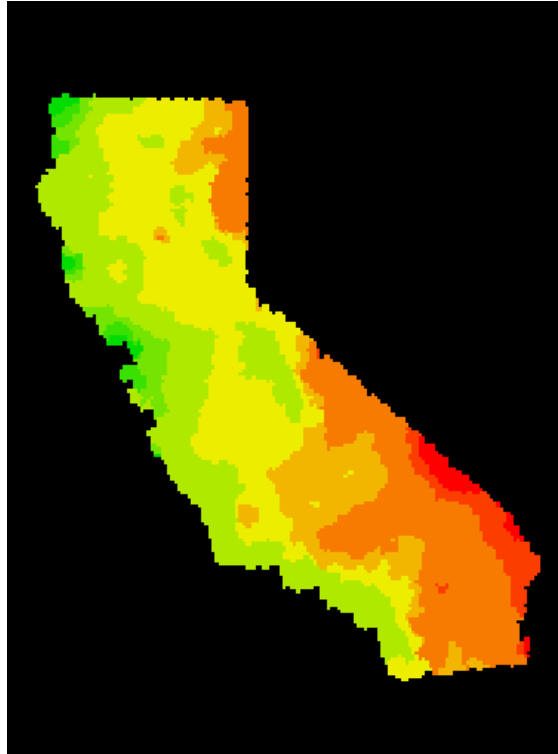


Figure 16. July grid of NFDR-TH values. This grid was created from Forest Service images, clipped to California, and re-projected to Albers for inclusion to the EES.

The grids produced through this process should be viewed as an experimental product. In some cases, there were missing data from the Forest Service archives, so not every month is represented by a complete set of daily moisture condition grids. In addition, some months have small gaps in coverage due to the interpolations we were obliged to use. Table 14 summarizes the data coverage for each month. There were also deficits in the spatial distribution of information. There is a lack of moisture data everywhere a weather station graphic appeared on the images. The interpolation of value that was necessary in these areas results in increased uncertainty in regard to accuracy of the data. For these reasons, the dataset is limited in the ability to accurately represent actual field moisture conditions.

CAMFER added the capability of accepting a gridded NFDR-TH input to the fire EES. The EESfires.ave script computes the centroid of each fire for which estimates are being produced, then determines the value of the NFDR-TH fuel moisture grid beneath this point in order to set a global variable with the appropriate value. Due to the poor spatial resolution of the grid, it is of relatively minor benefit to sample the grid outside the centroid of the fire polygon. The EES uses the date information in the fire input to determine which monthly average grid to use for the NFDR-TH input. The EES will run successfully with the NFDR-TH grid as input, producing emissions estimates based on the value of NFDR-TH at each fire. This functionality can be turned on or off depending on user preference and the availability of input data.

The results from a run of year 2000 polygons in the CDF database indicate a considerable difference between the generic default fuel moisture setting and the automatic determination of NFDR-TH spatial and temporal fuel moisture inputs. These results are summarized in Table 15. This table shows an approximate 60% increase in estimated particulates resulting from the use of spatial NFDR-TH inputs.

Table 15. Table of total emissions for year 2000 fires using default and spatial inputs of NFDR-TH. These data were produced with the EES and the CDF fires database.

Pollutant	Emissions in tons (Year 2000 fires)	
	Default NFDR-TH (20%)	Spatial NFDR-TH input
Total CO	470,541.0	771,062.0
Total PM 10	48,732.6	78,164.0
Total PM 2.5	41,348.8	66,327.2
Total CH ₄	18,819.5	30,840.2
Total NMHC	32,942.3	53,979.0
Total NH ₃	4,703.4	7,707.5
Total N ₂ O	949.4	1,398.5
Total NO _x	16,167.8	23,752.2
Total SO ₂	4,979.1	7,316.1

Discussion

Currently, the NFDR-TH grid input to the CAMFER EES is enabled. Ideally, the NFDR-TH input for any given fire would be taken from a grid corresponding to the “day” on which the fire occurred. This type of spatial input is not currently feasible given the necessary generalization of the data to monthly averages. These composites created for each month, or other suitable temporal resolution that represents the change in burning conditions as the season progresses, is coarse enough to average out unique, annual conditions. Since the NFDR-TH is based on meteorological conditions, the inter-annual variation will be a result of weather patterns that change from year to year. However, due to California’s relatively consistent Mediterranean climate, it is possible to generalize conditions over any one year. Monthly composites based on fire season 2000 weather are general enough to support historical analysis, but with the caveat that they are more applicable (and assumed to be more accurate) for years with similar weather conditions to fire season 2000.

Even with availability of daily moisture data, it may not be advantageous to require a daily NFDR-TH value as input. Often, the fire input data is not resolved to a daily time scale. Some fires burn over many days, complicating the selection of a daily grid to be used in emissions estimation. The application of daily NFDR-TH data from one year to future or previous years may not be appropriate on a daily basis. Generalized grids (by month) allow a more logical way to use one year of data as a proxy for moisture conditions in many other years. Finally, there are issues associated with data maintenance and storage of 365 grids for each year. Clearly, the storage of only 12 grids vastly simplifies processing, retrieval and the need for disk space.

The results of a year 2000 estimation run show a large increase in emissions (approximately 60% for estimated particulates) by using the spatial NFDR-TH fuel moisture input. These data indicate that, in general, the increased consumption associated with drier conditions (than the default 20% NFDR-TH input) results in a significantly higher emissions than was previously estimated. The use of the spatial, empirically based fuel moisture input results in increased confidence in emissions estimates.

Conclusion

We have demonstrated the capability of including the Forest Service NFDR-TH fuel moisture grid as a spatial input to the CAMFER EES. This empirically determined input reflects interpolated field conditions at a national scope. However, due to limited temporal availability, the use of these grids for historical fires is currently limited. Archiving of current data grids is now in progress. The disparities between estimates produced with and without a spatial fuel moisture input indicate that inclusion of the NFDR-TH grids is valuable for improving confidence in the emission estimates. Future work is needed to assemble the newly acquired fuel moisture data into a useable product. Use of data obtained directly from Forest Service servers will undoubtedly reduce error and increase accuracy of empirically based NFDR-TH grids used as input to the EES.

Section 3 – Daily Emissions Allocation

Introduction

The CAMFER Wildland Fire Emission Estimation System (EES) is capable of providing detailed emissions estimates that are spatially allocated, the spatial resolution being a function of the input data quality. These input data, and the resulting output, may or may not be temporally allocated. The CAMFER EES is designed to incorporate a date input (month-day-year, as a number format) in order to determine seasonality of the burn, which affects burning conditions. If the day of the burn ignition is known and present in the input data, the emissions from that fire are assumed to have originated on that day. This assumption, however, is not always accurate, especially for large fires.

For the purposes of air quality modeling, the California Air Resources Board (ARB) required that selected large fires be temporally allocated at a daily resolution. The air quality modeling also requires emissions to be spatially allocated to gridded areas of interest, rather than the per fire output that is standard to the CAMFER EES. While many large fire polygons are referenced by a single day in the California Department of Forestry and Fire Protection (CDF) database, these fires are known to have occurred over many days. This section describes the daily temporal allocation and spatial allocation of the Manter fire emissions to polygons used by the Central California Ozone Study (CCOS) for atmospheric modeling. CAMFER performed the same operation for the Plaskett II and McNally fires, delivering the results to ARB for the purposes of the CCOS modeling effort.

Methods and Results

The initial phase of the daily allocation task involved data acquisition. For the purposes of daily emission estimation, it is necessary to know the area burned on any given day. Ideally, this information is mapped using GPS, photo interpretation, or other techniques of suitable precision to geo-reference the fire boundary with minimal error. This type of data is not always available for large fires.

Due to the initial difficulty in obtaining daily burn data, CAMFER investigated the FARSITE model (Finney, 1997) as a way to create “estimated” fire progression polygons. The FARSITE model is a spatially allocated simulator of wildland fires. It is capable of producing fire progression polygons at high temporal resolution. However, the required inputs to FARSITE are complex and difficult to obtain. These requirements include:

- ASCII grid format inputs at 20 meter resolution or better of:
 - Elevation
 - Slope
 - Aspect
 - Fuel Type
 - Canopy Cover

- Temporally allocated weather file
- Temporally allocated wind file
- Rate of fire spread adjustment factors for each fuel type
- Temporally allocated fuel moisture file

CAMFER determined that the feasibility of obtaining these inputs in order to spatially decompose and temporally reference large fires was beyond the scope of this project. While we have not had universal success in finding spatial data for the fires of interest, it is worth noting that it would be even less likely that we could find the type of complex data needed for FARSITE runs. Additionally, the added pre-processing, modeling, and subsequent interpretation of FARSITE results would add considerable time and uncertainty to the eventual output of temporally allocated emissions estimates.

In lieu of this modeling approach, we were eventually able to obtain daily fire progression polygons for the Manter fire, a large fire occurring in the Sequoia National Forest in July and August of 2000. It was necessary to cull the most comprehensive file (polygon shapefile format) representing fire advancement from the voluminous and disorganized dataset provided to us. Due to the lack of documentation of the data, we assumed the file we chose was an accurate depiction of fire progression. These polygons are displayed in Figure 17. This image shows the total fire area decomposed into polygons of daily burn area.

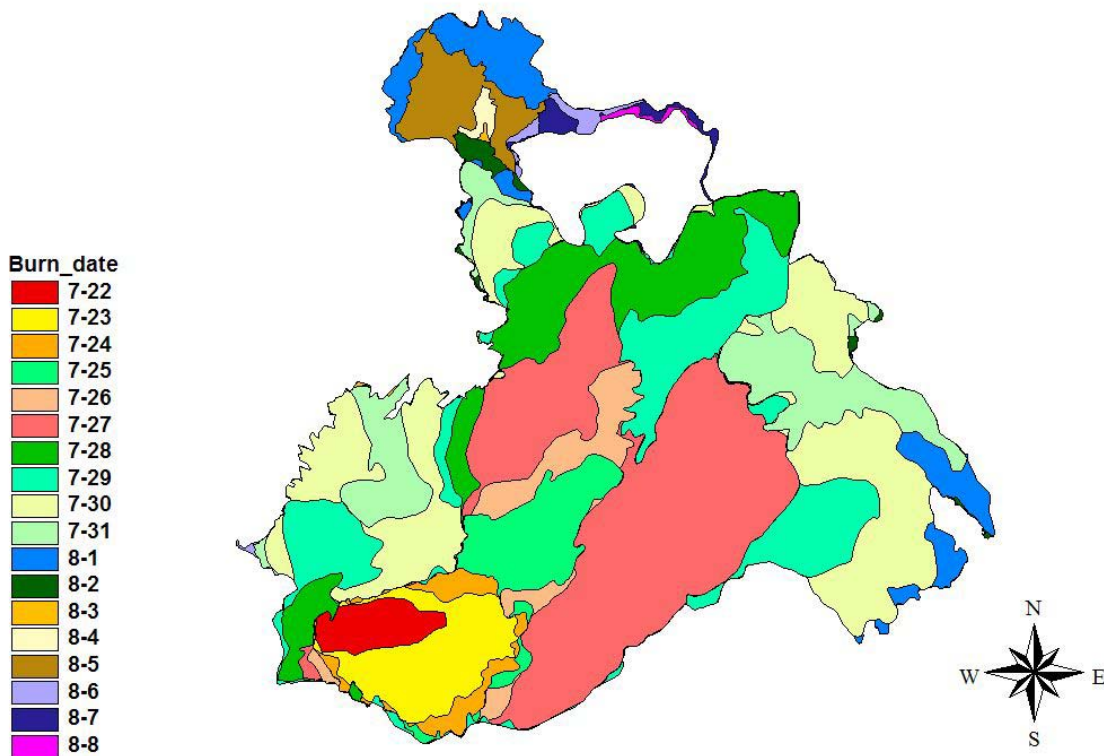


Figure 17. Manter fire daily progression. Each day of burning is represented by a polygon or a set of polygons, if the burning on that day was distributed over a large area. These polygons serve as input to the EES.

There were several problems with the file that represents the Manter fire. First, there were multiple polygons representing the same day. While this may be an accurate spatial depiction of the burn progression, it complicates emission estimation by storing values for one day in multiple records. Second, the polygons were not actually representative of daily burn area. Instead, each polygon represented *cumulative* area burned up to each day appearing in the attributes. CAMFER performed several pre-processing steps on the data in order to facilitate daily emission estimation. We dissolved the polygon file based on the date attribute (creating dissolvedmanter.shp) such that the area represented by each day was contained in only one record of the data table. Manually, we converted the polygons for each day to separate shapefiles, one for each day. With the GIS Avenue `dailymakr2.ave` script, the area for each day was subtracted from the proceeding day, in order to create polygons of daily area burned rather than cumulative area. These daily polygons were then put back together into a single shapefile (`daily.shp`) of true, daily polygons, each referenced by a unique id corresponding to the date on which the burning occurred.

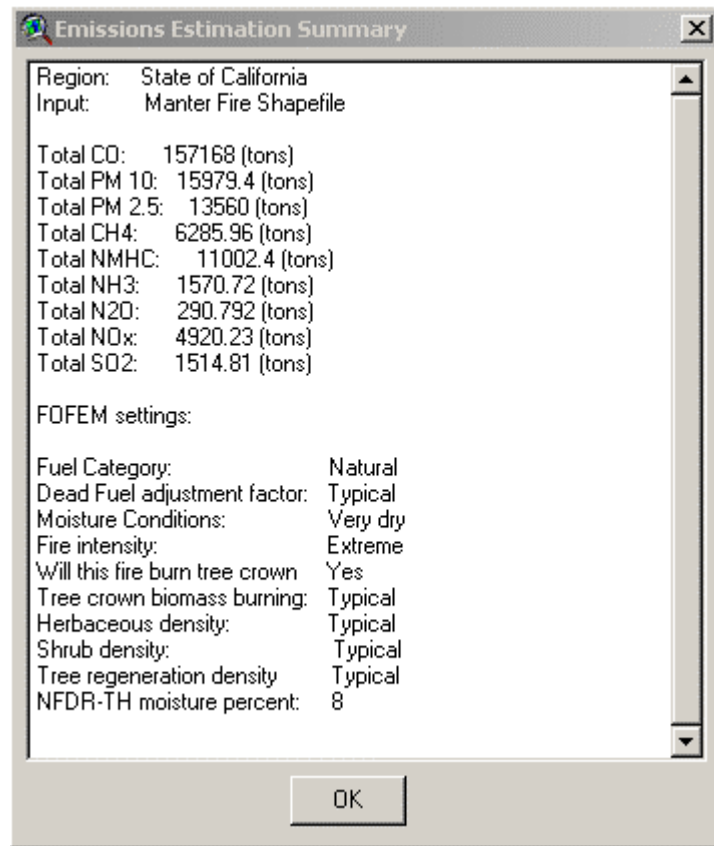


Figure 18. The output message box for the Manter fire. Input parameters appear at the bottom of the box.

Using the daily polygon file as input, we ran the EES, producing *daily* emissions estimates. We used the default EES settings, illustrated in Figure 18, except for the NFDR-TH fuel moisture input. In order to determine NFDR-TH, we inspected the

archived image of July 22, 2000 NFDR-TH values at the Forest Service Wildland Fire Assessment System web page. California was characterized by a broad area of the “6%-10%” category in the region of the Manter fire. We chose 8% as a logical input value that would be representative of burning conditions for this fire.

The differencing of the polygons (*spatial* subtraction) resulted in numerous, sliver polygons at the edges of the burns. Due to the lack of metadata, it was impossible for us to judge whether these slivers actually represented small areas of fire advance on the edges of the previous day’s burn, or whether they were artifacts of boundary discrepancy between data acquisition sessions on consecutive days. We assumed the slivers to represent actual burning and used the EES to process each individual polygon. The standard EES output of summarized emissions information (with filename, in this case, of *sumdaily.shp.dbf*), contained the total emissions mass from each day the fire burned, referenced by polygon id numbers. This table is illustrated as Table 16. These emissions data, joined with the date information assigned to each fire polygon, provide daily emission estimates as well as information about pre-burn fuel loading and area burned.

Table 16. *Sumdaily.shp.dbf*. This table shows the standard, summarized output of the EES. Using the polygon ID (fire ID) as the relate item and joining this table to the attributes of the input polygons spatially allocates the emissions and provides a date field.

Fire ID	PM10	PM2.5	CO	CH ₄	TNMHC	NH ₃	N ₂ O	NO _x	SO ₂
1	646.14	548.27	6,424.02	257.00	449.73	64.28	11.18	189.63	58.39
2	1,362.88	1,156.46	13,528.32	541.20	947.08	135.32	23.75	402.94	124.09
3	493.07	418.39	4,894.99	195.82	342.68	48.96	8.59	145.68	44.86
4	273.10	231.76	2,683.25	107.31	187.84	26.80	4.99	84.55	26.05
5	360.28	305.74	3,538.91	141.53	247.73	35.33	6.59	111.64	34.40
6	1,692.54	1,436.47	16,428.53	656.77	1,149.99	163.80	32.61	551.30	169.86
7	1,319.62	1,119.85	12,918.41	516.65	904.33	129.08	24.53	414.54	127.58
8	2,275.17	1,930.69	22,362.32	894.40	1,565.46	223.52	41.55	702.57	216.26
9	3,727.99	3,163.48	36,704.55	1,468.08	2,569.48	366.93	67.53	1,142.56	351.68
10	1,807.27	1,533.61	17,755.17	710.17	1,242.94	177.54	33.08	558.93	171.95
11	857.42	727.61	8,411.47	336.39	588.83	84.05	15.79	266.93	82.17
12	161.40	136.96	1,594.33	63.77	111.61	15.94	2.88	48.76	15.02
13	34.56	29.32	342.94	13.72	24.01	3.43	0.60	10.23	3.15
14	31.53	26.76	306.47	12.25	21.45	3.05	0.60	10.21	3.15
15	996.04	845.20	9,879.33	395.14	691.62	98.77	17.44	295.51	91.04
16	54.75	46.46	533.79	21.34	37.36	5.32	1.03	17.51	5.40
17	48.66	41.30	471.02	18.83	32.97	4.69	0.95	16.04	4.95
18	9.40	7.98	89.43	3.57	6.26	0.89	0.20	3.32	1.02

Using the daily shapefile input and the EES summarized emissions output file, we were able to transform the information into multiple formats, including grids. Once the spatial data had been converted to a grid, we used *distributr.ave* to allocate the emissions on a per cell basis. Conveniently, ArcView places a field called “Count,” which represents the number of cells produced from a given polygon value, in the attribute table of the grids. By joining the emissions to the grid, then running *distributr.ave*, the emissions per cell are computed by dividing total daily emissions by total cells per day. These gridded,

daily emissions can be produced at any desired resolution. Figure 19 shows a resultant 1 kilometer resolution grid for the Manter fire.

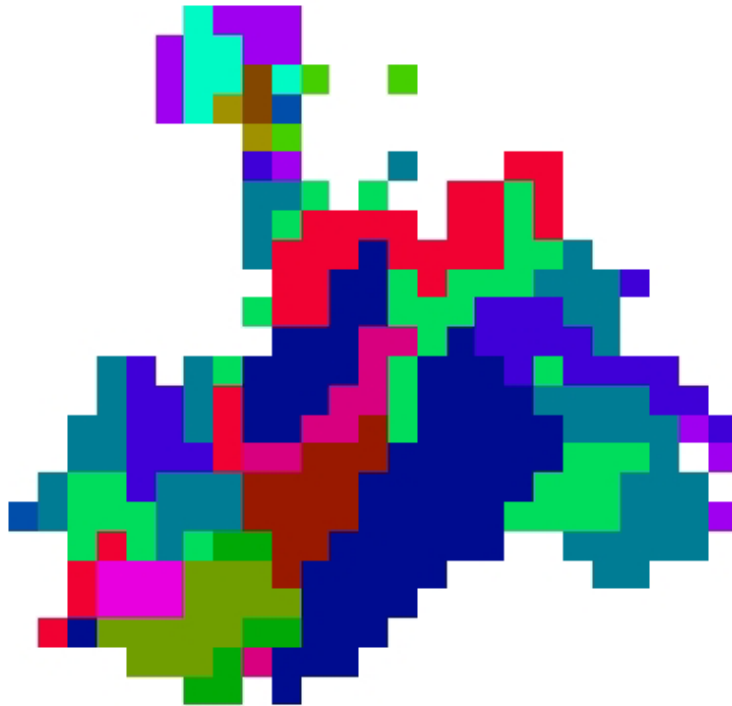


Figure 19. 1 kilometer grid of daily emissions for the Manter fire. At this resolution, small polygons of daily burning, apparent in Figure 17, are "washed out." Each day is represented by a different color.

For ARB modeling of air quality, we also allocated the emissions by CCOS polygons. Figure 20 shows an overlay of the Manter fire daily polygons and the CCOS domain polygons. As illustrated, there are a large number of combinations in terms of multiple days in one CCOS polygon as well as one day being distributed over multiple CCOS polygons. As the primary step in the process of quantifying these spatial relationships, we used ArcView to cross-tabulate the burn area each day by the CCOS polygon. We specified a 100 meter grid cell size for ArcView to use in the creation of a temporary grid used in the cross tabulation. This allowed us to check the area estimates against our "dailygrid," created at the same resolution. The results were consistent, but the CCOS allocation resulted in a few more hectares of burn area, likely due to a "washing out" of sliver polygons in the direct conversion to grid. The resultant table (ccostab3.dbf) indicated how much area in each CCOS polygon burned on each day. CAMFER created the ccosallocatr4.ave script to combine the data in this table with the data in the table of daily emissions. The resultant output table contains emission estimates for each day, each pollutant and each polygon of the CCOS domain. Due to size limitations, this table is not reproduced here. The method of data combination is detailed in the ccosallocatr4.ave script.

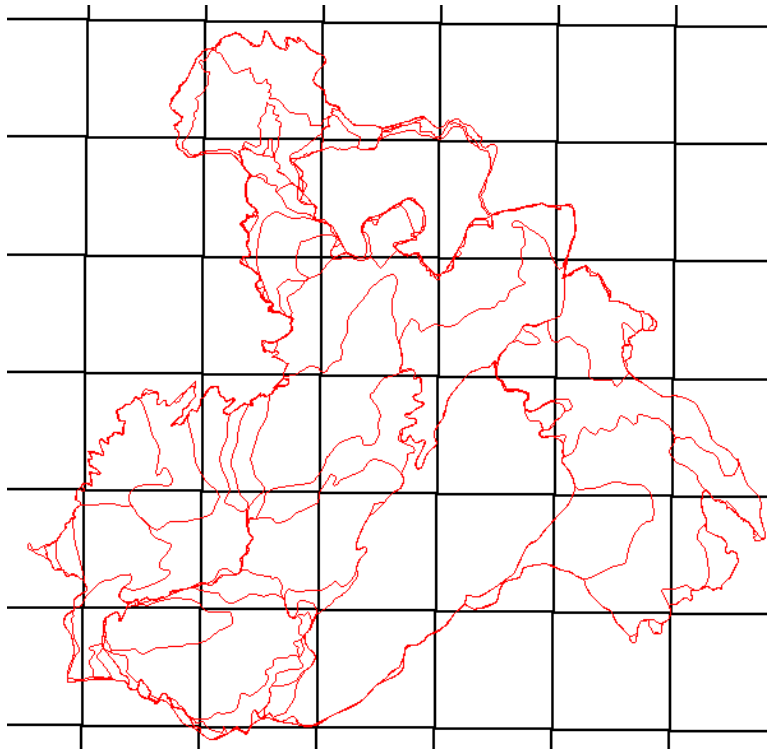


Figure 20. CCOS domain polygons in black and daily Manter polygons in red. Multiple days can be allocated to a single CCOS polygon and on day can be allocated over several CCOS polygons.

Discussion

The results indicate that spatial allocation on a daily temporal basis is possible given availability of fire progression data. Despite the uncertainty in the methods of data collection, with some pre-processing, the data can be used for emissions estimation and to create outputs in a variety of formats. Table 16 shows the magnitude of the emissions estimates for the Manter fire. Boundary discrepancies discussed earlier could be a source of error in this computation. In the spatial differencing process, numerous “archipelagos” of sliver polygons were created at places where fire boundaries of multiple days are coincident. It is not clear whether these sliver polygons are a result of small pockets of fire advancement between days, or whether they are the manifestation of errors occurring during data collection (if the boundary was actually unchanged between days, but was mapped multiple times with slightly different positional results).

The spatial representation of the data can take many forms, as illustrated by the grid, above. This map shows the loss of information that occurs with conversion of the estimates to lower resolution raster data. This loss of information is avoided by keeping the allocation framework in polygon format, as with the CCOS domain. This allows better accounting of emissions by avoiding the “washing out” effects of conversion to a large cell size. A large amount of information is retained, as evidenced by the 34x162 matrix of values created by `ccosallocatr4.ave` for the distribution of daily emissions into the CCOS polygons.

At a finer temporal resolution, burning occurs in two distinct phases: flaming and smoldering. The evolution of emissions from any burning area will be a function of the phase in which the fire is burning, thus the time since ignition. Future modeling may need to address this issue, but the CAMFER EES is currently incapable of temporal decomposition of emission production. With the current estimates, the simplest way to allocate emission hourly is to divide the daily estimates by 24. Other non-linear apportionment schemes exist for more accurate emissions distribution over a 24 hour period (AirSciences, Inc. 2002).

Conclusion

CAMFER allocated emissions from a large wildfire on a daily basis and in a variety of spatial formats. We have shown daily values of emissions, estimated with the EES, distributed over grid cells, into daily polygons, and over the CCOS domain polygons. The capability of this decomposition of emissions to finer spatial and temporal resolution is highly dependent on input data. While we assessed the feasibility of using a modeling approach to generate the input data, the demand for inputs to the model and resultant uncertainty in model output precludes the use of this approach for all but the most intensely measured fires. The CAMFER approach makes use of daily progression polygons, mapped in the field, for daily emissions estimation. The possibility of using remote sensing techniques to measure daily burning is constrained by a minimum pixel size of one kilometer. However, possible application of this technique is addressed in the 'Fire Mapping' section.

References

AirSciences, Inc. 2002 "Draft Final Report – 1996 Fire Emission Inventory"
Prepared for: Western Governors Association / Western Regional Air Partnership.
Online link:
http://www.wrapair.org/forums/FEJF1/emissions/FEJF1996EIReport_021208.PDF

Section 4 – Adding Additional Pollutants to Emissions Estimates

Introduction

The CAMFER Emissions Estimation System (EES) uses the Forest Service's First Order Fire Effects Model (FOFEM, Reinhardt et al. 1997) equations for the emissions estimation module of the EES. In order to make use of these equations in a Geographic Information System (GIS) that is capable of storing and processing of large amounts of spatial data, we coded the published FOFEM algorithms into Avenue, ESRI's scripting language for the ArcView software, as well as into Visual Basic

The EES also makes use of FOFEM tables of emission factors (reference table 4, Reinhardt et al. 1997) to derive the mass of individual pollutants that are emitted from fires. Previous versions of the EES were capable of estimating only those pollutants represented by emission factors in the published FOFEM tables: PM₁₀, PM_{2.5} and Carbon Monoxide (CO). However, a large number of gaseous and other emissions are produced by biomass burning (Helas 1995. Fearnside 2000. Conrad and Ivanova 1997. Cofer et al. 1991). In the interest of air quality monitoring and management, the California Air Resources Board (ARB) required the CAMFER EES to be expanded to include the capability of estimating a wider array of emissions species than originally incorporated to FOFEM. This section describes the expansion of emissions estimation capability in the CAMFER EES.

Methods and Results

The FOFEM emission factors are computed for PM₁₀, PM_{2.5} and CO based on functions of combustion efficiency and the ratio of flaming to smoldering combustion phases under different moisture regimes (Reinhardt et al. 1997). In order to preserve as much consistency as possible in the computation of emissions, CAMFER used the combustion efficiencies for flaming and smoldering phases as shown in the FOFEM documentation (reference Table 3, Reinhardt et al. 1997). The use of the FOFEM ratios of combustion efficiencies was essential to maintaining the functionality of the system with regard to expanded emissions estimation. This is because the ratios of flaming to smoldering combustion are adjusted based on different moisture regimes. In order to preserve the sensitivity of emissions estimations to changes in moisture regime, CAMFER used the ratios of combustion efficiency to generate the new emission factors.

The emission factors used in FOFEM were produced using the table of combustion efficiency in the FOFEM documentation and equations published in Ward and Hardy (1991). As a first step in the expansion of emissions estimations, CAMFER used an equation for Carbon Dioxide (CO₂) that is also reported in Ward and Hardy (1991) to create a table of CO₂ emission factors in the same format as the existing FOFEM table. As a result, we created a table of emissions factors for CO and CO₂, under three moisture regimes, that was produced based on ratios of flaming to smoldering combustion phases. In this way, we utilized a method for the addition of CO₂ emission factors that is consistent with the method of creation of the "stock" FOFEM emissions. This process is

illustrated in Table 17. The emission factors for CO and CO₂ formed the basis of subsequent emission factor computations.

Fuel Name	Combustion Efficiency		Combustion Phase Ratios by Moisture Regime					
	F	S	Wet		Normal		Dry	
			F	S	F	S	F	S
Litter, wood 0-1 inch	0.95	0.00	1.00	0.00	1.00	0.00	1.00	0.00
Wood 1-3 inches	0.92	0.00	1.00	0.00	1.00	0.00	1.00	0.00
Wood 3+ inches	0.92	0.76	0.50	0.50	0.70	0.30	0.80	0.20
Herb, shrub, regen	0.85	0.00	1.00	0.00	1.00	0.00	1.00	0.00
Duff	0.90	0.76	0.50	0.50	0.40	0.60	0.40	0.60
Canopy fuels	0.85	0.00	1.00	0.00	1.00	0.00	1.00	0.00
Weighted Average Emission Factor								
CO₂								
Litter, wood 0-1 inch			3482.7		3482.7		3482.7	
Wood 1-3 inches			3372.7		3372.7		3372.72	
Wood 3+ inches			3079.4		3196.8		3255.408	
Herb, shrub, regen			3116.1		3116.1		3116.1	
Duff			3042.8		2991.5		2991.456	
Canopy fuels			3116.1		3116.1		3116.1	
CO								
Litter, wood 0-1 inch			52.4		52.4		52.4	
Wood 1-3 inches			111.4		111.4		111.4	
Wood 3+ inches			268.9		205.8		174.4	
Herb, shrub, regen			249.2		249.2		249.2	
Duff			288.6		316.1		316.1	
Canopy fuels			249.2		249.2		249.2	

* CO₂ = 2(1833*Combustion Efficiency). Units in pounds of pollutant per tons of fuel consumed.
 * CO = 2[961-984(Combustion Efficiency)]. Units in pounds of pollutant per tons of fuel consumed.
 * Equations from Ward and Hardy (1991)
 * Combustion efficiencies and Flaming(F)/Smoldering(S) ratios from Reinhardt et al. (1997)

Table 17. Process used in the creation of carbon dioxide and carbon monoxide emission factors. The data at the upper part of the table is from FOFEM and the weighted average emission factors were computed using the equations below.

The CAMFER method of emission factor generation, proposed by Lobert et al. (1991), utilizes “emission ratios” to either CO or CO₂. This approach is based on the observation that emissions correlate with either CO₂ or CO depending on whether the compound is evolved primarily in the flaming or smoldering phase (Lobert et al. 1991. Battye and Battye 2002. Cofer et al. 1991). In the flaming phase, combustion efficiency is high, CO₂ and H₂O are the primary products of the reaction, and the high temperatures result in pyrolysis and/or volatilization of compounds including N₂O, NO_x, and SO₂. In the smoldering phase, combustion is not as efficient, temperatures are lower and a higher

proportion of CO, non-methane hydrocarbons, and NH₃ is produced (Lobert et al. 1991. Battye and Battye 2002).

These correlations indicate that the mass of various pollutants emitted through burning of biomass can be “predicted” based on the mass of CO₂ or CO that is emitted. The construction of the table of CO₂ and CO emission factors for “wet,” “moderate,” and “dry” conditions (table 1) enabled CAMFER to use emission ratios to predict additional emission masses based on the relationship:

$$EF_X = EF_{COorCO_2} * Mass_X / Mass_{COorCO_2}$$

Where EF is an emission factor expressed as mass of the pollutant emitted to the air per mass of biomass consumed. With one exception, CAMFER used *in situ*, empirical data reported in the literature for the computation of mass ratios. This data derives from an element (or mass) balance approach and involves direct sampling of smoke plumes above wildland fires to determine relative concentrations of pollutants above ambient levels (Einfeld et al. 1991, Radke et al. 1991, Susott et al. 1991). For emissions of CH₄, NH₃, N₂O, and NO_x, we relied on data reported in Radke et al. (1991) for mass ratios. This study seemed most appropriate due to the fact that values reported are averages of measurements from 10 separate fires from a variety of locations in Western states. We computed mass ratios for N₂O and NO_x relative to CO₂ but Radke et al. (1991) reports mass ratios to CO for CH₄ and NH₃ and CAMFER used these values directly. In the derivation of a TNMHC to CO mass ratio, CAMFER computed ratios from Einfeld et al. (1991) and Cofer et al. (1991) based on the reported “total” and “mixed” values, respectively. We averaged the two computed ratios in order to produce a mass ratio that would be representative of multiple ecosystem types. SO₂ is the only pollutant for which a mass ratio was derived using, in part, laboratory data. We used the average mole ratio reported by Battye and Battye (2000) converted to a mass ratio of SO₂ to CO₂.

CAMFER used the table of emission factors for CO and CO₂ with the compilation of mass ratios to produce emission factors for all the above pollutants. Since the new emission factors are correlated with CO₂ or CO, the new emission estimates are sensitive to changes in moisture regime that alter the relative amounts of flaming and smoldering combustion in fires. In this way, the new emission estimates are grounded in the same assumptions as the “stock” FOFEM emission estimates for PM₁₀, PM_{2.5}, and CO. In basing the expanded emissions estimates on the methodology inherent to FOFEM, CAMFER created an internally consistent table of emission factors. These emission factors are shown in Table 18 (a transposed version of emfac.dbf) for the three moisture regimes handled by the EES.

Discussion

Battye and Battye (2000) provide an excellent review of emissions factors and mass ratios culled from the literature. We used their report to “check” the derived emission factors (except methane, which was not reported, and sulfur dioxide) shown in Table 18. In all cases, the CAMFER emission factors are close to the averages reported by Battye

and Battye (2000), usually slightly less than one standard deviation above the average. This discrepancy could be due to the fact that CAMFER did not use data from laboratory test trials (except NH₃). Battye and Battye (2000) include data from laboratory studies in their averages. Since wildland fire burns under a diversity of fuel, moisture, topographic, and vegetation conditions that are impossible to mimic in a laboratory setting, we made the assumption that empirical data would better represent emissions as they impact air quality. It is also the case that the CAMFER system is not conducive to distillation of a single emission factor for each pollutant. This is the result of the complexity of the system: the use of a different emission factor for six different fuel components under three different moisture regimes. The weighting of the factors is in turn dependent on the fuel model corresponding to the ecosystem type being modeled.

Table 18. Complete set of emission factors included in the EES. The shaded portion of the table represents the added emission factors. The unshaded portion are the standard FOFEM emission factors.

Pollutant	Moisture Regime	Litter, wood 0-1 inch	Wood 1-3 inches	Wood 3+ inches	Herb, shrub, regen	Duff	Canopy fuels
<i>emission factor in pounds of emissions per ton of fuel consumed</i>							
PM10	Wet	9.30	14.00	26.60	25.10	28.20	25.10
PM10	Moderate	9.30	14.00	21.60	25.10	30.40	25.10
PM10	Dry	9.30	14.00	19.10	25.10	30.40	25.10
PM25	Wet	7.90	11.90	22.50	21.30	23.90	21.30
PM25	Moderate	7.90	11.90	18.30	21.30	25.80	21.30
PM25	Dry	7.90	11.90	16.20	21.30	25.80	21.30
CO	Wet	52.40	111.40	268.90	249.20	288.60	249.20
CO	Moderate	52.40	111.40	205.80	249.20	316.10	249.20
CO	Dry	52.40	111.40	174.40	249.20	316.10	249.20
CH4	Wet	2.10	4.46	10.76	9.97	11.54	9.97
CH4	Moderate	2.10	4.46	8.23	9.97	12.64	9.97
CH4	Dry	2.10	4.46	6.98	9.97	12.64	9.97
TNMHC	Wet	3.67	7.80	18.82	17.44	20.20	17.44
TNMHC	Moderate	3.67	7.80	14.41	17.44	22.13	17.44
TNMHC	Dry	3.67	7.80	12.21	17.44	22.13	17.44
NH3	Wet	0.52	1.11	2.69	2.49	2.89	2.49
NH3	Moderate	0.52	1.11	2.06	2.49	3.16	2.49
NH3	Dry	0.52	1.11	1.74	2.49	3.16	2.49
N2O	Wet	0.49	0.47	0.43	0.43	0.42	0.43
N2O	Moderate	0.49	0.47	0.45	0.43	0.42	0.43
N2O	Dry	0.49	0.47	0.45	0.43	0.42	0.43
NOX	Wet	8.23	7.97	7.27	7.36	7.19	7.36
NOX	Moderate	8.23	7.97	7.55	7.36	7.07	7.36
NOX	Dry	8.23	7.97	7.69	7.36	7.07	7.36
SO2	Wet	2.53	2.45	2.24	2.27	2.21	2.27
SO2	Moderate	2.53	2.45	2.33	2.27	2.18	2.27
SO2	Dry	2.53	2.45	2.37	2.27	2.18	2.27

Conclusion

CAMFER upgraded the EES to have the capability of producing emissions estimates for PM₁₀, PM_{2.5}, CO, methane (CH₄), Total Non-Methane Hydrocarbons (TNMHC), Ammonia (NH₃), Nitrous Oxide (N₂O), Oxides of Nitrogen (NO_x), and Sulfur Dioxide (SO₂). The modular nature of the EES facilitated this update in that the system runs and produces emissions estimates using the same method as previous versions, with only minor updates to several component scripts and the expansion of the table of emission factors. The table of emission factors (emfac.dbf) is part of the EES. However, the values can easily be updated as information becomes available with no change to the EES aside from the insertion of a new table. The complexity of the FOFEM emission estimation routines is preserved in the CAMFER EES and makes use of a wide array of emission factors for different fuel types and different moisture regimes. Emission factors are thus scaled by vegetation type, and abiotic conditions that affect the ratios of flaming to smoldering phases of combustion.

References

- Battye, William and Rebecca Battye. 2002. "Development of Emissions Inventory Methods for Wildland Fire." U.S. Environmental Protection Agency Contract No. 68-D-98-046. Online Link: <http://www.epa.gov/ttn/chief/ap42/ch13/related/c13s01.html>
- Cofer, Wesley R. III, Joel S. Levine, Edward L. Winstead, Brian J. Stocks. 1991. "Trace Gas and Particulate Emissions from Biomass Burning in Temperate Ecosystems." In: *Global Biomass Burning: Atmospheric, Climatic and Biospheric Implications*. Joel S. Levine, editor. MIT Press.
- Einfeld, Wayne, Darold E. Ward, Colin Hardy. 1991. "Effects of Fire Behavior on Prescribed Fire Smoke Characteristics: A Case Study." In: *Global Biomass Burning: Atmospheric, Climatic and Biospheric Implications*. Joel S. Levine, editor. MIT Press.
- Griffith, David W. T., William G. Mankin, Michael T. Coffey, Darold E. Ward, Allen Riebau. 1991. "FTIR Remote Sensing of Biomass Burning Emissions of CO₂, CO, CH₄, CH₂O, NO, NO₂, NH₃, and N₂O." In: *Global Biomass Burning: Atmospheric, Climatic and Biospheric Implications*. Joel S. Levine, editor. MIT Press.
- Lobert., Jurgen M., Dieter H. Scharffe, Wei-Min Hao, Thomas A. Kuhlbusch, Ralph Seuwen, Peter Warneck, Paul J. Crutzen. 1991. "Experimental Evaluation of Biomass Burning Emissions: Nitrogen and Carbon Containing Compounds." In: *Global Biomass Burning: Atmospheric, Climatic and Biospheric Implications*. Joel S. Levine, editor. MIT Press.
- Radke, Lawrence F., Dean A. Hegg, Peter V. Hobbs, J. David Nance, Jamie H. Lyons, Krista K. Laursen, Raymond E. Weiss, Phillip J. Riggan, Darold E. Ward. 1991. "Particulate and Trace Gas Emissions from Large Biomass Fires in North America." In:

Global Biomass Burning: Atmospheric, Climatic and Biospheric Implications. Joel S. Levine, editor. MIT Press.

Reinhart, Elizabeth D., Robert E. Keene, James K. Brown. 1997. "First Order Fire Effects Model: FOFEM 4.0, User's Guide." USDA Forest Service, Intermountain Research Station, General Technical Report INT-GTR-344.

Susott, Ronald A., Darold E. Ward, Ronald E. Babbitt, Don L. Latham. 1991. "The Measurement of Trace Emissions and Combustion Characteristics for a Mass Fire." In: *Global Biomass Burning: Atmospheric, Climatic and Biospheric Implications.* Joel S. Levine, editor. MIT Press.

Ward, Darold E. and Colin C. Hardy. "Smoke Emissions from Wildland Fires." 1991. *Environment International.* v17. pp.117-134

Section 5 – Development of Web and Desktop Tools for Fire Emission Estimation

Introduction

Sorry about this Nick. It seems like we should add a section summarizing the work VESTRA has done in tasks 6, 7, 8, 9. It can be pretty simple.

Mention the functionality of the products, the benefits, conversion to Visual Basic to support the new ArcGIS platform, the work with ARB to identify most relevant features that could be included within the contract constraints. Mention that the products, and all relevant scripts and code are provided on the data disc. Then a series of screen shots with example output would be good. This section might not fit the format used for the other sections.

Or, alternatively, you could add an additional appendix for this info, but it seems to me like it should be part of the body report.

Appendix

- **Wildland Fire Emissions Estimation System, Version 4 (Visual Basic),**
Programmer's Guide and Usage Notes
- **Wildland Fire Emissions Thematic Mapper, User and Configuration Guide**
- Avenue scripts used for geographic processing:

Analyzer2.ave
Assignr.ave
Avgmakr.ave
Ccosallocatr4.ave
Centroidmod.ave
Combinetables2.ave
Combinr.ave
Convertr.ave
Dailymakr2.ave
Dailymakr3.ave
Distributr.ave
Fdimport.ave
Gridmakr99.ave
Nibbler.ave
Rslinkr.ave
Startr.ave
Statmakr.ave

- Tables of comparison for CAMFER fire maps.

1996 Land Cover comparison
1996 Eco-region comparison
1999 Land Cover comparison
1999 Eco-region comparison

Wildland Fire Emissions Estimation System, Version 4

Programmer's Guide and Usage Notes

July 7, 2003

Created by:

VESTRA Resources, Inc.

962 Maraglia Street
Redding, CA 96002
Tel. (530) 223-2585
Fax (530) 223-1145



© 2003 VESTRA Resources, Inc.

Contents

Introduction	67
Installing the EES MXD	67
Key EES Usage Notes	67
General VBA Components	69
ThisDocument	69
Forms	69
Modules	70
Class Modules	71
Key EES Procedures.....	71
frmFuelInput	71
clsFOFEM	72

Introduction

The Wildland Fire Emissions Estimation System (EES) was developed by the University of California-Berkeley (UCB) using ESRI's ArcView 3.x software. VESTRA Resources, Inc. was contracted to migrate this system to ESRI's latest GIS software platform: ArcGIS 8. There are a number of upgrades associated with this migration, however the core EES functionality and calculations remain the same.

The ArcGIS version of the Wildland Fire Emissions Estimation System is written in Visual Basic for Applications (VBA) and deployed as a customized ArcMap document (MXD). Deploying the EES as an MXD allows easy access to the code for upgrades and other modifications.

This document provides an overview of the key elements of the Wildland Fire Emissions Estimation System. The basic modules and key procedures are described below and can be easily accessed through the Visual Basic Editor window of the MXD.

Installing the EES MXD

The Wildlands EES MXD, **ees4.mxd**, delivered on CD-ROM uses relative path names, so it should open on any computer so long as the corresponding **data** directory is in the proper place. The easiest way to ensure this is to copy the entire **ees4** folder from CD-ROM to the destination folder on your computer. This folder also contains the necessary emissions tables stored in the relative position required by the code.

A reminder when working with folders and files that originate on CD-ROM: In order to make changes to **ees4.mxd** and save output files in subfolders, the "Read Only" attribute must be unchecked (on the **ees4** folder and all its contents) after copying to your hard drive.

Key EES Usage Notes

Following are some salient points regarding the use of the Wildland Fire EES:

1. This version of the EES *requires* that the fire perimeter and vegetation shapefiles have a spatial reference defined (*i.e.*, have a .prj file). This requirement ensures that the necessary geoprocessing (intersecting the fire perimeter with the vegetation polygons) is performed correctly. All layers included on the CD-ROM have a spatial reference defined to California (*i.e.*, Teale) Albers. ArcMap is capable of projecting data on the fly, so the vegetation and fire layers do NOT have to have the *same* spatial reference. However, it is recommended to always use the same spatial reference for all layers. New shapefiles created by the “Fire Perimeter” tool inherit the spatial reference of the MXD’s dataframe, which is also California Albers in ees4.mxd.
2. The Wildland Fire EES MXD was developed using ArcMap version 8.2. The ees4.mxd is an ArcMap version 8.2 document. This MXD will not open under ArcMap 8.1, as MXD files are not backward compatible. However, VESTRA has performed limited testing under ArcMap version 8.3 (latest as of July 2003), and the EES appears to work fine under this version.
3. The Wildland Fire EES code requires that Microsoft Scripting be installed on any computer used to run the EES. Microsoft Scripting should already be available on any Windows system. However, if any errors pertaining to Microsoft Scripting or the “FileSystemObject” are raised, then the version of Microsoft Scripting may need to be updated. The CD-ROM contains the installation package for version 5.6 (the latest version as of 7/2/2003). The installation package can also be downloaded from the Microsoft website.
4. Anyone using this MXD can access the Visual Basic Editor window and, thus, can edit the code. Therefore, if many individuals will be using this or copies of this MXD, the manager(s) of this project may want to consider password protecting the code. To do so, open the Visual Basic Editor (Alt + F11). In the main menu bar, click on ‘Tools’, then ‘Project Properties’. In the window that is displayed, click on the ‘Protection’ tab. Check the ‘Lock project for viewing’ box and then enter a password. Upon opening the project again, a user will have to enter this password to view the code.
5. All of the buttons created in this MXD are contained on one toolbar. If this toolbar does not appear automatically (for instance, a previous user closed it), right-click on any toolbar, and, in the list that appears, select ‘Wildland Fire Emissions Estimation System’. Figure 1 below shows the toolbar in its initial mode. The editing buttons become enabled once ‘Create New Perimeter’ is clicked and a new fire polygon is created.

Figure 1 – EES Toolbar



6. The editing buttons are simply calling ArcMap editing functions and can be used in conjunction with the other editing capabilities of the ArcMap toolbar. Because these are calling the pre-existing functions, the behavior is similar. For instance, when editing geometry, the user must either click elsewhere on the screen or 'Finish Sketch' to save the edits. If they continue by stopping the edit session or with other edit operations before specifically finishing this sketch, those polygon edits may not be saved.

General VBA Components

A Visual Basic for Applications document is comprised of several types of sub-components, including **forms**, **modules**, **classes** and (in the case of ArcMap customizations) the custom class module **ThisDocument**. Following is a brief discussion of the components that make up the Wildland Fire EES:

ThisDocument

ThisDocument is a custom class module that represents the specific ArcMap document associated with a VBA project – it is the connection between the ArcMap interface and the underlying VBA code that comprises the EES. **ThisDocument** contains the event handlers and code associated with the buttons on the Wildland Fire EES custom toolbar (Figure 1). **ThisDocument** also contains the important enabling code that “watches” for certain edit events to trigger the display of forms and enable other buttons on the toolbar, as appropriate. An example of this behavior is when the “Attributes” form (**frmNewAttribute**) is displayed after the user double-clicks to complete the entry of a new fire polygon.

Forms

frmFuelInput: This is the primary form in the EES. It contains all functions and procedures associated with performing the emissions estimations, including the user input. Figure 2 depicts the default fuel input form.

Figure 2 – Fuel Input Form

Wildland Fire Emissions Estimation System - General Fuel Input

Welcome to the Wildland Fire Emission System for PC

Select a fire input theme or year

Select a fire theme for analysis.

Air Basins

Select a year for analysis.

Activate special GAP processing!

Define the fire input parameters

Fuel Category: Natural

Dead fuel adjustment factor: Typical

Moisture conditions: Very dry

Fire intensity: Extreme

Will this fire burn tree crowns: Yes No

Tree crown biomass burning: Typical

Herbaceous density: Typical

Shrub density: Typical

Tree regeneration density: Typical

Enter NFDR-TH moisture 20 %

Get NFDR-TH Moisture from grids

Path to NFDR-TH moisture grids: Browse...

Help Cancel Next

frmNewAttribute: Form called during creation of a new polygon using the custom tools; this form prompts the user for a year, month, and day from the user for the new polygon.

frmSplashScreen: Title screen displayed on startup of the map document.

frmSummary: Large text box for displaying the help text and the final summary of the emissions estimations.

Modules

mdlCreateField: Standard functions for creating different types of fields.

mdlCreateShapefile: Functions and procedures involved in creating and adding a new fire perimeter shapefile to the current map document.

mdlGeneral: Basic functions and procedures called by many different modules.

mdlGlobal: Global variables and the procedures to set them.

Class Modules

clsFOFEM: Functions and procedures to perform the FOFEM calculations for a given cover type and its area. These were placed in a class to allow for ease in upgrading to different methods for performing these calculations in the future, such as calling a stand-alone FOFEM function.

Key EES Procedures

Following are additional details of two key modules within the MXD – **frmFuelInput** and **clsFOFEM**. These are the two modules that contain the key procedures and functions for performing the emissions calculations. For more information on the flow between these functions and procedures, see the accompanying flowchart, **UCB Wildland Fire Emissions Estimation System – High Level Program Flow (EES4_ArcGIS_Flowchart.pdf)**.

frmFuelInput

- **RunEES** Sub – This is the ‘main’ sub routine that controls the flow of the calculations and calls the following procedures:
 - **SetParameters** Sub – Validates the input: verifies that a ‘Fire History’ layer exists, if the user chose to select by year; verifies that a ‘Landcov’ layer exists; verifies that the landcover and fire layer both have a spatial reference (this is required to use the geoprocessing tools needed to “clip” the landcover by the fire perimeter); if the user chose to use moisture grids, verifies that there is a grid for every month in the indicated path; creates a temporary directory within the .mxd workspace to store interim tables; and sets the workspace variables.
 - **CreateOutputTable** Sub – Creates the final output table. All of the output fields are added here; note that the field names are all hardcoded due to their large number.
 - **SelectFirePolysSS** Function – Selects all the fire polygons for the chosen layer if the user opted to perform the analysis on an entire layer or selects the fire polygons from a user-specified year from the Fire History layer. The selection set is returned from this function.
 - **GetMonthAndSeason** Sub – Gets the month of the specified fire polygon (from the ‘Month’ field, not the ‘Date’ field) and determines the season based on this month. If the ‘Month’ field does not exist or the month is invalid (*i.e.*, less than 1 or greater than 12) then the month is assumed to be 9 and the season is assumed to be fall.
 - **GetMoisturePerc** Function – This is only called if the user opts to get NFDR-TH moisture from the monthly grids. For a given fire polygon, the moisture grid for that month is loaded into ArcMap, and the cell value that corresponds to the center of the fire polygon (label point) is returned from this function.

- **GetCoverArea** Function – Within this function, the passed fire polygon and the landcover layer are intersected. The area of each covertype within that polygon is determined and stored in a temporary table, which is returned from this function. If the user opted to perform the GAP processing, the table that is returned contains the covertypes and areas for each of the three covertypes listed for one landcover polygon.
- **JoinDescInfo** Sub – Information from fireinfo.dbf and cnddbdesc.dbf are joined to the output table of all calculated emissions.
- **CalcSummary** Sub – Summarizes the output table by fire id (or unique id, if there was no 'FIRES_' field in the original table), adding all of the emissions for each. This is saved to another .dbf file, named similar to the original table. Also, a total summary of all pollutants estimated in the entire selection set is performed and written to a text file.

clsFOFEM

- **InitializeParameters** method – All string parameters (moisture condition, densities, etc.) are passed to and set in this routine, which is called from RunEES within frmFuelInput. The path to the directory that contains the emfac.dbf and cnddbcodes.dbf is also passed.
- **RunCalculations** method – Controls all the FOFEM calculations for a single passed covertype and area. The output table is also passed and updated directly by this routine. Note that covercodes that are not found in the cnddbcodes.dbf (*e.g.*, '99999') are not added to the output table.



Wildlands Fire Emissions Thematic Mapper
UC Berkeley research funded by the California Air Resources Board

User & Configuration Guide

July 1, 2003

Created by:

VESTRA Resources, Inc.

962 Maraglia Street
Redding, CA 96002
Tel. (530) 223-2585
Fax (530) 223-1145



© 2003 VESTRA Resources, Inc.

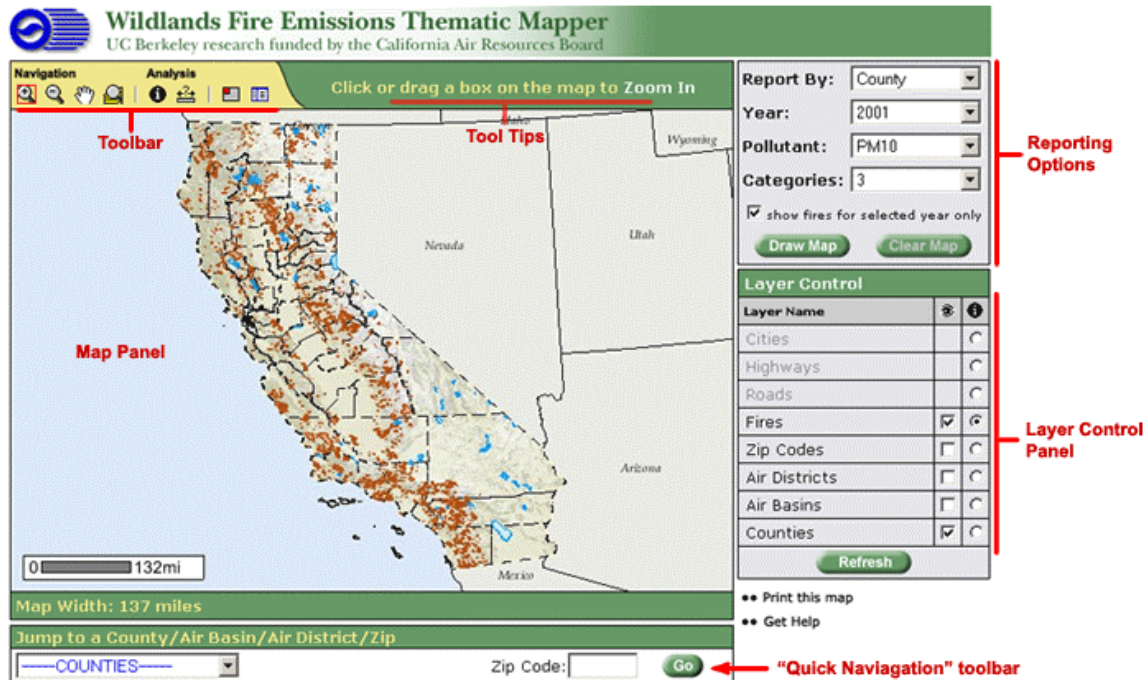
Contents

Chapter 1: Using the Wildlands Thematic Mapping Application.....	76
The Interface	76
Using the Reporting Options to Render the Map.....	77
Chapter 2: Configuring the Wildlands Thematic Mapping Application	79
The MapServices	79
Layer Index Constants	79
Controlling How Layers “Behave” in the Wildlands Mapper	80
Controlling the Results Returned by the Identify Tool.....	81
Making Changes to the Wildlands MapServices	83
Editing ArcIMS MapService Files (*.AXL).....	88
Configuring the Contents of the Reporting Option Menus.....	93
Other Configuration Constants (map_config.asp)	93
Appendix 1: Installation Checklist.....	94

Chapter 1: Using the Wildlands Thematic Mapping Application

This chapter is an introduction to the *Wildlands Fire Emissions Thematic Mapper* interface and its key functionality.

The Interface



The Toolbar

The Toolbar contains eight tools that allow you to navigate around the map, identify features on the map, and view a vicinity map and map legend.

Tool Tips

Tool Tips are messages about the usage of the map tools found on the interface. When you hover your mouse over a tool icon the Tool Tip tells you the tool's name. When you select a tool the message will change to tell you how the tool is used.

Layer Control Panel

The Layer Control Panel is a list of all the map layers that a user can make visible/invisible and set as the "active" layer for use with the Identify map tool. To turn a layer on/off, simply check or uncheck the box next to the layer name and press the "Refresh" button at the bottom of the panel. At some map scales layer names will be "grayed out" – these are scale-dependent layers, layers

that cannot be view beyond and/or beneath certain scales. To set a layer as your “active” layer for identifying, click the radio button next to the layer’s name. There can only be one active layer at any given time.

“Quick Navigation” Toolbar

Select a county, air basin, or air district from the drop-down list to jump to your area of interest, or enter a zip code into the text box provided and click “Go” to jump to a zip code.

Reporting Options

The Reporting Options panel allows you to select criteria for rendering the map by pollutant and fire year. Refer to the next section for detailed instructions on using the Reporting Options.

Using the Reporting Options to Render the Map

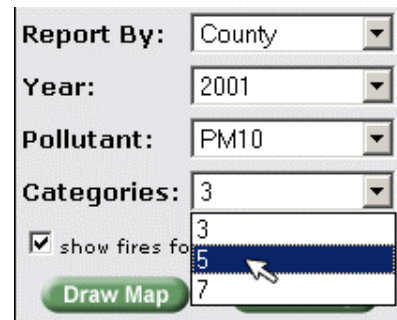
Step 1. Select your criteria using the drop-down lists.

Report By – Choose a political boundary to map: County, Air Basin, or Air District

Year – Choose any year between 2001 and 1990

Pollutant – Choose from the 10 pollutants listed

Categories – Specify the number of natural breaks to use in the rendering



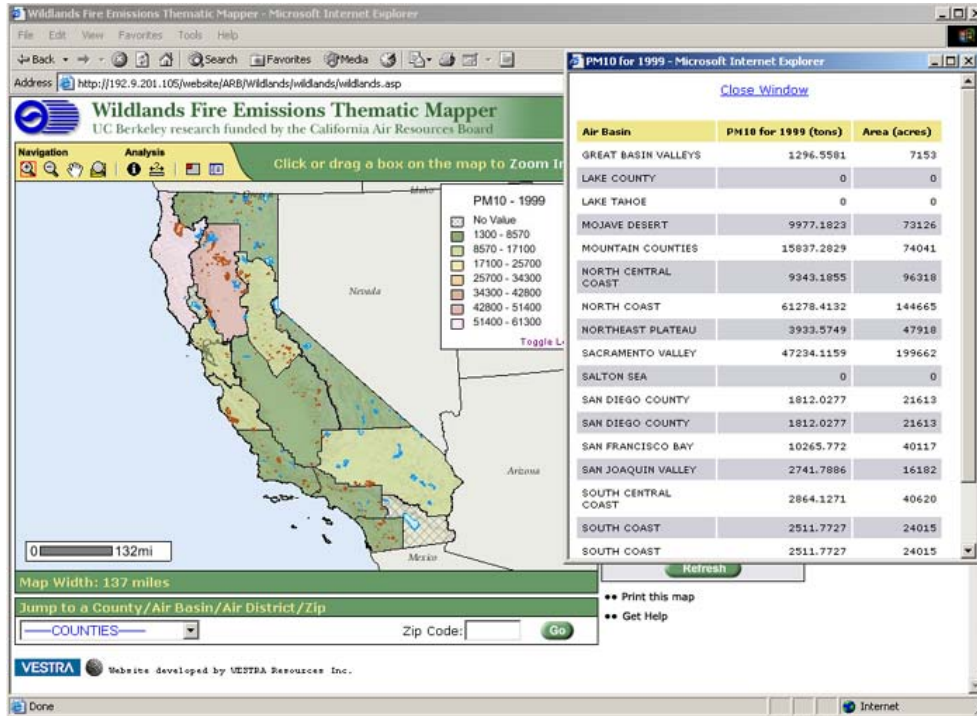
Step 2. Use the “show fires for selected year only” check box to specify whether you want to see *all* fire polygons (rust colored features on the map) after the map has been rendered, or just the fires that burned the year you have selected.



Step 3. Click “Draw Map”



Step 4. View results.



Chapter 2: Configuring the Wildlands Thematic Mapping Application

The *Wildlands Fire Emissions Thematic Mapper* has been designed so that all configurable components of the application are stored in a single file, **map_config.asp**. This chapter is intended to highlight the most pertinent sections of this file, and provide instructions for making changes to how the application is configured.

Note: the configuration file will need editing only on the rarest of occasions, if at all. For the most part, the contents of this chapter have been placed in order, from the most pertinent configurable aspects of the application, to those that will seldom need attention.

The MapServices

A MapService makes the contents of a map configuration file (.axl) accessible on the web. The *Wildlands Fire Emissions Thematic Mapper* uses two map configuration files, *wildlands.axl* and *wildlands_ov.axl*, to create two MapServices: **wildlands** and **wildlands_ov**. These MapServices are referenced on lines 11 and 12 in *map_config.asp*:

```
Const mc_MapSvcMain = "wildlands" ' Main map ArcIMS MapService
Const mc_MapSvcOV = "wildlands_ov" ' Overview map ArcIMS MapService
```

It is imperative that these two constants correctly refer to the two MapServices required for the application. For more information on creating MapServices see Appendix 1: Installation Checklist.

Layer Index Constants

Layer Index Constants are used to reference a map layer's position in a MapService, and play an important role in the application code. The constants can be found in the configuration file, *map_config.asp*, starting at line 27. Below is a sample listing of the *Layer Index Constants* list taken from *map_config.asp*:

```
Const mc_nLyrIndx_California_relief = 1
Const mc_nLyrIndx_Ocean = 2
Const mc_nLyrIndx_Neighbor_States = 3
Const mc_nLyrIndx_Counties = 4
Const mc_nLyrIndx_Air_Basins = 5
Const mc_nLyrIndx_Air_Districts = 6
...
Const mc_nLyrIndx_Cities = 12
```

As you can see from this list, the California shaded-relief image is the first layer in the main MapService, followed by the Ocean layer, Neighbor States, and so on, through to the last layer, Cities.

The *Layer Index Constants* are used throughout the mapping application code to correctly reference map layers in the main MapService. For this reason, it is of the utmost importance that these indices be updated whenever changes are made to the MapService. Specifically, any update that changes the number and/or order of the layers in the MapService requires that these indices be changed accordingly.

Updating the Layer Index Constants

VESTRA has developed a web-based utility to re-write *all* of the layer index constants once a change has been made to a MapService. See *Appendix 1: Installation Checklist* for details on installing the utility on the web server.

To use the application, open your web browser to http://arb.ca.gov/gismo/utilities/Create_Layer_Consts.asp -- you will get a web page called the **VESTRA Utility: Layer Constant Creation**.

Note: the URL given above, and all others used throughout this document, is based on the suggested installation procedures (see *Appendix 1: Installation Checklist*).

Enter the name of the server on which your MapServices reside, and the server port number (for ArcIMS this is usually 5300). When you've finished, click the "Get Map Services" button – this will populate a drop-down menu with a list of the map services currently running on that machine. Selecting the map service of your choice (wildlands) will generate a list of layer index constants for the layers of that MapService. Copy and paste this list from the text area into the map_config.asp file, and delete the old layer index constants.

Controlling How Layers “Behave” in the Wildlands Mapper

The Wildlands Mapper can be configured to control which layers can be turned on/off (i.e., visible/invisible) by the user, and which can be identified on. All of this functionality is controlled by an array, which is initialized in the **map_config.asp** file (line 49). This array, called **vLayerCtrls**, is referred to as the *Layer Control Array*.

A typical element in the array looks like this:

```
' Fires                                Layer name
vLayerCtrls(7, 0) = 1                  Layer Visibility Control Index
vLayerCtrls(7, 1) = True                Allow Identify?
```

Layer Visibility Control Index:

Can be one of the three possible values described below:

0 = User NEVER has control over visibility

1 = Layer visibility is controlled via the main layer control panel

Allow Identify: Determines whether a user can use the Identify Tool on this layer. Possible

values:

True = User CAN identify features on this layer

False = User CANNOT identify features on this layer

Controlling the Results Returned by the Identify Tool

You can control the results returned by the Identify tool via an array found in the **map_config.asp** file. The array, called **sIdFldCtrl**, is found near the end of the file, starting on line 127.

The array allows you to control:

1. Which fields are included in the Identify results table.
2. Field aliases to use as column headings in the Identify results table.
3. Field widths to better format the Identify results table.

A typical element of the array looks like this:

```
sIdFldCtrl(3) = "7;CNTYNAME;Name;200"
```

Field Index Field Name Alias Width

Field Index: Field index in the layer's attribute table. With ArcIMS this is 1-based (e.g., first record's index = 1).

Field Name: Field name in the layer's attribute table

Alias: Alias to be used in column heading; this can contain spaces and some special characters but it is best to avoid characters that have special meaning in HTML (e.g., "<", ">"). The alias should NOT contain apostrophes, single or double quotes.

Width: Column width is optional, but if it is included for any fields, it MUST be included for ALL fields entered in the token list.

The example above would create a identify results table with a single item, *Name*. To create a table with multiple items, add more field tokens to the string:

```
"1;HWYNAME;Hwy Name;200|5;ALT1_NAME;Alt. Name;200"
```

field 1 token field 2 token

Fields must be separated by the “post” (|) character.

Displaying ALL fields in the Identify results table

There are two ways of displaying *all* of the fields in the attribute table:

1. Set the array element to "" (null). This method will use the field names from the shape file as column headings.

```
sIdFldCtrl(3) = ""
```

2. If you want to use all of the fields AND have the ability to set access levels, field aliases, and column widths, then you must create a field control array element that includes all of the layer's fields.

Displaying a SUBSET of the fields in the Identify results table

If you would like only a subset of fields to be returned by the identify tool, list only those desired fields in the array element. Fields left out of the token list are NOT displayed in the table - this is how certain fields in a layer's attribute table can be ignored.

Updating the field control array

If you have recently updated a shapefile and it now contains an additional item(s), it is important to update the field control array element for that layer.

VESTRA has developed a web-based utility to re-write the entire field control array, or to re-write individual elements of the array. See *Appendix 1: Installation Checklist* for details on installing the utility on the web server.

To use the application, open your web browser to http://arb.ca.gov/gismo/utilities/Create_FieldControl_Array.asp -- you will get a web page called the **VESTRA Utility: Create Field-Control Array Template**.

Enter the name of the server on which your MapServices reside, and the server port number (for ArcIMS this is usually 5300). When you've finished, click the "Get Map Services" button – this will populate a drop-down menu with a list of the map services currently running on that machine. Selecting the map service of your choice (wildlands) will generate a list of the map layers in that map service.

Updating the field control array following changes to a Shapefile

If you have just updated a *single* shape file you may want to refresh the array element associated with that layer, rather than the entire array. To do this, find and select the map layer in the layer list, then submit your choice by click the "Create Field-Control Template" button. A new array element for this layer will be written to the large text area below. The map layer list box also allows you to select multiple layers at a time. Hold down the shift or control button to select multiple layers.

The new array element(s) will include ALL of the fields in the shape file.

Note: the alias item has been set to a default value of "alias" – you must change this to the column heading of your choice.

Updating the *entire* field control array

If you want to refresh the *entire* field control array you may do so by selecting ALL of the map layers from the layer list menu, then clicking the “Create Field-Control Template” button. To select all of the map layers click on the first and drag down.

Applying your updates

To apply the new array, or new array element(s), open the **map_config.asp** file, and find the existing field control array (line 127). If you have invested a lot of time in setting up the current array, it is *not* recommended that you replace your existing array with the new template – you will have a lot of work to *redo*. Instead, use the appropriate lines from the template array as guides in making the necessary changes to your existing array. The lines from the template are *especially* useful in determining the proper index number for each field.

Make adjustments to the array elements as necessary:

- To eliminate a field, or fields, from the identify results table, delete the field token associated with that field.
- Replace the text “alias” with the column heading you want to appear in the identify results table.

Checking the updated Identify Field Control Array for errors

VESTRA has developed a web-based utility to check the field control array for errors. The application verifies that:

- All field indexes are numeric.
- The field alias has been changed from placeholder value of “alias”.
- Field widths are numeric.

Using your web browser, go to

http://www.arb.ca.gov/gismo/wildlands/check_fieldcontrol_array.asp.

This application has a large text area that lists every layer in the **wildlands** map service along with a message informing you on the status of each layer’s field control array element.

Making Changes to the Wildlands MapServices

The Wildlands Mapper has been designed in such a way that layers can be added, removed, renamed or reordered in the ArcIMS MapService, without the need for changes to the application code itself. However, there are changes that *must* be made to certain configuration constants and arrays in the application when changes are made to the MapService.

As discussed in the previous sections, a custom feature of Wildlands Mapper is the ability to configure layer-level control over visibility, and “Identify” tool results. All of this functionality is controlled by two arrays: the *Layer Control Array*, and the *Identify Field Control Array*. Both of these arrays need to be updated when certain changes are made to the Wildlands MapServices (wildlands, wildlands_ov). Specifically, any update that changes the number and/or order of the layers in a MapService requires that the arrays be changed accordingly.

Adding layers to the MapService

When adding layers to the Wildlands MapService, changes must be made to the *Layer Index Constants*, *Layer Control Array* and the *Identify Field Control Array* (“vLayerCtrls” and “sIdFldCtrl” in “map_config.asp”). There is a one-to-one relationship between MapService layers and the array elements in both arrays.

To add a new layer to the MapService:

1. Make a backup copy of the MapService’s current .AXL file. One way to organize backups is to rename the copy by appending the date to the end of the filename. For example, “wildlands.axl” could be backed up as “wildlands_20030601.axl”. Store these backups in a folder other than the folder containing the current .AXL file.
2. Add the new layer to the MapService. Since the Wildlands MapService is fairly complicated, this will almost certainly involve editing the AXL file with a text editor – there is little that can be done with ArcIMS Author without compromising the manual edits that have already been made.

The suggested approach is to copy and paste an existing <LAYER></LAYER> tag into the appropriate place in the .AXL file (see next section – *Editing ArcIMS MapService Files* for more details). Note that each layer *must* have a unique ID. The ID is an attribute of the <LAYER> element (*i.e.*, <LAYER ... id="0" ... >). Layer ID’s do not have to be sequential – in fact, they do not even need to be numeric.

3. Refresh the MapService using ArcIMS Administrator or Manager.
4. Update the *Layer Index Constants* in **map_config.asp** to reflect the new layer order. The recommended approach is to use the *Layer Constant Creation Utility*. See previous section (*Layer Index Constants*) for additional details.
5. Add a new array element to the *Layer Control Array*. This array is called “vLayerCtrls”, and is located in the **map_config.asp** file, line 49. A short review is given here. See previous section (*Controlling How Layers ‘Behave’ In the Wildlands Mapper*) for additional details.

- 5.1. The array must be re-dimensioned to accommodate the additional element:

```
Dim vLayerCtrls(11, 1)   line 49 in map_config.asp
```

The first number in the parentheses is the upper bound of the array, with the lower bound always being zero (lower bound can’t be changed in VBScript). That means the array, as dimensioned above, contains 12 elements, (*i.e.*, layer control definitions for 12 layers). That also means that array element *n* corresponds to layer *n+1* in the MapService.

- 5.2. A new array element must be inserted as the appropriate element in the array. All array elements after the one inserted must be incremented by 1.

6. Add a new array element to the *Identify Field Control Array*. This array is called “sIdFldCtrl”, and is located in **map_config.asp**. A short review is given here. See previous section (*Controlling the Results Returned by the Identify Tool*) for additional details.

6.1. The array must be re-dimensioned to accommodate the additional element:

```
Dim sIdFldCtrl(11) line 127 in map_config.asp
```

The number in parentheses is the upper bound of the array, with the lower bound always being zero (lower bound can't be changed in VBScript). That means the array, as dimensioned above, contains 12 elements, (*i.e.*, ID field definitions for 12 layers). That also means that array element *n* corresponds to layer *n+1* in the MapService.

- 6.2. A new array element must be inserted as the appropriate element in the array. All array elements after the one inserted must be incremented by 1. The recommended approach is to use the utility (described in the section – *Editing ArcIMS MapService Files*) to create a “template” array element for the new layer. This can be copy/pasted into **map_config.asp** and edited appropriately.

Removing layers from the MapService

As with adding layers, removing layers from a MapService necessitates changes to the *Layer Index Constants*, *Layer Control Array* and the *Identify Field Control Array* (“vLayerCtrls” and “sIdFldCtrl” in “map_config.asp”). To remove a layer from the MapService:

1. Make a backup copy of the MapService's current .AXL file. Recommendation is to append the date to the end of the filename of the copy. For example, “wildlands.axl” could be backed up as “wildlands_20030601.axl”. Store these backups in a folder other than the folder containing the current .AXL file.
2. The suggested approach for removing a layer from the map service is to edit the .AXL file with a text editor and delete the appropriate <LAYER></LAYER> tag (see next section – *Editing ArcIMS MapService Files* for more details). No other changes need to be made to the .AXL file.
3. Refresh the MapService using ArcIMS Administrator or Manager.
4. Update the *Layer Index Constants* in **map_config.asp** to reflect the new layer order. The recommended approach is to use the *Layer Constant Creation Utility*. See previous section (*Layer Index Constants*) for additional details.
5. Remove the corresponding array element from the *Layer Control Array*.

5.1. The array must be re-dimensioned to reflect the removed element

```
Dim vLayerCtrls(11, 1) line 49 in map_config.asp
```

As mentioned previously, the first number in parentheses is the upper bound of the array, with the lower bound always being zero. That means the array, as dimensioned above, contains 12 elements. After removing an array index, this number would need to be changed to 10 (array

will then contain 11 elements).

- 5.2. Delete the appropriate element from the array. All array elements after the one deleted must be decremented by 1.
6. Remove the corresponding array element from the *Identify Field Control Array*.
 - 6.1. The array must be re-dimensioned to reflect the removed element

```
Dim sIdFldCtrl(11) line 127 in map_config.asp
```

As mentioned previously, the number in parentheses is the upper bound of the array, with the lower bound always being zero. That means the array, as dimensioned above, contains 12 elements. After removing an array index, this number would need to be changed to 10 (array will then contain 11 elements).

- 6.2. Delete the appropriate element from the array. All array elements after the one deleted must be decremented by 1.

Changing the order of layers in the MapService

Reordering layers in a MapService requires the reordering of the *Layer Index Constants* and the corresponding elements in the *Layer Control Array* and the *Identify Field Control Array* (“vLayerCtrls” and “sIdFldCtrl” in “map_config.asp”). . New elements will not be added or deleted from these arrays, but their order needs to be changed so they remain consistent with the order of the layers in the MapService.

To reorder the layers in the MapService:

1. Make a backup copy of the MapService’s current .AXL file. Recommendation is to append the date to the end of the filename of the copy. For example, “wildlands.axl” could be backed up as “wildlands_20030601.axl”. Store these backups in a folder other than the folder containing the current .AXL file.
2. The suggested approach for reordering the layers in the map service is to edit the .AXL file with a text editor and move the appropriate <LAYER></LAYER> tag (see next section – *Editing ArcIMS MapService Files* for more details). The order of the <LAYER> tags in the .AXL file determines their order in the maps made using that MapService (first layer in .AXL file is “bottom” layer on map).
3. Refresh the MapService using ArcIMS Administrator or Manager.
4. Update the *Layer Index Constants* in **map_config.asp** to reflect the new layer order. The recommended approach is to use the *Layer Constant Creation Utility*. See previous section (*Layer Index Constants*) for additional details.
5. Reorder the corresponding array elements in the *Layer Control Array*.

- 5.1. Cut and paste the appropriate array elements into their new order. The array elements then need to be renumbered sequentially.
6. Reorder the corresponding array elements in the *Identify Field Control Array*.
 - 6.1. Cut and paste the appropriate array elements into their new order. The array elements then need to be renumbered sequentially.

Renaming layers in the MapService

Renaming layers in a MapService is relatively straightforward. The suggested approach is to edit the .AXL file with a text editor and alter the appropriate layer's "name" attribute (contained in the opening tag of the layer; delete the appropriate <LAYER></LAYER> tag (see next section – *Editing ArcIMS MapService Files* for more details). No other changes need to be made to the .AXL file.

Once the layer is renamed, the MapService must be refreshed before the changes will be evident in the Wildlands web application.

Changing the location of the MapServices' source data (shapefiles)

The MapServices used by the *Wildlands Mapper* assume that a specific data structure is in place. Both MapServices have "hard-coded" paths that tell ArcIMS to look for the data in the following directory:

```
D:\ArcIMS_Data\AXL\ARB\Wildlands\data
```

If the data is not at this location, the MapService will fail to start (see Appendix 1: Installation Checklist – creating MapServices).

Should you want to place the data directory in an alternate location on the web server, you will have to edit the MapServices so that they point to the appropriate location. The suggested approach is to open the .AXL files in a text editor and look for the <WORKSPACES> tag, and its closing tag, </WORKSPACES>. In the **wildlands.axl** file you will find two tags enclosed in the <WORKSPACES> tags: <IMAGEWORKSPACE> and <SHAPEWORKSPACE>. The <IMAGEWORKSPACE> tag is used when a MapService includes an imagery layer(s), such as a shaded relief layer. The <SHAPEWORKSPACE> tag is used when a MapService includes shapefiles. Both tags have a *directory* attribute that is used to specify the location of the data. **If the location of the data directory differs in any way from that specified by the *directory* attributes, you will have to correct the path here before attempting to start a MapService.** The **wildlands_ov.axl** file does not contain an <IMAGEWORKSPACE> tag so only the <SHAPEWORKSPACE> will need to be modified.

Editing ArcIMS MapService Files (*.AXL)

ArcIMS Author is a useful tool, and a great place to start building an AXL file from the ground up. Once your AXL file is built, however, we recommend using a text editor (Notepad, WordPad) to do “routine maintenance”, such as changing layer names, adjusting upper and lower scale-thresholds, and changing symbol size and color.

Pitfalls and Problems with Author

- Author does not provide complete access to all of ArcXMLs attributes.

Author’s GUI interface cannot be used to set attribute values for a number of the tags in ArcXML. The <SIMPLEMARKERSYMBOL> tag, for example, has 9 attributes associated with it, only 3 of which can be set using Author.

- Every time you save updates to your AXL in Author, minor changes take place that you might not immediately notice.

Every time you save your AXL in Author it alters workspace names. For instance, a shape workspace called ‘shp_ws-134’ prior to saving your changes may be re-named to ‘shp_ws-73’ afterward. This will NOT prevent the MapService from functioning properly, BUT could be a source of frustration if you had taken the time to customize the workspace names.

Saving your AXL in Author often results in an altered envelope. The <ENVELOPE> tag is found just above the workspace tags, at the top of the AXL and is used to define the map’s initial extent.

Using “Parallel” AXL files

One way of updating your AXL file, and avoiding some of the pitfalls of Author, is to use “parallel” AXL files.

Make a copy of the AXL file you want to update and make your changes to the copy before altering the original. For instance, if you are making significant changes to the rendering of a particular layer, make the changes to the back-up AXL in Author. If you are satisfied with the changes, and you want to apply them to the original AXL file, open both AXLs in a text editor. In the back-up copy, find the layer you made the changes to, copy the layer, and then paste it over the old layer in the original AXL.

This method of updating your AXL files allows you to carefully track what changes are made to your AXL, and where.

Alternatively, if you are adding a new layer, or just changing the properties of an existing one, you can start a new AXL file altogether. Open Author and add the data layer you wish to add/alter to the view. Apply the new layer to the original AXL in the manner described above.

Adding a layer by directly editing the AXL

As mentioned, a new layer can be added to a map service (AXL file) without the use of ESRI's Author utility. Instead, you may edit an AXL file with a text editor (Notepad, WordPad, etc.).

Required ArcXML tags

Every map layer in the AXL file *must* start, and end with the <LAYER> tag.

For example:

```
<LAYER type="featureclass" name="Counties" visible="false" id="0">
```

Attributes of the <LAYER> tag:

Type: Specifies layer type. Use "featureclass" for shapefiles. Use "image" for raster image files, and GRIDS.

Name: Layer name alias. This is the name that will appear in the legend, identify results, etc.

Visible: Specifies layer visibility ("true" | "false").

Id: Unique id for the layer. The ID can be any combination of alpha and numeric characters.

Maxscale: Maximum scale to display the layer on the map. This attribute is optional, though it is critical that it be specified on layers using scale-dependent renderers for the web application to function properly.

Minscale: Minimum scale to display the layer on the map. This attribute is optional, though it is critical that it be specified on layers using scale-dependent renderers for the web application to function properly.

Following the <LAYER> tag is the <DATASET> tag, also required. This tag is used to define the data set used in the layer.

For example:

```
<DATASET name="cocoa" type="polygon" workspace="shp_ws-134" />
```

Attributes of the <DATASET> tag

Name: Specifies the name of the data file. For shapefiles, use the name of the data file without the .shp extension.

Type: Specifies feature type; polygon, line, or point

Workspace: References the workspace name where the data resides. For shapefiles the workspace id can be found in the <SHAPEWORKSPACE> tags at the top of the AXL file. For

images the workspace id can be found in the <IMAGEWORKSPACE>, also at the top of the AXL file.

Adding a New Layer -- Recommended Steps

The best way to add a new layer in a text editor is to copy the code from an existing layer and then paste the code into the AXL file where you want to new layer to reside. Alternatively, use a “parallel” AXL file, as discussed previously.

Note: the first layer listed in the AXL file is always the bottom layer. Any layers listed after the first layer will appear *on top of* this layer in the map. Generally speaking the first layers in a map service are the image layers (e.g., hillshade), followed by polygon features, line features, and point features.

When choosing an existing layer to copy, try to find a layer that is rendered similarly to how you wish to render the new layer – this can save you time by allowing you to “re-use” tags and structure.

Once you have pasted the new layer code in place make the necessary changes to the <LAYER> and <DATASET> tags so that they properly reference and describe the new layer you are adding. **Remember to change the ID attribute to something unique, and be sure that the workspace attribute points to the directory where the new data layer resides.**

If you are adding a new data layer from a workspace that isn’t already being pointed to via the <SHAPEWORKSPACE> or <IMAGEWORKSPACE> tags, you must create a new workspace. Simply copy an existing tag and paste it anywhere between the <WORKSPACE> tags at the top of the AXL file. **Correct the directory path so that it points to your new data layer, and be sure to give it a new name.** We recommend that you maintain the ESRI naming convention shown below:

Shapeworkspaces: shp_ws-(unique number)
Imageworkspaces: jai_ws-(unique number)

After adding a new layer, use Administrator to refresh the MapService.

Scale-dependent layers

The AXL code below shows an example of a scale-dependent layer:

```
<LAYER type="image" name="California relief" visible="true" id="10"  
minscale="1:80000" >  
<DATASET name="ca_hsel.sid" type="image" workspace="jai_ws-0" />  
</LAYER>
```

Notice that the *maxscale* attribute is set to 1: 15,000,000 and the *minscale* attribute to 1:80,000. The “California relief” layer will ONLY be visible when the map scale is between the *maxscale* and *minscale* values.

Scale-dependent symbols

The following piece of AXL code shows an example of scale-dependent symbology:

```
<LAYER type="featureclass" name="Cities" visible="true" id="3">
<DATASET name="cities" type="point" workspace="shp_ws-1" />
<GROUPRENDERER>
  <SCALEDEPENDENTRENDERER lower="1:400000" upper="1:1500000">
    <SIMPLERENDERER>
      <SIMPLEMARKERSYMBOL color="0,0,0" type="square" width="6" />
    </SIMPLERENDERER>
  </SCALEDEPENDENTRENDERER>
  <SCALEDEPENDENTRENDERER lower="1:200000" upper="1:400000">
    <SIMPLERENDERER>
      <SIMPLEMARKERSYMBOL color="0,0,0" type="square" width="8" />
    </SIMPLERENDERER>
  </SCALEDEPENDENTRENDERER>
  <SCALEDEPENDENTRENDERER lower="1:1" upper="1:200000">
    <SIMPLERENDERER>
      <SIMPLEMARKERSYMBOL color="0,0,0" type="square" width="12" />
    </SIMPLERENDERER>
  </SCALEDEPENDENTRENDERER>
</GROUPRENDERER>
</LAYER>
```

This sample AXL code defines the symbology for a “Cities” point layer. The LAYER tags encase 3 scale-dependent renderer tags, each rendering “Cities” as a black square of increasingly larger width – the symbol has an initial width of 6 pixels and has a maximum width of 12. As one zooms in on the map, the scale-dependent renderers create a larger and larger black square symbol. If this were *not* done, the symbol would appear to be getting smaller as a user zoomed in, and would become difficult to see.

The importance of defining layer-level scale-dependencies

In the Wildlands Mapper, it is critical to set the *minscale* and *maxscale* scale attributes of any map layer that has scale-dependent rendering. The *minscale* value should be set to the lowest scale threshold of the *last* scale-dependent renderer, and the *maxscale* value to the layer’s upper-most scale threshold.

Due to interdependencies between the MapService and the Wildlands Mapper code, failing to specify minimum and maximum scales for layers with scale-dependent renderers can create problems in the application. One such problem is that the layer list can get out of sync with what is seen on the map. Examine the following AXL code:

```
<LAYER type="featureclass" name="Schools" visible="true" id="14">
<DATASET name="gschools" type="point" workspace="shp_ws-1" />
<GROUPRENDERER>
  <SCALEDEPENDENTRENDERER lower="1:50000" upper="1:100000">
    <SIMPLERENDERER>
      <TRUETYPEMARKERSYMBOL font="ESRI Cartography" fontsize="18" character="229">
    </SIMPLERENDERER>
  </SCALEDEPENDENTRENDERER>
  <SCALEDEPENDENTRENDERER lower="1:1" upper="1:50000">
    <SIMPLERENDERER>
      <TRUETYPEMARKERSYMBOL font="ESRI Cartography" fontsize="24" character="229">
    </SIMPLERENDERER>
  </SCALEDEPENDENTRENDERER>
</GROUPRENDERER>
```

```
</SIMPLERENDERER>  
</SCALEDEPENDENTRENDERER>  
</GROUPRENDERER>  
</LAYER>
```

Note that the symbol for a school will not appear on the map above a scale of 1:100,000 – it is a scale-dependent symbol.

The code that creates the layer list on the application’s interface checks each layer to see if it is within its scale range – if it *is* within range, the layer is added to the layer list. A check is then done to determine whether the layer is visible. If the layer *is* visible then a “checked” check box is added beside the layer name, otherwise an empty check box is added. **If *minscale* and *maxscale* values are not specified for a layer it is considered to be within scale range**, and is added to the layer list. Because the “visible” attribute is set to *true*, a “checked” check box would appear beside the layer’s name, giving the impression that it is currently visible on the map.

Using the AXL code sample above, if the *maxscale* is not specified, it is likely that one could zoom out to beyond a scale of 1:100,000, at which time the school *symbol* would no longer be visible to the user. Yet the layer list would indicate – correctly – that the layer was still visible. Setting the *maxscale* attribute to the same scale as the upper scale-threshold of the first scale-dependent renderer will ensure that this problem never arises.

To fix this problem, the LAYER tag in the above example should read as follows:

```
<LAYER type="featureclass" name="Schools" visible="true" id="14" minscale="1:1"  
>
```

Note the inclusion of the “minscale” and “maxscale” attributes.

Antialiasing - Pros and Cons

Pros

- Antialiasing helps to make labels and symbols “crisp” and legible. When antialiasing is turned off, labels such as city names, street names and highway shields end up with a very “pixilated”, degraded look. True Type Marker Symbols and some Simple Marker Symbols also exhibit the same behavior without antialiasing.

Cons

- Antialiasing may significantly increase the time it takes to generate a map image. Limit antialiasing as much as possible.

Note: Antialiasing can be applied to Simple Label Renderers, True Type Marker Symbols, Simple Marker Symbols, Simple Line Symbols, and Simple Polygon Symbols. Antialiasing CANNOT be turned on through ArcIMS Author.

Configuring the Contents of the Reporting Option Menus

The Wildlands Mapper interface has four menus used to specify emissions reporting criteria: geographic boundary to report by (County, Air Basin, Air District), year, pollutant, and number of categories. The contents of each of these menus are driven by a series of arrays starting at line 242 in **map_config.asp**. Edit these arrays if you wish to modify the spelling/syntax used in the menus, or the order in which menu items appear. **If you re-order the array elements be sure to re-number them appropriately.**

Other Configuration Constants (map_config.asp)

In addition to the constants and arrays covered in the previous sections, there are a number of others that can be used to alter the basic configuration and functionality of the Wildlands Mapper. The types of constants that can be found in **map_config.asp** are summarized here:

- **MapService Names** – lines 11 - 12
There are constants to reference the two MapServices used in the Wildlands Mapper.

- **Colors, Fills, Symbols** – lines 170 - 196

There are a number of constants used to define the colors, fills, and symbols. The most significant of these is an array called sFillColor_RGB. This array contains the seven fill colors (defined using RGB values) that are used to symbolize the map when an emissions report is generated. Edit the RGB values to change how the map is rendered when a report is generated.

- **Field Constants** – lines 154 - 169

These constants reference critical fields by index number, and field name.

1. Installation Checklist

1. Install the shapefiles and AXL files

The shapefiles and AXL files are found on the application CD under **Wildlands Mapper\AXL\ARB\Wildlands**. Copy the **Wildlands** folder to the server; the suggested destination folder on the server is: D:\arcims_data\axl\arb. If an alternative location for the data is used, changes will have to be made to the AXL files (see *Changing the location of the MapServices' source data* in the “Making Changes to the Wildlands MapServices” section of Chapter 2). The AXL files used by the Wildlands Mapping application are:

- **wildlands.axl** (or latest version)
- **wildlands_ov.axl**

2. Install the web application

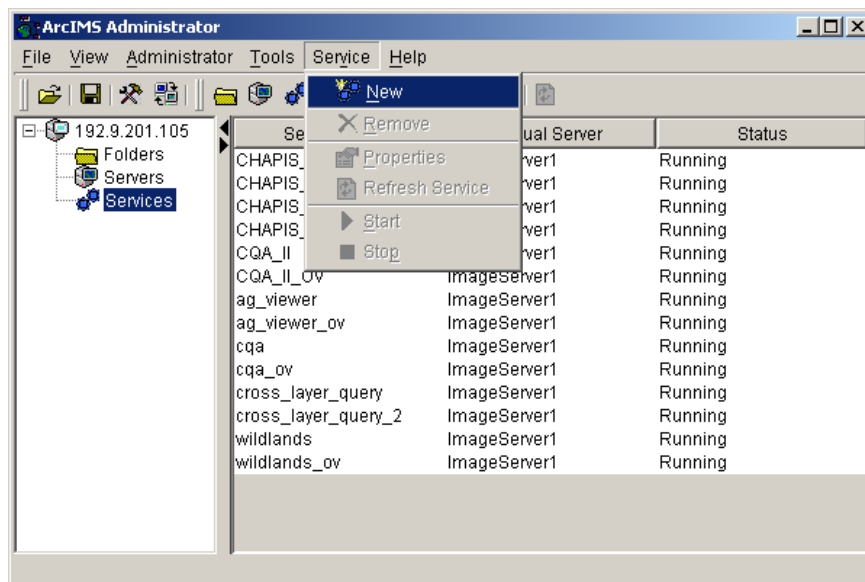
The web application is found on the application CD under **Wildlands Mapper\Website\ARB\Wildlands**. Copy the **Wildlands** folder to the server; the suggested destination folder is: D:\arcims_data\Website\arb.

Note: Ensure that all path/drive-letter references are appropriate for the system on which the Wildlands Mapper is being installed. In particular, check:

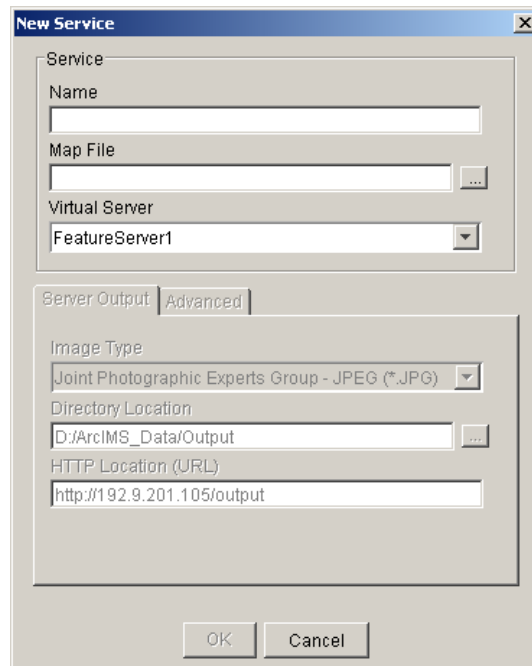
- **main_html.asp** (~ Line 10) – path to the ArcIMS DLL “**aims_ActiveX.dll**”; located in ArcIMS software install directory (usually on “C:” or “D:”).

3. Create Map Services

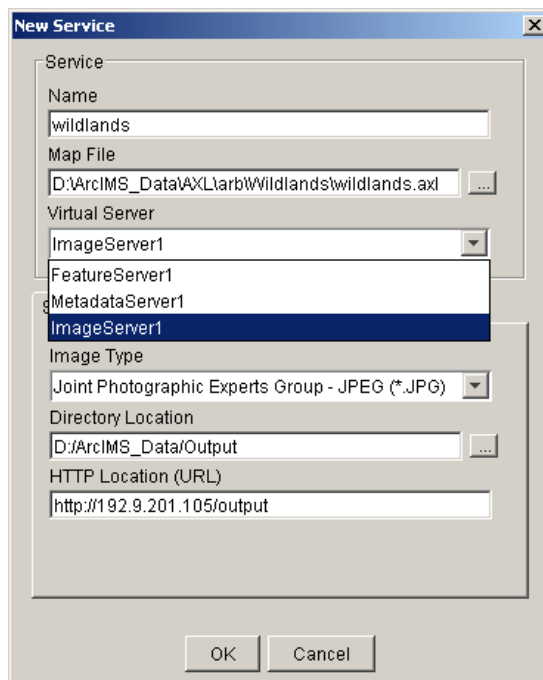
Create two new Map Services using ArcIMS Administrator. To create a MapService, start and login to Administrator. Click “Service...New” on the Administrator toolbar.



A “New Service” dialog box will appear. Click the button to the right of the “Map File” textbox to get an “Open File” dialog box.



Navigate to, and select an AXL file. Give the map service the same name as the AXL file, and specify **ImageServer1** as the Virtual Server.



Press OK and then save the configuration before exiting Administrator.

Map Services required for the Wildlands Mapping Application:

Type	Service Name	AXL File	Where found
Main Map	wildlands	wildlands.axl	D:\arcims_data\axl\arb\Wildlands
Overview Map	wildlands_ov	wildlands_ov.axl	D:\arcims_data\axl\arb\Wildlands

Note: Ensure that all path/drive-letter references in the AXL files are appropriate for the system on which the Wildlands Mapper is being installed – check the <IMAGEWORKSPACE> and <SHAPEWORKSPACE> tags (see *Changing the location of the MapServices' source data*).

4. Create a Virtual Directory (optional)

Although not necessary, a virtual directory can be created for the Wildlands Mapping application. A virtual directory can be created through the “Internet Services Manager”, accessible from “Start...Programs...Administrative Tools” (you must have administrative rights to perform this operation). This will open the “Internet Information Server” (IIS) window. In the “tree” view on the left, select the “Default Web Site”, right-click (or open the “Action” menu) and go to “New...Virtual Directory”. A wizard will guide you through the (short) process:

1. **Virtual Directory Alias:** Wildlands
2. **Website Content Directory:** Browse to D:\ArcIMS_Data\Website\arb\wildlands
3. **Access Permissions:** Accept defaults – *Read, Run, Scripts (Such as ASP)*. Do not allow *Directory Browsing*.

After establishing the virtual directory, the Wildlands Mapping application will be accessible via the following URL:

<http://arb.ca.gov/gismo/wildlands>

5. Installing the VESTRA Utilities (optional)

As mentioned in previous sections of this document, there are three web-based utilities that can be used to help reconfigure the *Wildlands Mapper*. The utilities are found on the application CD under **Wildlands Mapper\Website\utilities**. To install these utilities on the web server, copy the **utilities** folder from the application CD; the suggested destination folder is: D:\arcims_data\Website. Once the directory is in place, create a virtual directory called **utilities** (see Step 4 above). Allow directory browsing.

After establishing the virtual directory, the utilities will be accessible via the following URL:

<http://arb.ca.gov/gismo/utilities>